

Organic Photodiodes: The Future of Full Color Detection and Image Sensing

Ross D. Jansen-van Vuuren, Ardalan Armin, Ajay K. Pandey, Paul L. Burn,* and Paul Meredith

Major growth in the image sensor market is largely as a result of the expansion of digital imaging into cameras, whether stand-alone or integrated within smart cellular phones or automotive vehicles. Applications in biomedicine, education, environmental monitoring, optical communications, pharmaceutics and machine vision are also driving the development of imaging technologies. Organic photodiodes (OPDs) are now being investigated for existing imaging technologies, as their properties make them interesting candidates for these applications. OPDs offer cheaper processing methods, devices that are light, flexible and compatible with large (or small) areas, and the ability to tune the photophysical and optoelectronic properties – both at a material and device level. Although the concept of OPDs has been around for some time, it is only relatively recently that significant progress has been made, with their performance now reaching the point that they are beginning to rival their inorganic counterparts in a number of performance criteria including the linear dynamic range, detectivity, and color selectivity. This review covers the progress made in the OPD field, describing their development as well as the challenges and opportunities.

1. Introduction

Color image sensing (i.e., capturing color images) was first achieved by Edmond Becquerel in 1848 when he produced short-lived color photographs using silver halide films.^[1] It then took just under a century to develop the first film-based color camera,^[2] and the idea of capturing pictures electronically followed in the late 1970s^[3] after the invention of the first image sensor – the charge-coupled device (CCD) in 1970.^[4] The first electronic camera was produced in 1975,^[5] and further developments have since led to cheaper, more compact versions with superior picture quality. As a result, digital cameras are now widespread and can be found in smartphones, portable computers, and vehicles. Many of the advances in image sensor technology have relied on digital imaging, in particular the use of complementary metal-oxide semiconductor (CMOS) devices, which were developed in the 1990s by Fossum et al.^[6,7] Figure 1 shows that the forecasted market for CMOS image

sensors is expected to reach nearly \$18 billion in 2018. Camera phones are predicted to continue to be a significant, although reduced, market for CMOS image sensors, but new applications in medical, scientific, automotive and industrial contexts will account for more growth in the coming years.^[8] Thus CMOS image sensor suppliers are tailoring new designs and pixel-cell architectures to serve applications outside the traditional stand-alone digital camera market and embedded photography in smartphones. The emphasis is no longer focused on increasing the resolution (more megapixels) onto a chip. Instead but greater attention is being placed on making detectors “smarter”,^[9,10] smaller, packed with more analog-to-digital functions with a wider range of optical formats, as well as having different dynamic range specifications and signal-to-noise ratios, a lower power consumption, wireless communication, and the ability to

interact with a variety of interfaces.^[11] Figure 1 also demonstrates the changing landscape of the image detector market and the diversity of applications that such devices are increasingly being required to fulfil. Although OPD-based image sensors are still in the product development stage,^[12] it is not difficult to envisage them making their way into many types of products and applications, given the unique properties that distinguish them from traditional electronic devices and the progress that has already been made with their development. Although the background and characteristics of OPDs will be discussed, the focus here is on approaches reported for color separation.

Generally, there are four key steps by which a pixelated image is captured within an image sensor: first, photons are absorbed by the photoactive material(s) resulting in the generation of electron-hole pairs; second, the electrons and holes move under an applied bias towards the electrodes where they are extracted and collected (for each pixel); third, the accumulated charge from each pixel in the two-dimensional array is read out – the process by which this occurs gives rise to the different image sensors, which include CCDs, charge-injection devices (CIDs), CMOS image sensors and image pickup tubes;^[8] finally, the detected charges are converted into digital data, which is then processed to produce the final image by the application-specific integrated circuit (ASIC).^[14]

The different components and characteristics of the image sensor can be modified in order to improve their performance

Dr. R. D. Jansen-van-Vuuren, Dr. A. Armin,
Dr. A. K. Pandey, Prof. P. L. Burn, Prof. P. Meredith
Center for Organic Photonics & Electronics
the University of Queensland
Queensland 4072, Australia
E-mail: p.burn2@uq.edu.au



DOI: 10.1002/adma.201505405

and facilitate their use in other applications. These include: (i) the image processing software;^[14–17] (ii) the image sensor architecture and layout;^[18–22] (iii) the individual pixel sensor arrangement (typically “passive” or “active”);^[12,23] (iv) the integration of “smart functions” onto the image sensor chips;^[24] (v) the design and arrangement of the color separation system;^[25–27] or (vi) the use of a different photodetector material, e.g., amorphous Si/SiC heterostructures,^[28] organic semiconductors,^[29–31] quantum dots,^[32] nanoribbons/nanofilms,^[33] or nanorods.^[34] Importantly, the type of photodetector material and color separation system associated with the image sensor play a dominant role in defining the quality of the final image since they determine the spectral sensitivity, linear dynamic range, color accuracy and resolution.^[35] In addition, the photodetector material plays a large part in determining the physical properties of the image sensor (flexibility, size, and weight), which then determines the properties and applications of the sensing device.^[36]

Photodiodes (PDs) offer a simple device structure^[37] and can essentially be grouped into those photodetectors that absorb across a broad wavelength range (broadband or panchromatic) and those specifically designed for color imaging in which a narrow wavelength band is targeted (narrowband or monochromatic). However, it will become apparent that these two approaches are closely intertwined.

The main materials currently used for visible wavelength image sensing include inorganic semiconductors: silicon (Si), gallium arsenide phosphide (GaAsP), gallium phosphide (GaP) and InGaAs (indium gallium arsenide). Of these, hydrogenated amorphous (*a*-Si:H) or crystalline (*c*-Si) silicon are the most commonly used in photodetectors for color imaging.^[38] Silicon-based photodetectors comprise the sensor cells (or discrete light-sensing elements – photosites^[14]) which collect the incoming photons and convert these to electrical signals which are read out by a scanning procedure (the mode used depends on the type of image sensor), resulting in the digital signal representative of the charge at each pixel. This signal is then passed on to the ASIC, which together with the microprocessor, is responsible for the readout and processing of the photo-signal. Silicon photodiodes typically consist of a *p*-type and *n*-type semiconductor heterojunction between two heavily doped layers as electrodes. They convert light into electrical signals by photon absorption that results in the spontaneous formation of charge carriers. The subsequent photocurrent is therefore a measure of the light intensity and the response is generally linear. Silicon and several other inorganic semiconductors have high photon to free carrier external quantum yields. The reasons for this are complex and related to low recombination, efficient carrier transport (high mobilities of order $10^2 \text{ cm}^2/\text{Vs}$) and their relatively high dielectric constants, which mean low exciton binding energies. However, in spite of the good electrical properties of inorganic semiconductor-based photodiodes (PDs), they have a number of limitations that can restrict their application. For example, silicon has poor mechanical flexibility,^[39,40] making the simplification of optical systems and incorporation of silicon PDs within tubing or other bendable configurations a major challenge. Crystalline silicon has high carrier mobilities with long lifetimes that can lead to crosstalk between neighboring pixels.^[38] In terms of



Ross D. Jansen-van Vuuren obtained his PhD degree in 2012 at the University of Queensland. The focus of his research was the development of green-sensitive organic photodetectors to replace silicon in conventional image sensors, potentially enabling filterless, color-selective photodetectors. He then spent 8 months

investigating ways in which tertiary educators based in developed nations could partner with and share resources with scientists based in under-resourced “majority world” countries. He was then appointed as a Postdoctoral Research Fellow at the University of Queensland in the Centre for Organic Photonics & Electronics (COPE) where he works on the development of poly(dendrimer)s for OLEDs with applications in large, flexible lighting modules.

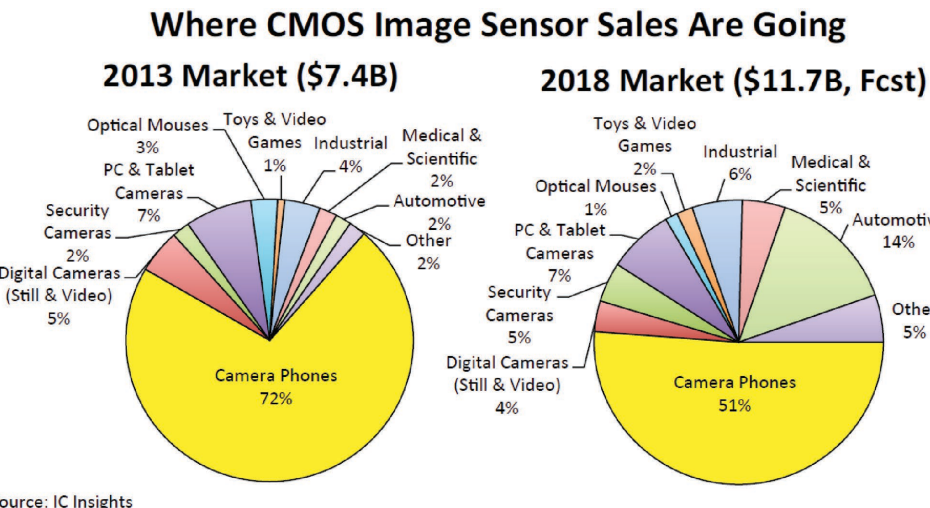


Ardalan Armin obtained his PhD degree in 2015 at the University of Queensland, studying electro-optical properties, charge transport and photo-physics of disordered semiconductors. He was then appointed as a Postdoctoral Research Fellow at the University of Queensland in the Centre for Organic Photonics & Electronics

where he is working on organic and organohalide perovskite photodetectors and solar cells.



Paul L. Burn is a Fellow of the Australian Academy of Science and the Royal Society of Chemistry. He is currently a Professor of Chemistry and the Head of the Centre for Organic Photonics & Electronics, and holds a Vice Chancellor’s Research Focused Fellowship at The University of Queensland, Australia. He received his PhD from the University of Sydney before moving to Cambridge University during which he held the Dow Research Fellow at Christ’s College, Cambridge, England. In 1992 he moved to the University of Oxford and then in 2007 to The University of Queensland as an Australian Research Council Federation Fellow. His research focuses on the development of organic (opto)electronic materials and their application in technologies such as thin film photovoltaic devices, photodiodes, organic light-emitting diodes for displays and lighting, and sensors.



Source: IC Insights

Figure 1. A comparison of the 2013 and 2018 CMOS image sensor markets, showing where CMOS image sensor sales are going. Reproduced with permission.^[8] Copyright 2014, IC Insights.

the optical properties, both amorphous and crystalline silicon absorb light broadly over the visible spectrum, meaning that it is difficult to achieve color discrimination with the material alone, and the absorption is relatively weak,^[33,36] particularly in the violet-blue region (400-460 nm),^[42,43] thus requiring the use of relatively thick photoactive junctions. Furthermore, the fact that silicon has a smaller band-gap than required for visible detection (the band-gap of Si is ≈ 1.1 eV at 300 K^[39]) means that infrared (IR) filters are required in order to avoid unwanted IR sensitivity.^[40]

The emergence of organic semiconductors as an alternative photodiode material has opened up the field of photo-detection and imaging to a new set of possibilities. This has been timely given the rise in demand for new PD designs and pixel-cell architectures to serve applications outside traditional digital camera technologies, e.g., in machine vision or the medical arena such as large-area, flexible X-ray imagers or for endoscope-based imaging. OPDs can now rival and on some metrics outperform silicon photodiodes, and are moving towards becoming more established as a ‘technology’. However, despite the potential that organic semiconductors have to offer, there are still a number of significant challenges to be overcome before OPD-based image sensing devices can compete within the market. Here, the approaches that have been adopted in developing OPDs for color image sensing will be examined against the backdrop of the development of inorganic PDs, since most of the approaches taken have drawn from this well-established earlier technology. It will also highlight the major milestones achieved and some of the challenges that still need to be overcome to enable commercialization of OPDs.

Initially the approaches that have been taken to achieve color image sensing in conventional inorganic semiconductor-based devices will be discussed, before examining how this has translated to OPDs. The figures of merit (FOM) of PDs will be introduced and the means to optimize these in OPDs will be discussed. This will be followed by a discussion of the development of spectrally broad and narrowband OPDs, with a focus

on the materials and the device architectures employed. Finally, the future outlook for the field will be discussed.

2. Color Image Sensing in Conventional Inorganic Semiconductor-based Devices

Two general strategies for color imaging have been developed for inorganic semiconductor-based PD devices: the first consists of sensors that make use of an auxiliary structure that is not a part of the photoactive layer of the pixel, such as a color filter array (Figure 2a-d), and the second consists of sensors that are able to discriminate photons based on wavelength via specialized methods of photocarrier collection within the active layer of the PD (Figure 2e,f). It is important to understand these methods as they set the context and have been drawn upon in developing the OPD-based color sensor technologies that are discussed later.

2.1. Color Separation Achieved by an Auxiliary Structure that is not Part of the Photoactive Layer (Group 1)

There are four main approaches to achieve color images with inorganic-semiconductor-based, broadband (panchromatic) PDs. The first approach commonly used within consumer digital cameras involves the use of a color filter array (CFA) placed over each sensor cell (Figure 2a). In this strategy, the incident light is filtered onto individual pixels of the imaging array. Although there are several arrangements of filters, a common system employs the Bayer filter,^[40] which consists of a mosaic of red (R), green (G) and blue (B) filters such that there are twice as many Gs as there are R and B, thereby representing the human visual system (HVS).^[35,46] Once the image has been captured, there follows a complex “demosaicing” process, which relies on the use of algorithms to extrapolate a set of complete red, green, and blue values for each point of the Bayer pattern image, ultimately resulting in the formation of a

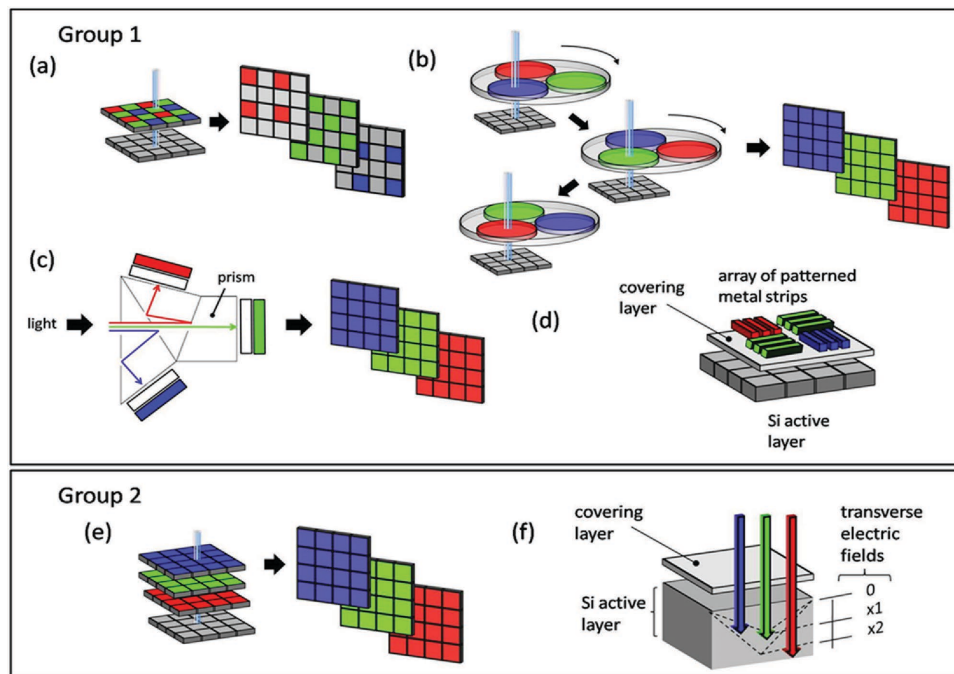


Figure 2. Color separation systems for digital cameras. Group 1 – those incorporating an auxiliary color separation system: (a) Bayer filter mosaic; (b) sequential triple exposure with R, G and B filters; (c) prism separation system and three sensor arrays (3-CMOS or 3-CCD); (d) the integrated color pixel (ICP). Group 2 – image sensors that achieve color separation through an internal mechanism: (e) the Foveon X3® image sensor; (f) the transverse field detector (TFD).

full color image. Some of the major challenges associated with this technology are related to improving the sensitivity as up to two thirds of the incident light is typically absorbed by the color filters,^[47] which limits the quantum efficiency and spatial resolution of the individual pixel sensors, and puts a constraint on reduction of the pixel size.^[47,48] Furthermore, the demosaicing processes associated with the reconstruction of the final image can result in degradation of the color quality^[47,48] and “color constancy” (the perceived color of objects remaining constant under varying illumination conditions)^[49–51] of the final image.

The second method involves taking three sequential exposures, each with a different optical filter (RGB) mounted in a color wheel, before combining the three separate images to form the final picture (Figure 2b). This method is mainly used for professional studio cameras (still-life), as subject motion causes distorted color images.^[35]

The third approach (Figure 2c) mainly applies to video imaging systems and involves the use of a beam-splitter that is able to separate the light into its red, green and blue components, which are then focused onto three discrete image sensors (a three-chip system). This system is commonly referred to as 3-CCD or 3-CMOS. Although considered the best in image quality and resolution, 3-CCD cameras are generally more expensive than single-sensors and the potential for miniaturization is somewhat limited.^[35,52]

The fourth approach is an emerging technology - the integrated color pixel (ICP), which involves replacement of the CFA with an array of metal strips in a specific pattern, enabling color separation during image capture (Figure 2d). The patterned metal layers (which may be 1D or 2D) are placed above each photodetector and control the transmission of light to the

photodetector within the pixel.^[26,53] A key feature of the ICP approach is that it can improve the efficiency of the filtering without degrading the resolution.

Other approaches to color discrimination in Group 1 include the use of a micro color splitter (MiCS), which achieves color separation without absorbing any of the incoming light,^[54] the use of silicon subwavelength (SW) gratings on quartz substrates as transmission color filters,^[55] plasmonic hole arrays,^[56,57] SW plasmonic nanostructures^[58] and the use of a CMOS buried double junction (BDJ) p-n photodetector structure.^[59] The continual research and development effort towards improved color filter-based imaging is recognition that it hampers the efficacy of current color PDs.

2.2. Color Separation Obtained within the Photoactive Layer (Group 2)

The first method within this grouping involves the direct measurement of red, green and blue by a single pixel, which is achieved by stacking color pixels in a three-layer arrangement (similar in many respects to the layers of a chemical emulsion color film), as shown in Figure 2e. The Foveon X3 direct image sensor^[60–62] is based on this approach and has three pixel layers embedded in silicon. The approach is based on the fact that red, green, and blue light penetrate silicon to different depths,^[42] thereby enabling an image sensor that essentially captures light of each of the colors in every pixel. The approach obviates the need for color filters and maximises light utilization and sensitivity. The stacked image sensors are also able to increase the geometric fill factor of the photodetector as separate pixels

are no longer required for each color. However, the spectral selectivity in these image sensing devices and the resultant color reproducibility is still insufficient to meet the demands of modern applications,^[63] and the cross-talk between layers still represents a major device challenge.^[64]

A second approach is to use transverse field detectors (TFDs),^[65] which rely on manipulation of the electric field across the device to generate carriers at specific depths within the device (Figure 2f). Martínez et al. recently combined TFDs with color filters to demonstrate an imaging system capable of obtaining 12 times more information than the human eye.^[66]

Photoactive layer materials can also play an important role in regulating the color recognition ability of an image sensor. In the context of realizing filter-free color separation, several materials have been investigated including vertical silicon nanowires,^[67,68] amorphous Si/SiC heterostructures,^[69,70] nanowires^[71] and nanosheets,^[72] quantum dots,^[32,38,73] and more recently, organic semiconductors, which are the main focus of this review and introduced in Section 3.

2.3. The Problem of Color Constancy

Given the availability of digital cameras, it might be thought that the various approaches to color separation within inorganic semiconductor-based image sensors are already adequate. However, what is not generally appreciated is that the current color discrimination methods result in images whose color characteristics deviate considerably from the actual color perceived by the observer (color constancy), especially under conditions of varying, uncontrolled illumination and wide ranges of brightness.^[15,49,74] That is, the colors in a collected image will vary depending on the characteristics of the illuminant (e.g., its intensity and spectral content).^[75] The main reason for the lack of color constancy in these image sensors stems from their broad spectral response and the need to include a color filter, which necessitates the reconstruction of the final image.^[76] This is one of the great challenges in color imaging and significant effort has gone into the development of image processing technologies and algorithms to overcome the deficiencies of the photodiode response.^[77,78] However, thus far the different approaches have failed to deliver sensors with the required color accuracy.^[79–84] Thus, any new color PD imaging technology must provide a pathway to achieve illuminant-independent color constancy.

3. Organic Photodiodes (OPDs)

Organic photodiodes (OPDs) have the potential to meet the present and future needs of PDs and the remainder of this article will focus on their development and, in particular, on strategies for color separation. Before doing so, it is important to understand the figures of merit (FOM) by which PDs are judged in order to enable an informed comparison, and these are defined following a brief introduction to OPDs.

The first OPD was demonstrated in 1981 by Kudo and Moriizumi^[85] and even at this early stage, it was recognized

that the use of organic semiconductors had the potential to produce photodiodes capable of controlling the spectral response without the need for color filters. The device had a merocyanine/Rhodamine B bilayer as the active component in the photodiode, in analogy to the p-n junction within Si PDs. In this case, the authors describe the merocyanine as behaving as a p-type (prefers to carry holes) semiconductor, and the Rhodamine B as an n-type (prefers to carry electrons) semiconductor, where this distinction is based on the ionization potential and electron affinity of each of the materials. It is worth noting that: (i) such types of semiconductor are typically referred to as electron donor (D) materials and electron acceptor (A) materials, respectively, in the field of organic optoelectronics; and (ii) although the p- and n-convention from inorganic semiconductors is a convenient descriptor for organic semiconductors as well, in the strictest sense molecular solids should not be described as such but rather referred to as preferentially supporting positive or negative charge transport (or materials of low ionization potential or high electron affinity). However, for simplicity, we will continue to adopt the p- and n-convention for the organic semiconductors, realizing these limitations. The concept of using such materials with differing ionization potential and electron affinity is now the widely used strategy for achieving efficient OPDs. To understand why this is the case we will briefly describe the mechanism by which an OPD works.

In OPDs, as with organic solar cells (OSCs), photons from the incident light are absorbed as they travel through the organic semiconductor layer, providing they are of equal or greater energy than the optical gap. Since organic semiconductor materials are generally low dielectric constant media (static $\epsilon \approx 3\text{--}4$), the excitation leads to the formation of a neutral bound state called an exciton (essentially a bound electron-hole pair) rather than free charges. The lack of direct separation of the exciton into free charges is due to the weak screening of the Coulomb interaction of the generated electron-hole pair. For this reason, the free charge generation quantum yield in an homojunction (an active layer comprised of a neat material) is low, which results in the maximum external quantum efficiency (EQE, discussed in more detail in the next section) at short-circuit voltage ($V = 0$) being poor (usually $\approx 1\%$).^[86] Thus, strategies to overcome the exciton binding energy (usually of the order of 0.3–0.5 eV, i.e., $>>kT$ at room temperature)^[87] are essential for high EQEs. The widely used and successful approach to obtaining improved free charge generation in OPDs (as with OSCs) is to combine an electron ‘donor’ (D) with an electron ‘acceptor’ (A) while maintaining a D-A energy offset that is greater than the exciton binding energy in order to enable electron or hole transfer^[88,89] (see Figure 3). This has been achieved in two ways: by forming a D/A planar heterojunction (a ‘bilayer’, as in the work of Kudo and Moriizumi^[85]), or by mixing the donor and acceptor in a blend to form a distributed heterojunction across the bulk of the thin solid film (a bulk heterojunction (BHJ) layer).^[90,91]

At first sight, OPDs appear to operate in the same way as D/A-based OSCs. However, there are a number of key differences between OPDs and OSCs. Firstly, unlike OSCs, OPDs use an external electric field to assist free charge carrier extraction. In addition, there are some strict requirements for OPDs

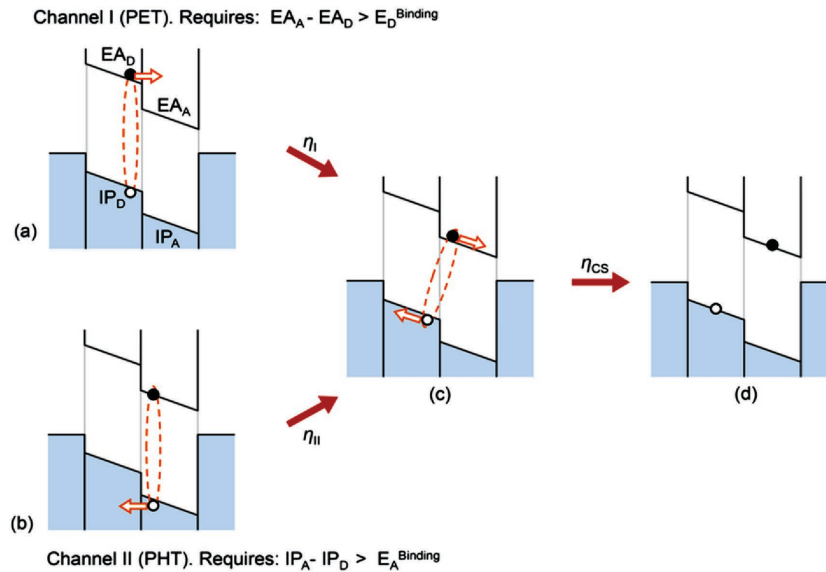


Figure 3. Photoexcitation of the electron donor (a) and acceptor (b) with energetic requirements for efficient exciton dissociation at the organic donor–acceptor interface shown in each case. Electron affinity (EA) [often equated to the lowest unoccupied molecular orbital (LUMO) energy], and ionization potential (IP) [often equated to the highest occupied molecular orbital (HOMO) energy]. (a) to (c) electron transfer or Channel I; and (b) to (c) hole transfer or Channel II are shown in the figure where $E_{D(A)}^{\text{binding}}$ denotes the binding energy of the donor (acceptor) excitons. These two charge generation pathways result in interfacial charge transfer (CT) states (c) that dissociate to separated charges (d). Reproduced with permission^[9]. Copyright 2014, American Chemical Society.

that are not entirely applicable to OSCs, e.g., performance parameters such as open-circuit voltage and fill factor are not as relevant for OPDs whilst a key parameter for OPDs is the dark current under reverse bias (ideally the dark current should be zero).^[92] Finally, for OPV devices the objective is to harvest light across the solar spectrum whereas selective color sensitivity is the more important issue for imaging OPDs.

In 1994, Yu and co-workers were the first to demonstrate BHJ OPDs, which were comprised of the semiconducting polymers poly(3-n-octylthiophene) (P3OT) or poly[2-methoxy-5-(2'-ethylhexyloxy)-1,4-phenylenevinylene] (MEH-PPV) blended with the electron-accepting fullerene C₆₀; the OPD devices gave a sensitivity greater than that of UV-enhanced commercial Si-photodiodes, albeit at a reverse bias of 15 V.^[93] In addition, the ITO [indium tin oxide (anode)]/P3OT:C₆₀/Al diode was found to give a uniform spectral response from 350–630 nm compared with inorganic photodiodes, which have significantly decreased sensitivity at shorter wavelengths. Since then, OPDs have matched or outperformed silicon photodiodes in a range of metrics, including the linear dynamic range (LDR),^[94,95] the specific detectivity^[96] the speed of response,^[97] the dark current^[98] and spectrally flat (or consistent) internal quantum efficiencies (IQEs).^[99]

Furthermore, and in line with the focus of this article, organic semiconductors enable color selectivity without the need for color filters whilst offering additional structural advantages over inorganic semiconductors such as the ability to fabricate photodiodes onto mechanically flexible,^[100–102] or large surfaces,^[103] or used as ultra-thin devices.^[104] Finally, it is important to note that OPDs can be produced by vacuum or solution processing techniques. While many molecular materials are processed by evaporation,^[105] there are examples whereby they are solution

processed.^[37,106] Macromolecules such as dendrimers and polymers can be processed from solution using techniques such as aerosol-jet printing,^[107] spin-coating,^[108] inkjet-printing,^[109,110] screen printing,^[111] or spray-coating.^[112–115]

3.1. Organic Photodiode Figures of Merit

In ordered, non-excitonic semiconductors such as silicon where both charge generation quantum yield and transport are nearly optimal, the EQE and the dark current are the two primary parameters that influence secondary performance indicators such as the linear dynamic range (LDR) and specific detectivity (D*). However, in organic photodiodes the FOM are more complex due to the intricate relationship between the light absorption, charge generation and charge extraction in these devices. In this section we will discuss the FOM for OPDs (considered as intrinsically disordered or partially ordered materials) and how they are dependent on the electro-optical properties of the organic semiconductor active layers and the device structure.

Table 1 summarizes important performance metrics for OPDs and the factors that influence these, which are either device-related or dependent upon the properties of the semiconductor employed. What is clear is that a combination of both device and materials engineering is required in order to realize OPDs with FOM that compare favorably with conventional inorganic-based PDs. We will now discuss the key points of these metrics in order to provide the reader with a clear understanding of what they signify, and to enable a correct comparison and assessment of the performance of reported OPDs. For further discussion on FOMs the reader is referred to other reviews.^[30,32]

Table 1. Figures of merit and factors that affect them in OPDs.

Performance criteria		Dependent upon	References
External Quantum Efficiency (EQE), %	Material and device	- Active layer optical constants - Charge generation quantum yield - Charge transport (including mobility and recombination, voltage and active layer thickness) - Device optics - Gain	[104,116,117]
Spectral response (FWHM)	Material and device	- Inter-chromophore interactions - Photoactive chromophore (optical gap engineering) - Light matter interaction within the cavity (device)	[118–120]
Spectral response (λ_{\max})	Material and device	- Photoactive chromophore - Light matter interaction within the cavity (device)	[118,121]
Upper limit of the spectral bandwidth	Material	- Photoactive chromophore	[94]
Cross-talk between pixels (Spatial resolution)	Material and device	- Charge carrier mobility - Parasitic current	[105,114,122,123]
LSF (Line Spread Function)			
Speed of response, also known as 'operation frequency' or 'operation bandwidth' of signals detected (Hz)	Material and device	- Electron and hole mobilities - Device capacitance - Range of light intensity and modulation frequency of the photo-response - Charge trapping - Device thickness - Applied voltage	[97,124–127]
Specific detectivity (D*)	Device	- Noise current, responsivity and device area - Morphology	[94,183]
Dark current (J_d) Noise	Device	- Thickness - Morphology - Mobility, trapping and doping - Electrode work function - Defect density (e.g., surface roughness, particles)	[129–132]
Linear dynamic range (LDR)	Material and device	- Photoactive chromophore - Noise current (J_d) - Slower carrier mobility - Device thickness - Bias voltage - Bimolecular recombination rate	[95,126,133]
Flexibility (mechanical strain)	Material and device	- Thickness - Morphology - Defect density (e.g., surface roughness, particles)	[113,134]

3.1.1. EQE and Responsivity

The EQE [also known as the incident photon-to-current efficiency (IPCE)] represents the ratio between the extracted electrons and the number of incident photons, with the higher the EQE the better. It is also very common to express the EQE in a more practical format: the responsivity (R), which is essentially the ratio between the output current and the input light power

[units = Amperes/Watt (A/W)]. Responsivity should not be confused with sensitivity, which refers to the lowest detectable light level of a PD, which is related to the signal/noise (S/N) ratio and is therefore heavily influenced by the detection bandwidth.^[40] The responsivity and EQE can be calculated as follows:

$$R = \frac{J_{\text{ph}}}{L_{\text{in}}}, \quad (1)$$

and

$$\text{EQE} = \frac{Rh\nu}{e}, \quad (2)$$

where: J_{ph} is the photocurrent density, L_{in} is the irradiance of incident light, e is elementary electron charge and $\hbar\nu$ is the energy of the incident photon, respectively. Assuming a constant light source and therefore a fixed number of photons per unit time, it is the photocurrent that determines the EQE.

For broadband (panchromatic) photodetectors, the ideal situation is that the combination of donor and acceptor materials absorb across the desired wavelength range, to generate a spectrally invariant EQE. However, for imaging applications that require color discrimination, the situation is a little more complex as a high EQE is only required in the desired spectral window. In this case it is therefore important to ensure that both the donor and acceptor absorb only the desired wavelengths. For example, if the donor is designed to absorb at a specific wavelength, then the residual light absorption by the electron acceptor material outside the desired wavelength range will lead to additional charge generation and degradation of color separation. For, example, soluble derivatives of fullerenes, e.g., phenyl-C₆₁-butyric acid methyl ester (PC₆₁BM), are typically used in OPDs due to their excellent electron accepting and transporting properties, but these absorb light in the UV-blue region.^[118b,135–137] The use of alternatives to PC₆₁BM along with other approaches to overcome this challenge is discussed in Section 3.3.1.

The thickness of the photoactive layer (junction) also influences the EQE in OPDs, as it is strongly dependent upon the charge carrier mobilities of the organic donor and acceptor materials employed and the optical field distribution within the junction. Most photoactive organic semiconductors have modest charge carrier mobilities for electrons and holes, i.e., mobilities that fall in the range of 10^{-5} to 10^{-3} cm²/V.s in the vertical or “diode” direction,^[138,139] which puts an upper limit on the maximum thicknesses that can be used in devices. The limitations imposed by poor mobility can partly be compensated by the fact that OPDs are operated under a reverse bias.^[140] However, the level of dark current increases (simultaneously) under reverse biasing conditions.^[141] A popular approach to reduce the dark current is to raise the thickness of the photoactive layer in order to achieve a higher shunt-resistance.^[126,142] However, due to problems with charge recombination and space-charge effects in thick organic semiconductor films,^[143] there is often a trade-off between higher EQE and the lower dark current in OPDs.^[141,144]

3.1.2. Spectral Response (FWHM and λ_{max})

As mentioned in the previous section the light absorption profile of the active organic semiconductor layer is a major factor in the EQE response of the detector.^[105,118b,145–147] For broadband OPDs, the material needs to absorb over a wide wavelength range. For narrowband devices, the organic semiconductors should absorb either blue, green or red light - corresponding to color matching functions^[148] or the colorimetric functions of a standard observer^[50,149,150] A four-color system (blue, green, orange-yellow and red) has also been investigated to accurately represent color

irrespective of the illuminant conditions: the benchmark for the design of organic materials for illuminant-independent color separation is a quasi-Gaussian spectral response with a Full-width-at-half-maximum (FWHM) ≤ 100 nm.^[151] To fulfill such a fundamental spectral response requirement, the donor and acceptor materials can be engineered (section 3.3.1) and/or the electro-optics of the device can be manipulated (section 3.3.2).

3.1.3. Cross-talk Between Pixels

The origin of pixel cross-talk can be electrical (photocurrent leakage) and/or optical (light deflection and scattering within adjacent pixels), with both contributing to reduced color and luminance resolution. A pixel size of ≤ 10 μm is usually suitable for commercial imaging applications, with the smaller the pixel size the larger the amount of cross-talk between adjacent pixels.^[152] A balance between the pixel size and the cross-talk can be achieved by separation of the pixels. Furthermore, in traditional imagers such as CMOS and CCDs, reducing the pixel dimension to below 1 μm also leads to a sharp decrease in effective photoactive area to below 30% because of an increased density of electrical read-out elements,^[114,152] since the silicon is used for both the photodiode and electronic functions.

The use of OPDs can be advantageous in this regard as vertical integration with the read-out electronics (i.e., the silicon is only used for the electronics) can lead to a spatial pixel fill factor as high as 100%. Broadband OPDs (usually for X-ray imaging applications) have been fabricated using pre-patterned pixels with dedicated electronics and readout lines on which a continuous layer of the organic material is processed.^[122,153,154] The reports of image sensors in which the organic absorbers are integrated with active-matrix backplanes,^[122,155,156] have all had relatively large pixel areas (>100 micrometers) so cross-talk has not yet been an issue.^[105,122] Furthermore, the high absorption coefficients of organic semiconductor thin films should lower the evanescent waveguide coupling between adjacent pixels and minimize the optical cross talk. Moreover, due to the typically low mobilities of organic semiconductors, the lateral current is very small - hence electrical cross-talk between the pixels is not as large a concern as it is in silicon-based imagers.^[38,114,157]

3.1.4. Dark and Noise Current

The dark current is primarily defined by the electronic properties of the device such as the electron and hole mobility, the doping and trap density and the work functions of the electrodes.^[131] Organic semiconductors typically act as intrinsic semiconductors under relevant biasing conditions.^[158,159] Since their optical gap is relatively large (>1.5 eV), the thermally generated free charge density is expected to be $<10^5$ cm⁻³.^[159] However, this ideal condition is never achieved and a finite native doping density of $>10^{14}$ cm⁻³ is often observed for organic semiconductors.^[159,160] Even taking the real doping density into account, the actual dark current is always larger than what is potentially predicted due to defects (e.g., ITO spikes and particles), which decrease the shunt resistance. It has been shown that employing thick active layers^[126,142] and electron/hole

blocking layers^[161,162] can effectively suppress the dark current with values reported of $<10^{-9}$ A/cm². Any current generated in the absence of light (signal) defines the noise level. Although in practical applications the dark current is subtracted from the signal (which includes the dark- and photocurrent), its random fluctuations cannot be mathematically eliminated. These fluctuations include shot noise, which is due to the random arrival of quanta of the electric current, and Poissonian-distributed electrons and thermal fluctuations in the charge density in the semiconductor.^[163] Noise current, i_{noise} (in units of A), is the root mean square of the random fluctuations in the dark current at a detection bandwidth, B , and can be written in a general form:

$$\begin{aligned} i_{\text{noise}} &= \left[i_{\text{shot}}^2 + i_{\text{thermal}}^2 + i_{1/f}^2 + i_{\text{g-r}}^2 \right]^{1/2} \\ &= \left[2ei_d B + \frac{4kTB}{R_{\text{sh}}} + i(f, B)_{1/f}^2 + i(f, B)_{\text{g-r}}^2 \right]^{1/2}, \end{aligned} \quad (3)$$

where k is the Boltzmann constant, T the absolute temperature, and R_{sh} the shunt resistance of the photodiode. While the two first terms, shot and thermal noise are “white”, i.e., independent of frequency (f), the third and fourth terms $i(f, B)_{1/f}^2$ and $i(f, B)_{\text{g-r}}^2$ denote frequency dependent noise components

conventionally referred to as 1/f noise^[164] and generation-recombination (g-r) noise,^[165] respectively. These components are complex and cannot be readily defined in terms of device metrics such as dark current, bandwidth and shunt resistance. In absence of the third and fourth components, the total measured noise current (in units of A) scales with the square root of the electrical bandwidth for a given photodiode. However, due to the frequency dependence of the noise current induced by these terms, the total noise will have a complex functionality at low frequencies. Very often, i_{noise} is inferred based on the dark current and the shunt resistance with the assumption that 1/f and g-r noise are negligible. However, this is not necessarily true, as these noises are not always smaller than the first two components. Therefore, the actual noise current in an OPD (a stack of disordered semiconductor and conductor layers) is complex and is not necessarily fully described by the shot and thermal noise. The experimentally measured noise current in OPDs has been shown to be frequency dependent,^[126,142,162] at least at lower frequencies. Precise measurement of the 1/f noise has been employed to obtain information about percolation pathways in disorder semiconductors.^[166,167] Moreover, it has been observed that the measured noise at a given detection frequency can be several times larger than the sum of the shot and thermal noises (see Figure 4).^[117,126,168] Therefore,

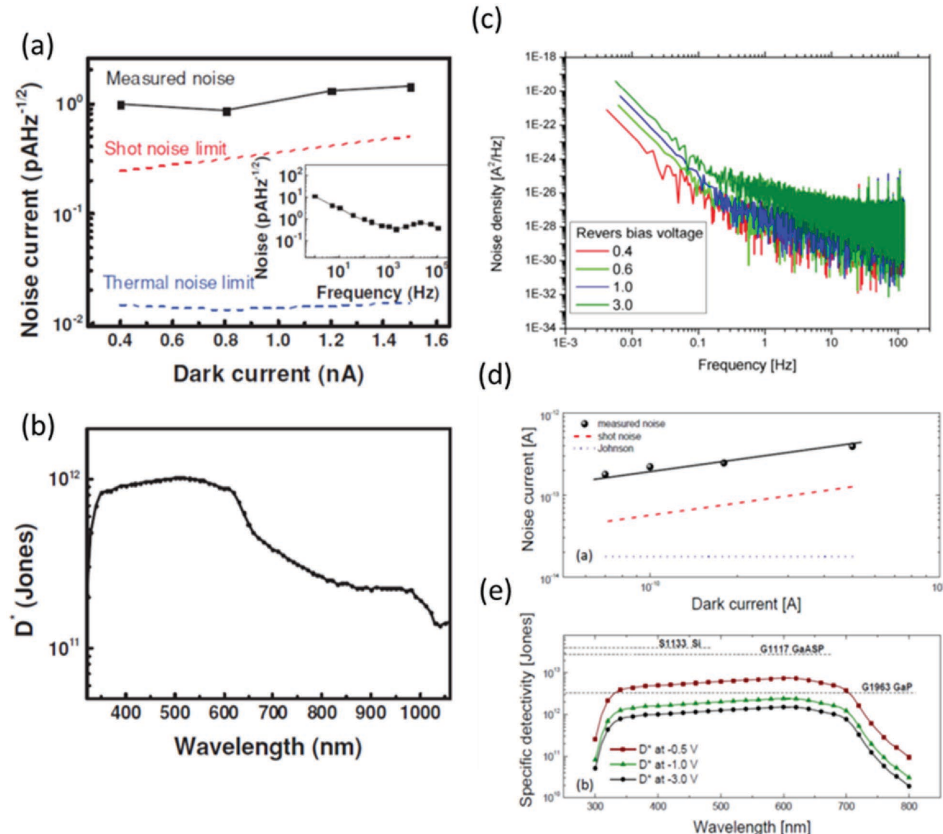


Figure 4. (a) The measured noise of the PbS:P3HT:PCBM:ZnO photodetector; the shot noise and thermal noise limits are also shown (inset: the frequency-dependent noise current measured at -3 V); (b) specific detectivity of the dual-QD photodetector at different wavelengths; (c) The noise spectral power of a PCDTBT(B3):PC₇₁BM(B4) photodiode showing the frequency dependence of the noise density at frequencies <100 Hz. (d) comparison between the measured noise, shot noise and thermal noise for broadband B3:B4 photodiode. (e) specific detectivity of the broadband PCDTBT OPD at different reverse bias voltages in comparison with those of commercial visible sensitive photodiodes. Figures (a) and (b) are reproduced with permission.^[172] Copyright 2014, John Wiley & Sons. Figures (c) to (e) are reproduced with permission.^[126] Copyright 2014, John Wiley & Sons.

using Equation (3) and ignoring its last two terms can result in an underestimation of the noise current and overestimation of a more important metric: the specific detectivity.

3.1.5. Noise Equivalent Power (NEP) and Specific Detectivity (D^*)

The importance of the noise current becomes clearer when determining the minimum detectable signal. The noise equivalent power (NEP) is the minimum light power which can be detected by a PD at a S/N ratio ≈ 1 when the electrical bandwidth = 1, i.e., the power corresponding to the noise current. Therefore from Equation (1), the NEP (in units of $\text{W}/\sqrt{\text{Hz}}$) can be written as

$$\text{NEP} = \frac{i_{\text{noise}}}{R\sqrt{B}}, \quad (4)$$

The reciprocal of the NEP is the detectivity, D . The detectivity can be normalized to the square root of the device area, A , to obtain the specific detectivity with units of $\text{cm Hz}^{1/2}\text{W}^{-1}$:

$$D^* = \frac{\sqrt{A}}{\text{NEP}} = \frac{R\sqrt{AB}}{i_{\text{noise}}}. \quad (5)$$

Using Equation (2) and Equation (5), the specific detectivity can be expressed in terms of the EQE

$$D^* = \frac{e\lambda\sqrt{AB} \cdot \text{EQE}}{hc i_{\text{noise}}}. \quad (6)$$

D^* has a unit of $\text{cm Hz}^{1/2}\text{W}^{-1}$ or Jones (J) and conceptually is the S/N ratio of a PD with an effective area of 1 cm^2 on which an optical power of 1 W is incident and detected at a bandwidth of 1 Hz . To evaluate D^* of an OPD, the noise power spectral density must be quantified. As indicated above, inferring the D^* based upon a simplified version of Equation (3) (i.e., only taking shot and/or thermal noise into account) rather than its experimental evaluation from the measured noise is misleading and can result in an overestimation of the detectivity. The use of the measured noise, which is more appropriate and accurate,^[40,95,120,142] is not universally adopted, and this makes it difficult to compare OPDs reported by different groups. Figure 4 shows two examples of noise and detectivity, as evaluated for OPDs.

There are two main strategies to increase the specific detectivity of PDs: increasing the EQE (responsivity) and suppressing the noise current – as seen from Equation (6). Although increasing the device area can apparently be beneficial in achieving a higher detectivity, this will increase the dark current at a faster rate and compromises D^* . In the absence of gain, the EQE is limited to a value of 100% (singlet fission can potentially increase the EQE to a maximum of 200%^[169]), assuming no loss in the absorption efficiency and ideal charge generation and extraction. Therefore, in these cases the noise current is the dominating parameter in defining the detectivity of the photodetector. Specific detectivities as high as 10^{13} J in the visible have been reported using organic semiconductors by suppressing the dark current and employing hole blocking layers.^[95,108,126] The EQE can however be increased to larger

values in the presence of gain and photo-multiplication. Guo et al. have reported using poly(3-n-hexylthiophene) (P3HT, **B1**, see Figure 5) and poly(9-vinylcarbazole) (PVK, **B2**) blended with zinc oxide (ZnO) nanoparticles (NP) to increase the gain in order to obtain an EQE $> 10^5$ and specific detectivity of $\approx 10^{15}\text{ J}$ for the UV and $\approx 10^{14}\text{ J}$ for detection in the visible,^[117] which is higher than silicon and GaP at room temperature.^[49] Dong et al. report hybrid nanocomposite OPDs in which the measured total noise current was dominated by the shot noise within a frequency range of 1 Hz to 10 kHz (Figure 4a); these OPDs demonstrated a D^* of $\approx 10^{12}\text{ J}$ for detection in the visible (Figure 4b).^[169] Armin et al.^[126] report specific detectivities exceeding 10^{12} J using thick junctions of poly[N-9-heptadecanyl-2,7-carbazole-alt-5,5-(4',7'-di-2-thienyl-2',1',3'-benzothiadiazole)] ‘PCDTBT’ (**B3**) in blends with PC₇₁BM (**B4**) – see Figure 4c–e. Chen et al. (separately) also report high EQE values of 5500% and 7000%, respectively, for photodetectors based on bulk heterojunction layers doped with NIR dyes.^[171,172] Chen et al. achieved EQEs of 8000% at 350 nm and a bias of -4.5 V with composites of P3HT, fullerene, and CdTe nanoparticles,^[173] whilst Li et al. reported EQEs of 16700% in P3HT(**B1**):PC₇₁BM(**B4**)-based OPDs.^[174] Similarly, Wang et al. have reported OPDs comprising P3HT(**B1**):PTB7-Th(**B5**):PC₇₁BM(**B4**) that show broad absorption (from the UV to the NIR) and exhibit EQEs of 90700% (at 390 nm and a bias of -25 V).^[175]

3.1.6. Dynamic Range

The operational light intensity range of an image sensor is described by the dynamic range (DR). This quantifies the ability of the light sensor to adequately capture the variations in light intensities across and within any scene to be captured and is expressed as the ratio of the maximum (I_{max}) and minimum detectable current (I_{min}), where I_{min} is limited by the noise current (defining the minimum detectable power) of the photodetector. In order for OPDs to be simply used in real-life applications, a linear DR (LDR) is desired. Within the LDR, the photocurrent versus intensity is a linear function; i.e., it is a derivative, in which the responsivity is a constant.^[40,176] The LDR can be expressed as an order of magnitude of current (or equivalently light power) over which the response is linear.

At low light intensities where the bimolecular recombination (i.e., when the recombination is quadratically proportional to the carrier density) is negligible compared to the extraction rate, the photocurrent is linear with respect to the light intensity. When the light intensity increases, depending on the charge mobility of the active materials^[176] and recombination rate coefficient,^[143] the photocurrent will deviate from linearity at a certain light intensity and photocurrent I_{max} . After this point the responsivity decreases. The reason behind this deviation is predominantly the formation of space charges when the charge carrier concentration increases, resulting in a lowering of the bimolecular lifetime with respect to the charge carrier transit time.^[143,176] The lower limit of the linearity range I_{min} is theoretically i_{noise} . However, it has been shown that under some circumstances (e.g., in the presence of gain^[117]), decreasing the light intensity results in OPDs losing their linear response.

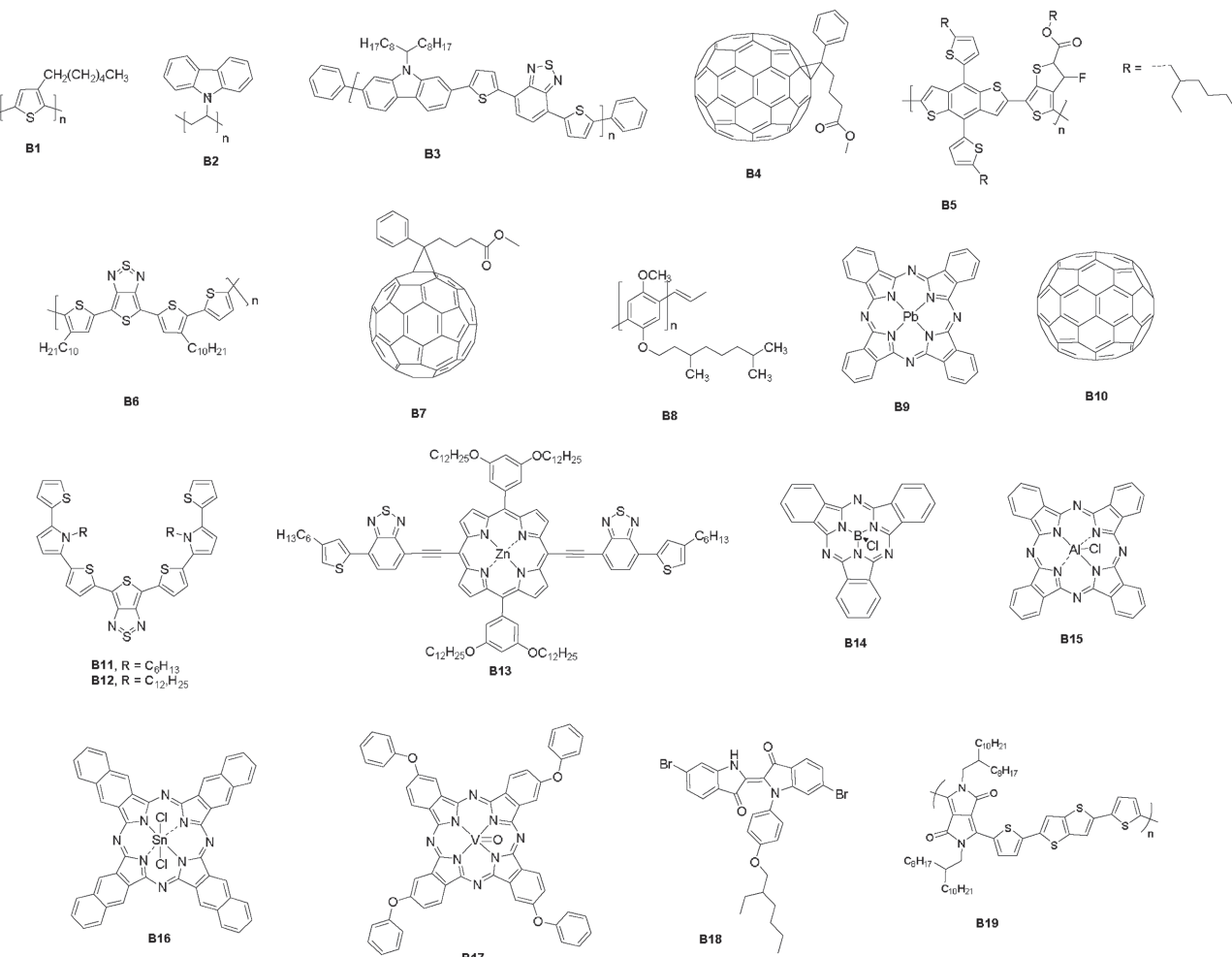


Figure 5. Example chemical structures of molecules and polymers (**B1** – **B19**) used in fabricating spectrally broadband (**B**) OPDs.

Therefore, it is important to measure the LDR experimentally with both upper and lower limits rather than by inferring it through assuming a theoretical lower limit.

As stated earlier, the LDR can be simply expressed as number of orders of magnitude over which the photodetector operates linearly, and the normalized dB unit is the conventional way to express the LDR.

$$\text{LDR} = 20(10) \log \frac{I_{\min}}{I_{\max}}. \quad (7)$$

However, there is an inconsistency in the OPD literature with both ‘20Log’ (conventionally used in and adapted from an electrical engineering context in expressing the linearity of power versus voltage) and ‘10Log’ used to convert the ratio between maximum and minimum currents to dB. Although both of these expressions are correct as definitions, this issue can create confusion, e.g., when an LDR based on 20 log for an OPD is compared with an inorganic photodiode whose LDR is based on a 10 log scale.^[94]

In general, to improve the LDR, the noise level needs to be lowered in order for I_{\min} to decrease. Increasing the space

charge formation threshold will result in an increasing I_{\max} . In OPDs this can be done by: increasing the slower carrier mobility;^[176] decreasing the junction thickness;^[176] minimizing the series resistance;^[176] and employing donor:acceptor systems with non-diffusion limited (suppressed) bimolecular recombination.^[143] The highest reported values of LDR in OPDs are those by Armin et al.^[126] and Guo et al.^[95] [9 orders of magnitude (180 dB) for visible], Fang et al. (12 orders of magnitude for UV)^[133] and Dong et al. (7 orders of magnitude for UV to NIR).^[170] Various strategies have been proposed to improve the LDR based on increasing the photocurrent.^[175–179]

3.1.7. Speed of Response

The speed of response (SR) in OPDs corresponds to the time taken to generate and extract the generated electrons and holes. When used in an optical communication system, the response time of an OPD determines the bandwidth available for signal modulation and data transmission. For imaging applications, the photodetector response should be fast enough to capture all levels of light variation in the scene. The temporal bandwidth is

defined as the frequency of input light modulation at which the photo-response is -3 dB lower than the continuous wave (CW) response. The -3 dB bandwidth is limited by the carrier transit time, characteristic RC -time or both^[152,180] and is given by

$$\frac{1}{f_{-3dB}^2} = \frac{1}{f_t^2} + \frac{1}{f_{RC}^2}, \quad (8)$$

where f_t and f_{RC} are the carrier transit time limited and RC limited bandwidths respectively and are defined as:^[181]

$$f_t = \frac{3.5}{2\pi t_{tr}}, \quad (9)$$

and

$$f_{RC} = \frac{1}{2\pi RC}, \quad (10)$$

where t_{tr} is the carrier transit time, R is the total series resistance (which includes the photodiode series resistance, sheet resistance, contact resistances and load resistances in the measurement circuit). It is important to note that decreasing the active layer thickness can potentially increase the frequency bandwidth since the transit time is $t_{tr} = d^2/\mu V$, where d is the thickness of the active layer, μ charge carrier mobility and V the applied voltage. However, decreasing the thickness also results in increasing the capacitance and therefore the RC -time. In general, the temporal bandwidth should be optimized based upon the thickness, mobility and applied voltage. For example, Armin et al. have recently shown that the transit time used in Equation (8) (adopted from inorganic systems) must be that of slower moving carriers for OPDs.^[126] The slowest extracted species is not necessarily composed of the slower carriers (the species with lower mobility) but can include faster carriers that are slow to exit the device due to the optical field distribution within the device structure when a thick junction is employed.

Conventional imaging applications require typical frame rates of around 100 frames/s with typical integration times and data transfer times in the order of milliseconds.^[122] The best strategies for achieving a high frequency response are to minimize the carriers transit time to the electrodes and any parasitic capacitance formation in the device. OPD-based image sensors operating at a speed of 100 kHz have been reported.^[97,182]

For individual OPDs, different temporal bandwidths have been reported depending the operating wavelength and spectral bandwidth: 430 MHz ($500 < \lambda < 750$),^[124] 100 kHz to 1 MHz (for visible),^[126] 10 to 100 MHz (blue),^[183] and 400 kHz (visible).^[184] We draw the attention of the reader to the diverse range of proposed strategies to increase the speed of response.^[103,183,185–187]

3.2. Spectrally Broadband OPDs

The spectral bandwidth limits of the photoresponse of broadband OPDs are primarily defined by the absorption of the photoactive layer. However, the measured EQE is also dependent on the charge generation and collection efficiency^[188] as well as any optical cavity effects arising from the use of multi-layer devices and partially reflective electrodes. For example, Lupton et al.^[119] have shown that introducing semi-transparent electrodes can be used to increase the Q-factor of the cavity (the active layer sandwiched between transport layers and electrodes), and therefore the active layer can be used to tune the absorption and the EQE. Furthermore, it has been shown that the effect of layer thicknesses on the spectral response is particularly important even without the presence of a high Q-factor cavity,^[189] with minor thickness variations (10–20 nm) in thin junctions (<300 nm) introducing large differences in the spectral response of the OPDs. By increasing the junction thickness, the EQE of a broadband OPD can be flattened and its dependence on the thickness reduced, as shown in Figure 6. Figure 6a shows that by increasing the junction thickness the photo-generated carrier profile changes from an interference-governed regime to Beer-Lambert-like when the thickness is increased to 700 nm. This significantly flattens the EQE response, which can be seen in Figure 6b where the flat photoresponse of an 800 nm thick junction is compared with that of a 100 nm thick junction.

Efforts to develop broadband OPDs have essentially fallen into two main categories, namely UV–Vis–NIR OPDs and IR blind-visible OPDs (blind referring to the fact that the OPDs do not absorb in a particular spectral region). With respect to the creation of UV–Vis–NIR OPDs, photo-responses ranging from the visible out to 1450 nm have been reported by

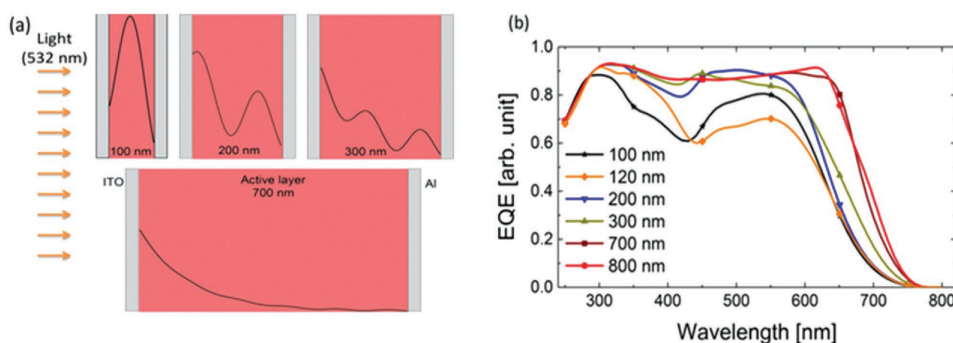


Figure 6. Comparison of absorbed photon distribution profiles and simulated EQEs for PCDTBT(B3):PC₇₁BM(B4) devices with different junction thicknesses: (a) simulated photon distribution profile as a function of junction thickness under light illumination; (b) simulated EQE spectra for a blend ratio of 1:4 (by weight), as a function of thickness Reproduced with permission.^[126] Copyright 2014, John Wiley & Sons.

Gong et al. using a photoactive film of poly(5,7-bis(4-decanyl-2-thienyl)-thieno(3,4-b)diathiazole-thiophene-2,5) PDDTT (**B6**, see Figure 5) – a narrow optical gap polymer, blended with PC₆₁BM (**B7**).^[94] Arnold et al. have achieved a broader spectral range by using a carbon nanotube/polymer-based device, in this case with P3HT (**B1**) and MMDO-PPV (**B8**).^[190] Su et al. have reported UV–Vis–NIR OPDs with a photo-response out to 1100 nm based on planar and hybrid planar-mixed molecular heterojunction OPDs comprised of a lead phthalocyanine (**B9**) as the donor, with C₇₀ (**B10**) as the acceptor.^[96] These UV–Vis–NIR OPDs have been developed to extend the photo-response to beyond the band-edge of silicon, where InGaAs photodiodes are commonly used (Figure 7a). Other efforts to achieve a broadband response similar to that of silicon (300 to 1100 nm) include the use of narrow optical gap donors such as **B11** and **B12**,^[191] and **B13**,^[192] as well as tandem structures consisting of complementary narrowband absorbing molecules including phthalocyanine-based compounds **B14**–**B16** (as heterojunctions with PC₆₁BM, **B7**),^[193] and bulk heterojunctions of poly[2-methoxy-5-(2-ethylhexyloxy)-1,4-phenylenevinylene] (MEH-PPV) with vanadyl 2,9,16,23-tetraphenoxy-29H,31H-phthalocyanine (**B17**).^[194] While NIR sensitivity can be achieved using narrow optical-gap organic semiconductors, Yang et al. have shown that for P3HT(**B1**):PC₆₁BM(**B7**) devices with junction thicknesses of several micrometers, it was possible to achieve a NIR photo-response by utilising absorption by charge-transfer states, although the devices were not particularly efficient.^[195]

Figure 7a and Figure 7b show the EQEs for the UV–Vis–NIR and silicon matching OPD devices, respectively, in comparison with commercial inorganic PDs. It is important to note that in these devices the EQEs of the OPDs are significantly less than their inorganic counterparts at longer wavelengths and are not spectrally flat.

However, while IR detectors are important, for digital photographic cameras the responsivity of the silicon in the IR is undesired and requires the use of additional filters. IR-blind visible light detection has been achieved for a number OPD materials and device combinations. For example, the intermediate optical gap polymer P3HT (**B1**) blended with PC₆₁BM (**B7**) in different device structures (Valouch et al.,^[196] Ramuz et al.,^[141] Baierl et al.^[184,197] and Wang et al.^[198]) provide for IR-blind visible light detection. The spectral response window at short wavelength is limited to the glass (substrate) absorption edge (\approx 350 nm) and the long wavelength absorption onset of the P3HT:PC₆₁BM blend (\approx 650 nm). More recently the carbazole-based polymer, poly[N-9'-heptadecanyl-2,7-carbazole-*alt*-5,5-(4',7'-di-2-thienyl-2',1',3'-benzothiadiazole)] (PCDTBT, **B3**), which has a slightly narrower optical gap, has been blended with PC₇₁BM (**B4**)^[126] in order to realize a constant EQE (\approx 70% at -1 V) over the visible spectrum (Figure 7c). Kim et al. have constructed visible broadband OPDs with P3HT in blends with a non-fullerene, solution-processable indigo acceptor **B18**.^[199] These demonstrated relatively flat EQEs of \approx 80% and a D^* of \approx 10¹² cm Hz^{1/2} W⁻¹ from 350–650 nm, i.e., an IR-blind

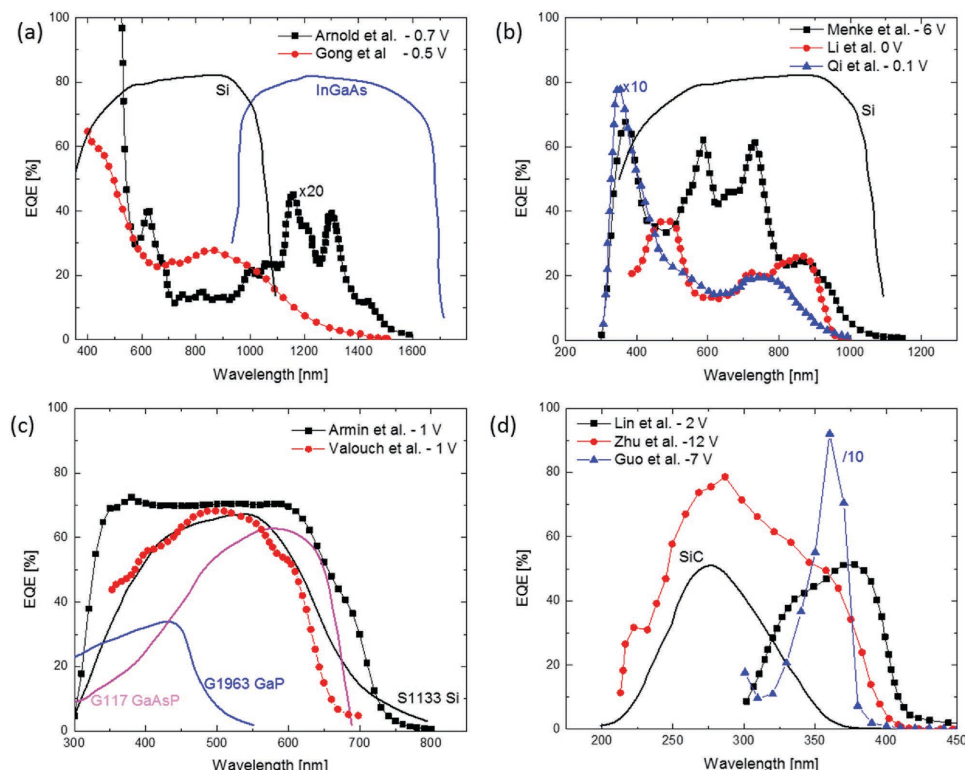


Figure 7. Various broadband OPDs in comparison with a range of conventional inorganic semiconductor PDs. (a) Broadband UV–Vis–NIR OPDs based on a narrow optical-gap polymer (Gong et al.,^[94] and Arnold et al.,^[190]) in comparison with silicon and InGaAs photodiodes; (b) a comparison between silicon and broadband Vis–NIR OPDs developed by: Qi et al.,^[191] Menke et al.,^[193] and, Li et al.,^[203]; (c) PCDTBT(**B3**)-based^[126] and P3HT(**B1**)-based^[196] visible OPDs in comparison with commercial visible band photodiodes; (d) UV-sensitive OPDs^[117,201,202] compared with a commercial SiC photodiode.

spectral response. However, based on the reported non-unity logarithmic slope of the photoresponse, the LDR is likely to be incorrect.

Efforts have been made to realise visible- and IR-blind UV photodetectors (useful for various applications such as flame detection, chemical sensing or astronomical observation^[200]) using organic semiconductors. The work of Lin et al.,^[201] Zhu et al.^[202] and Guo et al.^[117] show a superior spectral response in comparison with traditional SiC UV photodetectors (Figure 7d).

Table 2 summarizes some of the major figures of merit for broadband OPDs compared with conventional Si-based imaging sensors (Hamamatsu S2251 and OSI Optoelectronics (Planar diffused UV-enhanced Si PDs)).

Color images can be achieved with broadband absorbing OPDs and a color separation system such as a CFA in a similar fashion to that used with inorganic sensing devices [Section 2, Figure 2, Group 1 b]. Yu et al. were the first to apply this approach using poly(3-alkylthiophene:PC₆₁BM-based OPDs incorporated within a line scanner.^[204,205]

By incorporating the OPDs in linear arrays, 2D images could be recorded by scanning a visible image line by line. Instead of pixelating the organic semiconducting layer, a continuous layer was used, with the pixel dimension determined by the electrodes. Color filters were placed sequentially above the photodiode array enabling the selective

spectral responses shown in **Figure 8a**. The photocurrent signals corresponding to variable grey levels of incident light intensity were converted to digital signals (256 gray levels by an 8-bit (2^8) A/D circuit) before transfer.^[204] **Figure 8b** shows the desirable linear intensity dependence of the polymer-based pixel sensors. The red, green and blue images were then superposed in order to attain the full-color image (Figure 8c). The same approach was used for P3HT:PC₆₁BM OPDs that had a flat photoresponse from ≈ 400 –600 nm.^[149,205] Despite the poor resolution resulting from the large pixels (635 μm), the result was an outstanding proof-of-principle achievement.

Although not yet commercially available, FUJIFILM Corporation has now demonstrated image sensors with considerably smaller pixel sizes (lengths less than 3 μm) working on similar principles.^[211,212] The image sensor had an EQE of 65% (at 550 nm) and a DR of 60 dB.^[212] More recently, FUJIFILM and Sony have reported the development of an image sensor with an OPD layer ‘laminated onto CMOS circuits’ that had an extended dynamic range of 88 dB (pixel sizes of 3.0 μm), which was achieved by using larger lens aperture settings and reducing the shot noise.^[213] In spite of these advances, the use of color filters for OPDs suffer the same deficiencies as when they are used with inorganic PDs, although without the need for IR filtering.

Table 2. A selected summary of broadband OPDs with performance metrics comparable to those of typical color image sensing inorganic PDs: [†]Hamamatsu S2551^[209] and ^{*}Planar diffused UV-enhanced Si PDs^[210] (OSI Optoelectronics). The chemical structures of some of the materials can be found in **Figure 5 (B)** and **Figures 13 and 16 (N)**.

Materials used (Device structure)	λ range (nm)	LDR (dB)	J_d (nA/cm ²) (V)	D* ($\times 10^{11}$ cm Hz ^{1/2} /W) (λ , nm; V)	NEP $\times 10^{-14}$ (W/ $\sqrt{\text{Hz}}$)	R (A/W) (V or λ , nm)	EQE _{max} , % (λ , nm) (V)	Year	Ref
PEN/PEDOT:PSS/ PCDTBT(B3):PC ₇₁ BM(B4)/ Al or Au	400–720	–	0.15 (−5)	345 (−5 V)	–	–	55 (−5)	2015	[111]
P3HT(B1):PC ₆₁ BM(B7) (with a-IGZO ETL)	300–650	–	10 (−2)	30 (550)	–	–	64 (0)	2015	[206]
EHTPPD-MT:PC ₆₁ BM(B7) BHJ	300–800	–	–	–	–	0.18 (532)	23 (0)	2015	[37]
ITO/PEDOT:PSS/P1: PC ₆₁ BM(B7)/BCP(N30)/Al	300–1200	–	0.25 (−0.1)	140	–	0.16	–	2015	[120]
PEDOT:PSS/ T1:P3HT(B1):PC ₇₁ BM(B4)/ PFN/PEDOT:PSS	400–750	–	10	–	–	–	34 (−1)	2014	[110]
P3HT(B1):PC ₆₁ BM(B7)	300–700	–	360 (−1)	3.15	9.5×10^{-13}	0.18 (−6)	35 (0)	2013	[207]
ITO/PEDOT:PSS/C ₆₀ (N19)/ BCP(N30)/Al	300–700	90	–	3.6	–	–	40 (−6)	2013	[95]
P3HT(B1):PC ₆₁ BM(B7)	350–725	60	7 (−1.5) 20 (−4)	–	–	–	52 (−4)	2015	[114]
ITO/PEDOT/PDD-TT(B6):PC ₆₁ BM(B7)/ Al	300–1450	>100	–	420 (500)	–	0.17	26 (800)	2009	[94]
P3HT(B1):PC ₆₁ BM(B7)	300–700	–	1 (−1 V)	70	2.8	–	70 (0)	2008	[141]
ITO/PTCDA/p-Si	550–1000	–	–	–	–	–	85 (650, −10)	1989	[208]
Si (Hamamatsu S2551) [†]	340–1060	–	1 (−0.01)	150	3.9	0.6 (920); 0.37 (663)	–	2015	[209]
Planar diffused UV-enhanced Si PD (OSI Optoelectronics)*	190–1100	–	–	–	3.6	0.5 (980); 0.33 (633)	–	2015	[210]

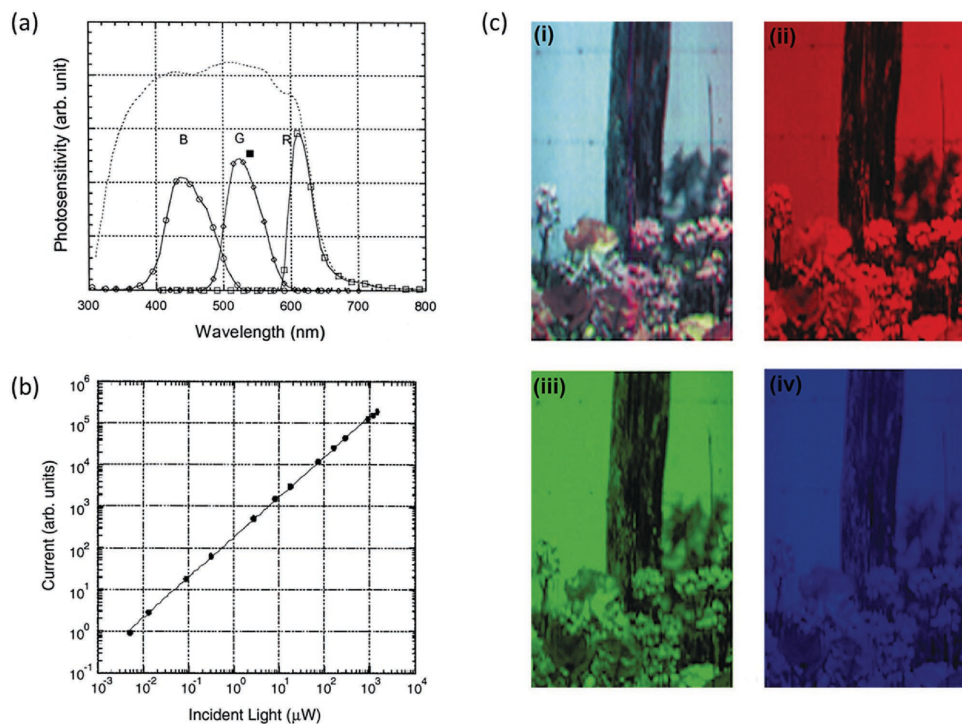


Figure 8. Poly[thiophene]:PC₆₁BM OPD with color filters. (a) Spectral photoresponses of red, green and blue pixels achieved with a P3HT:PC₆₁BM photosensor using colour filters; b) the intensity-dependence of these BHJ-based sensor pixels. (Figures (a) and b) reproduced with permission from^[205] 2000, Elsevier); (c) (i) a full-color image and the corresponding red (ii), green (iii) and blue (iv) mono-color images taken by the P3OT:PC₆₁BM 1×102 OPD array. Adapted with permission.^[204] Copyright 1998, John Wiley & Sons.

3.3. Narrowband Absorbing OPDs

To avoid the need for color filtering, it is necessary to have OPDs that absorb and respond in a narrow wavelength band. Narrowband OPDs can be obtained by three different general approaches based around a combination of materials and device architectures: (i) by designing the materials to have the required absorption spectra; (ii) by modifying the device architecture in order to optimize the light-matter interaction by optical effects; and (iii) manipulation of the electro-optics of the device. The next few sections of this review will focus on the collective findings of research in these three areas. Materials can be used to fabricate OPDs based on the different pixels for either a three-color sensor (RGB, the conventional sensor^[204]) or a four-color sensor, such as has been proposed by Jansen-van Vuuren et al.,^[151] or for multilayer devices which enable monochrome color sensing (Figure 8). We will now consider the materials that have been trialled within such device structures.

3.3.1. Materials-based Approach

There are a limited number of materials that have a narrow absorption band and are blind outside the desired wavelength range; hence there are fewer reports on this strategy for OPDs. In general, molecules that have narrow spectral band widths possess excited states whose geometries are similar to the ground state (i.e., with very few vibrational levels superimposed on the electronic absorption bands of the molecule - both in

the ground and excited states),^[214] and this usually requires the chromophores to have a certain level of rigidity and planarity – resulting in absorption and fluorescence spectra with well-resolved vibronic bands.^[215] Since higher efficiencies (and therefore sensitivities) can be obtained through the use of donor–acceptor blends,^[91] the absorption properties of both the donor and acceptor materials need to be considered. The following section will outline and discuss the range of donor and acceptor combinations that have been studied for blue, green and red absorbing layers based on small molecules, dendrimers, and polymers. In each case where possible the FWHM and efficiency of the OPD will be given with a fuller summary of the performance metrics given (where reported) in Table 3.

3.3.1.1. Blue-sensitive OPDs: In principle, blue-sensitive OPDs are the simplest to prepare as the chromophore can be chosen to absorb at short wavelengths and be blind to longer wavelengths. Fukuda et al.^[147] have developed a three-color sensor based on different organic materials with pixels that separately absorb blue, green and red light (see Figure 9 a(i)). The organic materials were initially selected by a simple screening of the literature and relatively simple OPDs (ITO/organic layer/Al) comprised of neat solution-processed films were prepared. The blue OPD had an active layer of poly(9,9-di-*n*-octylfluorenyl-2,7-diyl)-co-1,4-benzo-(2,1,3)-thiadiazole (F8BT, N1) while for reference the green and red OPDs used doped poly(9,9-di-*n*-octylfluorene) (PFO, N2): rhodamine 6G (N3) and nickel tetrakis(*tert*-butyl)phthalocyanine (N4), for the green and red

Table 3. A summary of the optoelectronic and device properties of B-, G- and R-sensitive OPDs in comparison with the three separate color sensors that comprise the Hamamatsu silicon RGB color sensor (S7505-01).^[246]

OPD	Device Structure	FWHM (nm)	λ_{\max} (nm)	EQE/% (at bias V or Field V/cm)	J_d /nA/cm ² (bias)	S/AW ⁻¹ (bias)	Year	Ref
B	ITO/PEDOT:PSS/mMTDATA:C ₆₀ (N19)/Al	—	—	—	0.1 (−0.5)	0.13 (−6)	2014	[238]
	ITO/PPR/BBOT/LiF/Al	50	440	—	10 (0)	—	2014	[239]
	ITO/PEDOT:PSS/ST-dendrimer(N8):PC ₆₁ BM(B7)/Al	100	435	22.5 (−2) 14.5 (−0.5)	3 for 25 (0)	—	2014	[225]
	ITO/F8BT(N1):NPh ₃ -silole(1:1)/LiF/Al	89	470	25 (−15 MV/m)	—	—	2013	[222]
	ITO/F8BT(N1):NPh ₃ -silole (1:1)/LiF/Al	—	—	52 (−26 MV/m)	—	—	2013	[221]
	ITO/F8BT(N1):DMTPS(N5)/LiF/Al	125	470	7.6 (2 × 10 ⁵ V)	—	—	2010	[217]
	ITO/C ₆₀ (N19)-doped Coumarin 30 (N40)/Alq ₃ (N36)/Al	—	410	64 (−10)	9.5 (−5)	—	2010	[136]
	ITO/BCP(N30)/Co-TPP(N37):Alq ₃ (N36)	75	420	20 (2.25 × 10 ⁶ V/cm) <1.0 (2.0 × 10 ⁶ V/cm)	0.08	2005	[240]	
	Silicon: S6428-01	90	460	—	4.4 × 10 ^{−4} (−1)	0.22	2015	[241]
G	ITO/MoO _x /DM-2,9-DMQA(N41):BSubPC(N14)/Al	115	553	57 (−3)	53 (−3)	—	2015	[242]
	ITO/MoO _x /Al/DM-2,9-DMQA (N41):BSubPc(N14) (1:1)/MoO _x /ITO	115	580	41.2 (−3)	—	—	2015	[242]
	SiO ₂ /Cytop/anthracene derivative(N20)	75	≈530	—	—	—	2014	[231]
	ITO/PEDOT:PSS/dendrimer N12:PC ₆₁ BM(B7)/Al	130	510	8.2 (−1) 2.1 (0)	7.6 (0)	—	2013	[118]
	ITO/MoO _x /DMQA(N15):BSubPc(N14)/Al	160	575	60 (−5)	37	—	2013	[105]
	ITO/R6G(N3):PFO(N2)/LiF/Al	94	560	0.009 (−1.5)	—	—	2009	[147]
	Glass/Cr/Au/NPD(N22)/DFPP(N21)/Ag	150	505, 580	2.2 (0)	—	—	2008	[233]
	Silicon: S6429-01	70	540	—	4.4 × 10 ^{−4} (−1)	0.27	2015	[243]
	ITO/pentacene (OFET OPD)	≈180	584, 674	—	—	0.19	2015	[244]
R	ITO/PEDOT:PSS/PCDTBT(B3):PC ₇₁ BM(B4)/C ₆₀ (N19)/Al	85	645	34 (−1)	0.01 (−1)	0.1 (−1)	2015	[142]
	ITO/PEDOT:PSS/Ni(t-Bu) ₄ Pc(N4)/LiF/Al	≈120	610	0.83 (−3)	—	—	2011	[234]
	ITO/PEDOT:PSS/P6T(N25)/BP3T(N26)/CuPc(N24):C ₆₀ (N19)/BCP(N30)/Al	160	620	—	—	—	2010	[235]
	Glass/Ormocer/Cr/Au/MPP(N23)/CuPc(N24)/Ag	110	620, 660	2	—	—	2008	[233]
	ITO/CuPc(N24):BPPC(N31)/Au	240	540, 640	—	—	0.03 (−3)	2006	[237]
	ITO/TiOPc(N28)/F ₁₆ ZnPc(N29) ₅ /BCP(N30)/Ag	—	≈640	—	—	—	2003	[236]
	Silicon: S6430-01	90	660	—	4.4 × 10 ^{−4} (−1)	0.16	2005	[245]

devices, respectively. The FWHM of the blue OPD was ≈120 nm (photocurrent) although the EQE was only 0.12% at -2.3 V due to it being a homojunction.^[147] Indeed, homojunctions generally tend to give low EQEs.^[216]

When F8BT (N1) was blended with various electron-accepting materials, the blue-sensitive OPD performance was improved.^[217–222] For example, a 40 wt% blend of 1,1-dimethyl-2,3,4,5-tetraphenylsilole (DMTPS, N5) in N1 improved the EQE to 7.6% under an electric field of 2×10^5 V/cm in ~250 nm-thick OPDs.^[218] Importantly, the wavelength selectivity of the device was unaffected by the presence of the N5 due it absorbing exclusively in the near UV.^[217,223]

The PFO derivative ‘F8T2’ (N6) in blends with fullerene derivatives PC₆₁BM (B7) and the *N*-tosylated aziridino fullerene ‘TsAF’ (N7) provided OPDs with FWHMs of ≈100 nm ($\lambda_{\max} = 460$ nm)^[183,224] although a tail from the fullerene derivatives was evident, particularly for the N6:B7 (1:4) OPD device.

Pandey et al. have reported blue-sensitive OPDs based on solution processed pentathiophene-cored dendrimers (N8 and N9, Figure 10) in blends with PC₆₁BM (B7).^[225] N8 was found to

give rise to superior device performance, with an EQE of 23% at −2 V and a FWHM of the absorption peak being around 100 nm (if one was to use a cut-off filter at 400 nm) for a device with the structure: ITO/PEDOT:PSS/N8:B7/Al. However, the PC₆₁BM again contributed to a small but unwanted photoresponse at longer wavelengths. As previously mentioned, although the fullerenes are excellent electron acceptors, their absorption outside the desired spectral window generally leads to a reduction in color selectivity (due to the photoresponse from the fullerene).^[136]

3.3.1.2. Green-sensitive OPDs: Green-sensitive OPDs have been reported using a small number of chromophores including rhodamine, quinacridone, perylene diimides, subphthalocyanines and ketocyanines. Two major challenges associated with shifting from blue to green sensitive OPDs are: (i) the need to prevent blue light absorption (which is difficult to avoid due to electronic transitions resulting from higher excited states in almost all organic molecules) and (ii) ‘broadening effects’, which extend the spectral response, and are caused by intermolecular interactions of the chromophores in the solid state.

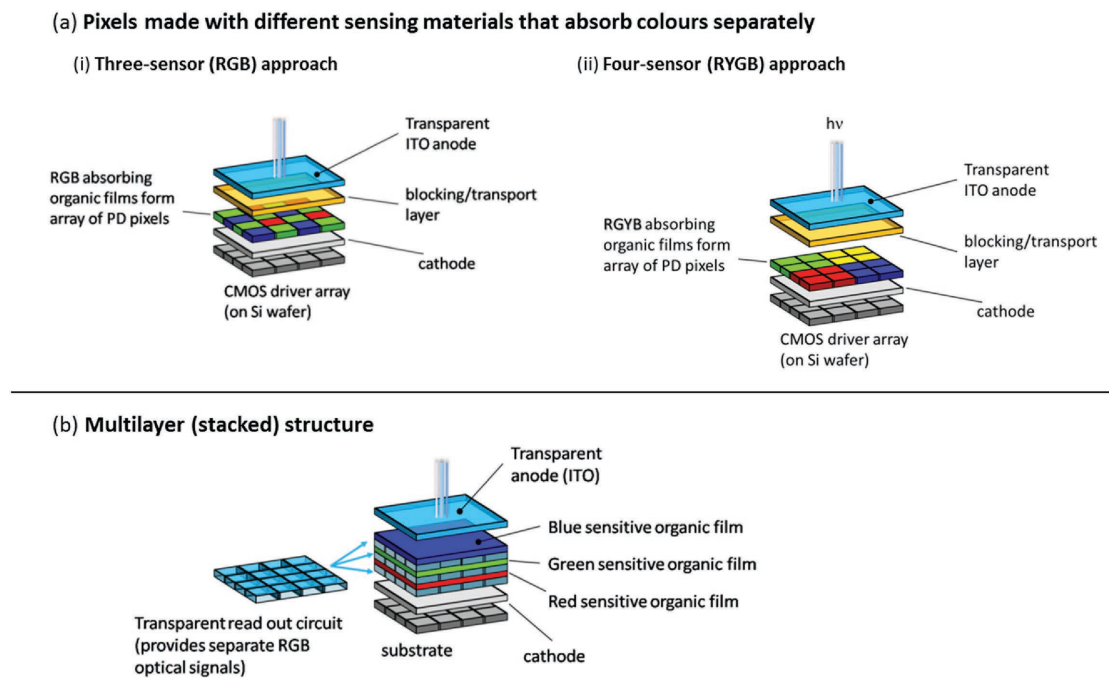


Figure 9. (a) pixels made with different sensing materials that absorb colors separately, i) three different organic materials that each respond to one of the primary colors of the spectrum (RGB) constitute the pixels for an image sensor (no color filters or any external color separation is applied); ii) four different materials are used (RYGB); (b) a multilayer (stacked) structure, in which the blue-, green- and red-sensitive organic semiconductor layers span the width of the image-sensing device.

Ketocyanines are a family of dyes that at least in part meet the requirement that absorption at wavelengths shorter than the main band is small.^[118] Jansen-van Vuuren et al. found that encapsulating a ketocyanine chromophore (**N10**, Figure 11a) with dendrons (dendrimers **N11** – **N13**) reduced the inter-chromophore interactions, resulting in a narrowing of the FWHM of the solid-state absorption profiles (Figure 11b).^[118b] The FWHM of the absorption profile was reduced from 117 nm to 89 nm when biphenyl dendrons were attached at the α -N of

the ketocyanine (compound **N12**) (Figure 11 b). From the same figure, it can be seen that the absorption profile was influenced by the position of attachment of the dendrons to the chromophore (**N11** cf. **N12**). In OPD devices, when non-dendronized ketocyanine **N10** was blended with PC₆₁BM (**B7**), the device had a narrow absorption profile (narrower than when pristine), but the spectral photoresponse of the **N10:B7** OPD was almost 200 nm. In comparison, when dendrimer **N12** was blended with **B7**, the device had an EQE of 8% at -1 V and a FWHM

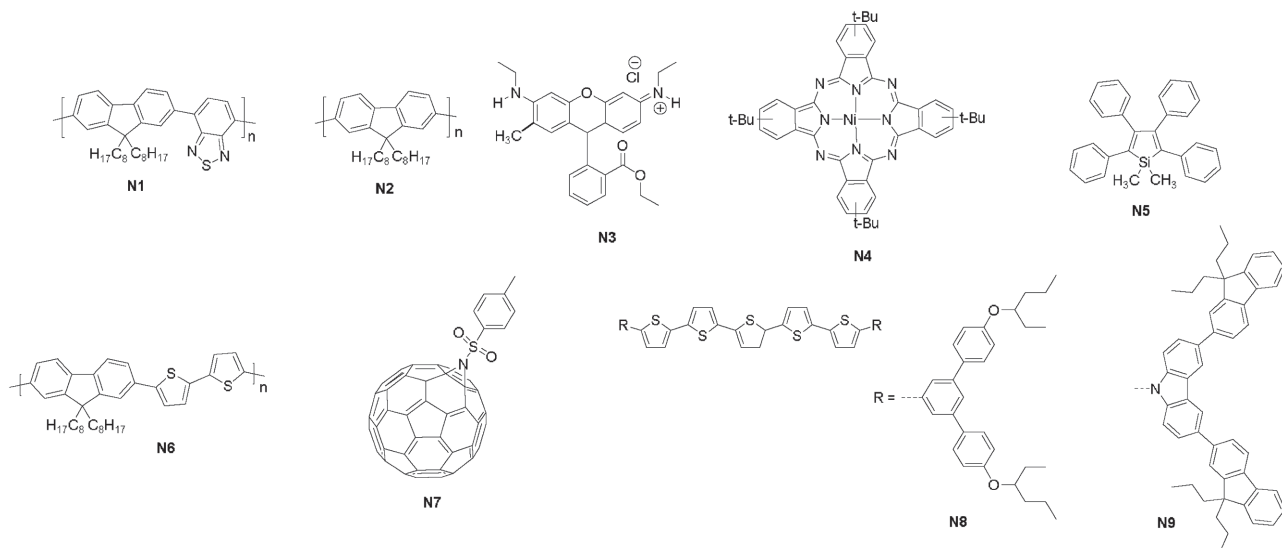


Figure 10. Chemical structures of materials used in fabricating filter-less OPDs. Blue-sensitive OPDs were constructed with narrowband (**N**) materials **N1**, **N2** and **N5** – **N9**.

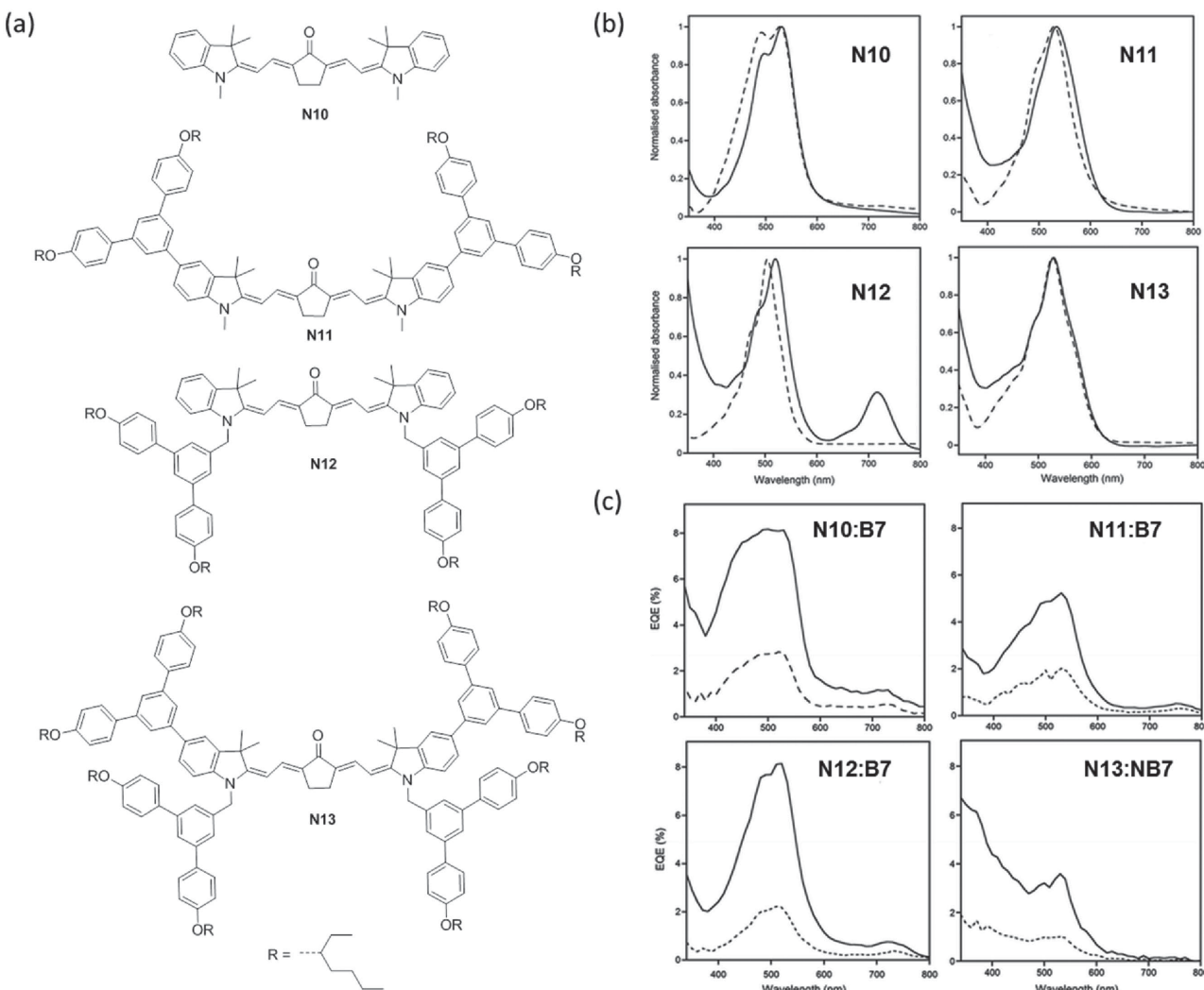


Figure 11. (a) Chemical structures of green-sensitive ketocyanine chromophore (**N10**) and dendrimers (**N11-N13**); (b) absorption profiles of films of ketocyanine compounds: pristine (dotted line) and in blends with PC₆₁BM, **B7** (solid line); (c) EQEs of ITO/PEDOT:PSS/**N10-N13:PC₆₁BM(B7)**/Al at 0 V (dotted line) and at -1 V (solid line). Figure adapted with permission.^[118b] Copyright 2013, The Royal Society of Chemistry.

of the photoresponse of 130 nm (Figure 11c). It is important to note that even with this spectral width, the **N12:B7**-based device still provides up to 60% color recognition accuracy for color imaging applications.^[151] However, the key point is that the EQE of all the devices had a component caused by the direct absorption of light by the fullerene (between 400–450 nm); in the case of **N12**, the blend with PC₆₁BM also has a peak at \approx 730 nm, which was proposed to arise from a charge-transfer complex that is formed in the solid-state blend.^[226]

By doping 30 wt% of R6G (**N3**) into PFO (**N2**), Fukuda et al. fabricated a green-sensitive OPD with an EQE of 33% at -34 MV/m (thickness of **N3** = 130 nm) and an absorbance FWHM of \approx 95 nm.^[227] The spectral photoresponse (EQE) of the device was unfortunately not provided. The effect of doping four different silole derivatives (as visible-blind electron accepting materials) within a film of **N3** was subsequently investigated. The most favorable EQE and FWHM were achieved when **N3** was blended with 1,1-dimethyl-2,5-bis(*N,N*-dimethylaminophenyl)-3,4-diphenylsilole), but was only 0.3%

(at -30 MV/m), respectively at a λ_{max} of 560 nm.^[228] Neither the absorption spectrum nor the EQE spectral photoresponses were shown for the blends so the FWHM could not be ascertained.

Lee et al. (Samsung Electronics) took a different but effective approach to obtaining a narrow green-sensitive photoresponse, which involved a donor–acceptor combination in which the absorption spectra of the two chromophores overlapped in the green region.^[105,229] Two sets of donor and acceptor materials were then used to construct four different devices: the donor materials employed were boron sub-phthalocyanine chloride (**N14**) and *N,N*-dimethyl quinacridone (**N15**), whilst the acceptor materials were pentafluoro-phenoxo-substituted boron sub-phthalocyanine chloride (**N16**) and a di-*n*-butyl-substituted dicyanovinyl terthiophene (**N17**), although **N14** was also trialled as an acceptor (due to its lower LUMO level) (Figure 12a and Figure 12b). Four OPDs were fabricated in the configuration ITO/MoO_x/blend(A – D)/Al (where MoO_x = molybdenum oxide, typically used as a ‘hole-collection, electron-blocking layer’) by thermal evaporation with blends (A-D) being A (**N14/N16**), B

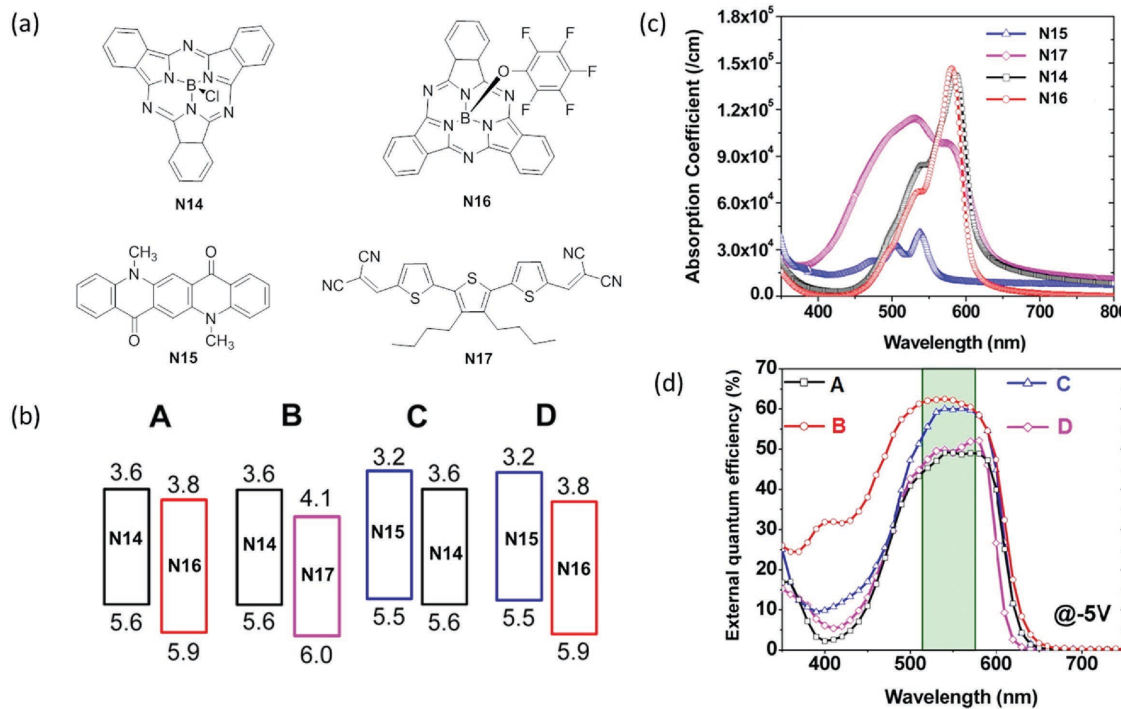


Figure 12. (a) Chemical structures of green-absorbing ‘donor’ materials **N14** and **N15** and green-absorbing ‘acceptor’ materials **N16** and **N17** (**N14** also acts as an ‘acceptor’ in device C); (b) reported energy levels of the four green-absorbers in devices A–D; (c) absorption spectra of **N14** – **N17** (as pristine films); (d) EQEs of devices A–D (at –5 V). b) and c) adapted with permission.^[105] Copyright 2013, American Chemical Society).

(N14/N17), C (N15/N14), and D (N15/N16) (see Figure 12b). The light absorption and optoelectronic properties of the OPD blends were dependent on the materials combinations, with device B demonstrating the highest EQE (63% at –5 V), but with a large FWHM of 211 nm, whilst C demonstrated an EQE of 60% (at –5 V) with a spectral photoresponse FWHM of 132 nm (Figure 12c). Importantly, the EQE photoresponse of devices A, C, and D showed a markedly reduced blue-light component in comparison with device B, although no explanation was provided.

Another example of a green-absorbing molecule is that developed by Meiss et al., which was 2,3,10,11-tetra-*n*-butyl-1,4,9,12-tetraphenyl-diindeno-[1,2,3-*cd*:1',2',3'-*lm*]perylene (‘Bu₄-Ph₄-DIP’) (N18, Figure 13a).^[230] Devices fabricated with an ‘n-i-p’ configuration containing BHJ blends of N18 with C₆₀ (N19) demonstrated that the donor–acceptor ratio and substrate heating during deposition strongly influence the photoresponse of the devices. The optimal device (N18:N19 = 1:1 by weight) displayed an EQE of 36% at $\lambda_{\text{max}} = 570$ nm with a FWHM of ≈120 nm (Figure 13 b), but there was still a significant photoresponse in the blue. Lim et al. have developed an organic photoconductor based on a solution-processable green-sensitive tri-*iso*-propylsilyl ethynyl anthracene derivative (N20, Figure 13c) as a single crystal (formed by slow evaporation of chloroform solutions).^[231] The crystal was placed on a “Cytop” (an amorphous transparent fluoropolymer with excellent insulating properties^[232]) coated SiO₂ dielectric on a highly n-doped Si substrate and gold source and drain electrodes were evaporated on top of the crystal. The device demonstrated a responsivity >10 A/W and specific detectivity of the order of 10¹¹ J,

attributed to a “gain-generation mechanism by systematic analysis of the photocurrent behavior as a function of the interfacial properties, optical power and applied bias”.^[231] The UV–Vis absorption spectra and responsivity of the device as a function of illuminated light wavelength is shown in Figure 13(d): the FWHM of the responsivity was >150 nm.

Lastly, Lamprecht et al. showed that it was possible to realize a green-sensitive OPD using *N,N*-diperfluorophenyl-3,4,9,10-perylenetetracarboxylic diimide (DFPP, N21) as an n-type material with a transparent (visible-blind) hole accepting material, *N,N*-di-[(1-naphthalenyl)-*N,N*-diphenyl]-1,1'-biphenyl)-4,4'-diamine (NPD, N22) in a bilayer configuration.^[228] The chemical structures of N21 and N22 and their separate absorption spectra are shown in Figure 14a and Figure 14b, respectively. A device with the structure glass/Ormosil/Cr/Au/NPD(N22)/DFPP(N21)/Ag was fabricated (Figure 14c (i)) and its spectral response is shown in Figure 14f: the EQE was low (≈2%, the operating voltage was not provided), but the FWHM of the green device was a respectable 90 nm.

3.3.1.3. Red-sensitive OPDs: A red-sensitive OPD has been demonstrated using a bilayer device comprised of *N,N*-di-3-pyridylperylene-3,4:9,10-bis(dicarboximide), MPP (N23), which absorbs the incoming blue and green photons, and a bottom layer of copper-phthalocyanine (CuPc, N24), which is the red-sensitive component (see Figure 14).^[233] The excitons were generated in this device within a 10 nm region at the junction of the two layers, and a low EQE of ≈2% was achieved (Figure 14f) with a FWHM of ≈110 nm. The interesting aspect of this approach is that the N23 layer did not generate any

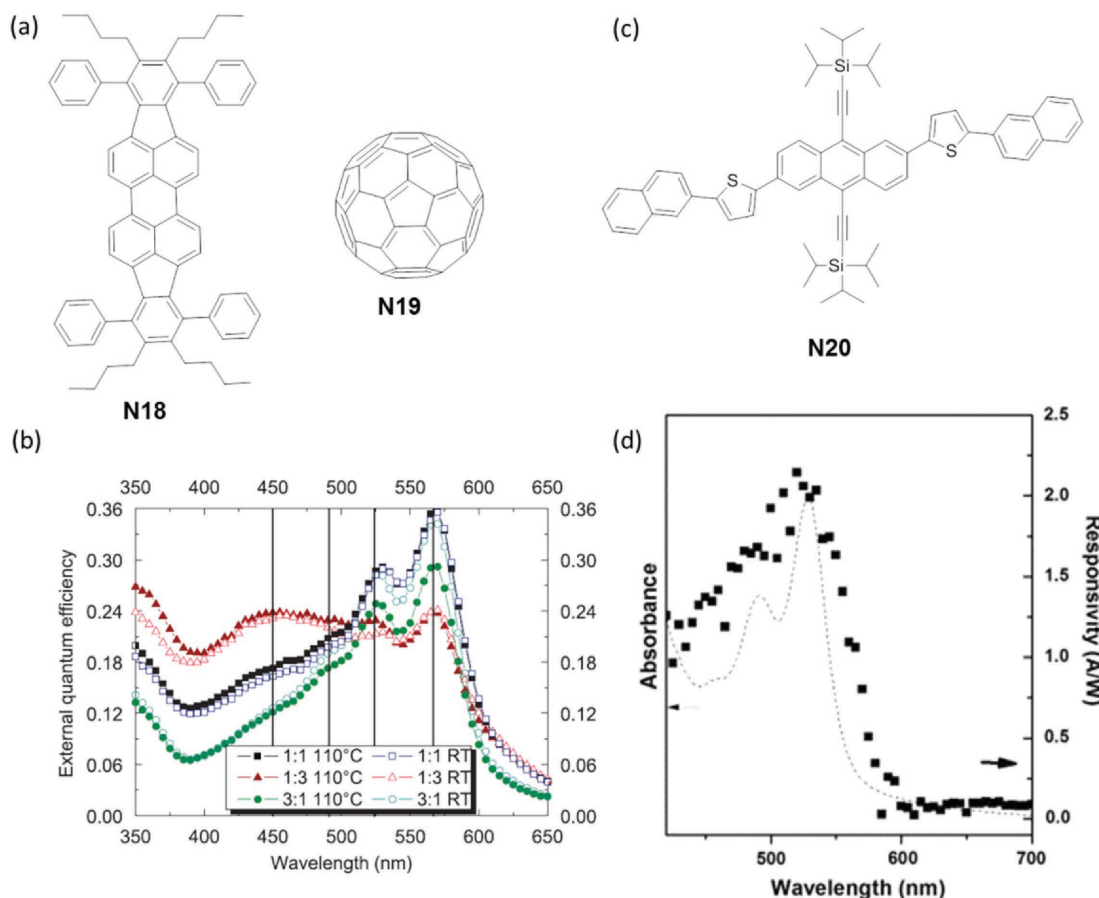


Figure 13. (a) Chemical structure of compounds **N18** and **N19**; (b) EQE of the **N18:N19** devices plotted against the wavelength; each curve represents a different mixing ratio of Bu4-Ph4-DIP (**N18**):C₆₀(**N19**); (full symbols: deposited on heated substrate; empty symbols: substrate at room temperature). The lines show the absorption maxima of **N18** and **N19**. (c) chemical structure of green absorber **N20**; d) absorption spectrum for **N20**. b) Reproduced with permission.^[230] Copyright 2011, Elsevier; (d) reproduced with permission.^[231] Copyright 2014, Elsevier.

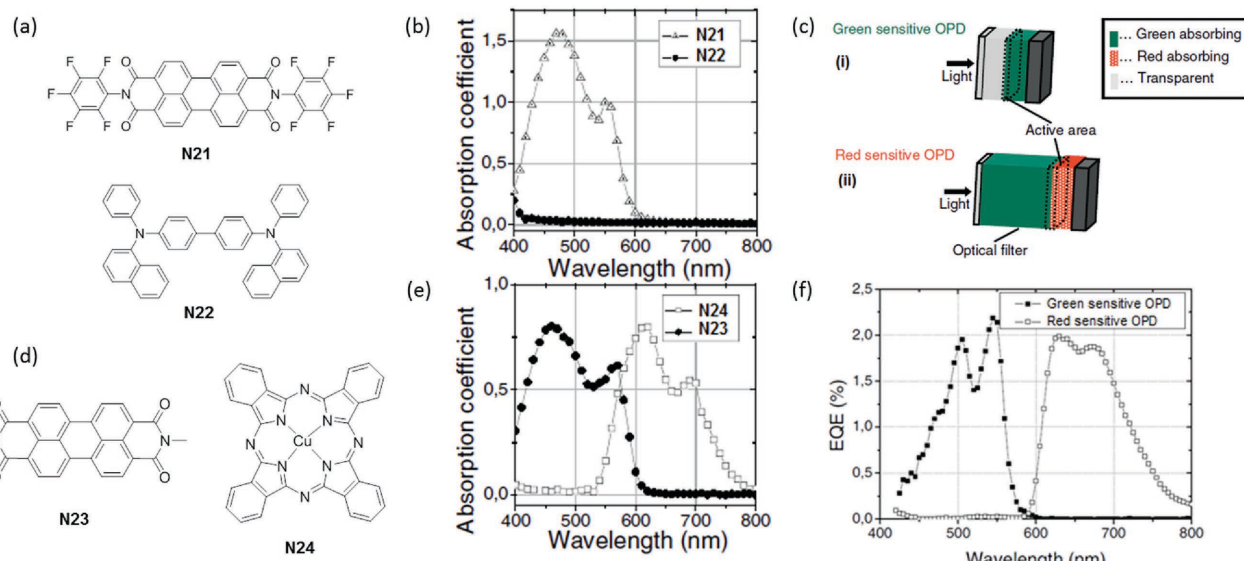


Figure 14. (a) Chemical structures of green-absorbing DFPP (**N21**) and transparent p-type NPD (**N22**); (b) the absorption profiles of **N21** and **N22** (as thin films); (c) OPD device architectures; (d) chemical structures of green-absorbing **N23** and red-absorbing **N24**; (e) the absorption profiles of **N23** and **N24** (as thin films); (f) the EQE photoresponse of the green-sensitive (**N21/N22**) and red-sensitive (**N23/N24**) OPDs. Reproduced with permission.^[232] Copyright 2008, John Wiley & Sons.

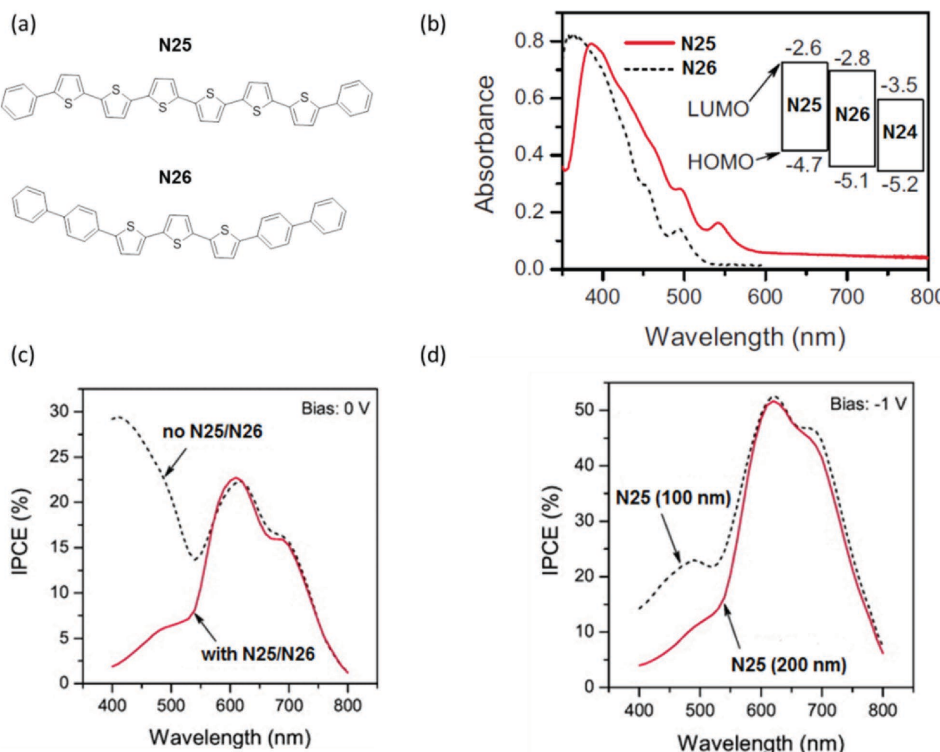


Figure 15. (a) Chemical structures of N25 and N26; (b) absorption spectra of films of N25 (P6T) and N26 (BP3T) and energy levels of N25, N26 and red-absorbing N24; (c) IPCE spectra of the BHJ devices demonstrating the difference made to the spectral profile by including a layer of N25/N26; (d) IPCE spectra of the BHJ devices with a 100 nm or 200 nm thick N25 layer. b), c) and d) adapted with permission.^[235] Copyright 2010, AIP Publishing LLC.

photoresponse, which led to selectivity in the red. Given the long wavelength absorption spectra of the phthalocyanine, it is not surprising that there have been further reports of their use in OPDs.

A series of three red-sensitive OPDs consisting of differing regioisomeric ratios of nickel-tetrakis(tert-butyl)phthalocyanine (N4, Figure 10) were fabricated in the configuration: ITO/PEDOT:PSS/N4(A, B or C)/LiF/Al.^[234] As might be expected for neat films, the EQEs were low, with the best reported for device 'A' (0.8% at -3 V). Furthermore, the FWHM was reasonably large (\approx 130 nm).

Higashi et al. employed the same approach taken by Lampricht et al. to circumvent the problem of undesired blue and green light absorption by including additional blue/green-absorbing and exciton-blocking layers in a red-sensitive device, with CuPc (N24) acting as the red absorber in this case (and C₆₀ (N19) as the acceptor).^[235] The materials used to construct these layers included the p-type semiconductors: α,ω -diphenyl-sexithiophene (P6T, N25) and α,ω -bis(biphenyl-4-yl)-ter-thiophene (BP3T, N26) (see Figure 15a). The active layer was comprised of CuPc (N24) blended with C₆₀ (N19) and the purpose of the layer of N25 was to absorb incident blue and green light (Figure 15b), whilst the layer of N26 was expected to block energy transfer from N25 (i.e., excitons formed on N25) to the N24:N19 layer due to its larger optical gap (Figure 15b, inset). In devices constructed as planar heterojunctions of N24 and N19 (with and without the additional layers), it was found that although the dark and photocurrent were reduced due to the additional layers (making the device thicker), clear rectifying behavior was

observed. The external quantum efficiency of the device with the extra layers showed reduced blue-light sensitivity whilst maintaining a spectral response to red light, in comparison with the device made without the layers (Figure 15c). However, in a device in which N24 and N19 were blended together, the thickness of the layer of N25 was found to affect the spectral contrast (SCR, defined as the ratio of the quantum efficiency at 620 and 450 nm): doubling the thickness of the N25 layer to 200 nm resulted in a quantum efficiency of 57% at 650 nm and -1 V, an SCR of 7.4 and a FWHM of \approx 200 nm in the red (Figure 15d).

In 2000, Forrest et al. demonstrated a 32-layer OPD consisting of CuPc (N24) and 3,4,9,10-perylene-tetracarboxylic bis-benzimidazole (PTCBI, N27) that was designed for a high-speed response under irradiation of red laser light^[124] (see Figure 16). The EQE and FWHM at a bias greater than -10 V were \approx 75 % and \approx 300 nm, respectively. In an effort to reduce the number of layers whilst retaining the performance metrics, Kaneko et al. expanded this work to multilayer red-sensitive OPD devices consisting of titanyl phthalocyanine (N28) and fluorinated zinc phthalocyanine (N29) with only five alternating layers and using BCP (N30) as the exciton blocking material, thus maintaining a constant overall photoactive active layer thickness.^[236] The film absorption spectra of N28 and N29 are shown in Figure 16b: it can be seen that the FWHM for each profile are broad: 250 nm and 260 nm, respectively. The configuration of the 10-layer (i.e., N28/N29 counting as two layers) OPD devices was ITO/[TiOPc(N28)/F₁₆ZnPc(N29)]₅/BCP(N30)/Ag with the PCE at 0 V being 0.02%. The spectral photoresponse was not shown so the FWHM could not be determined. Although the sensitivity

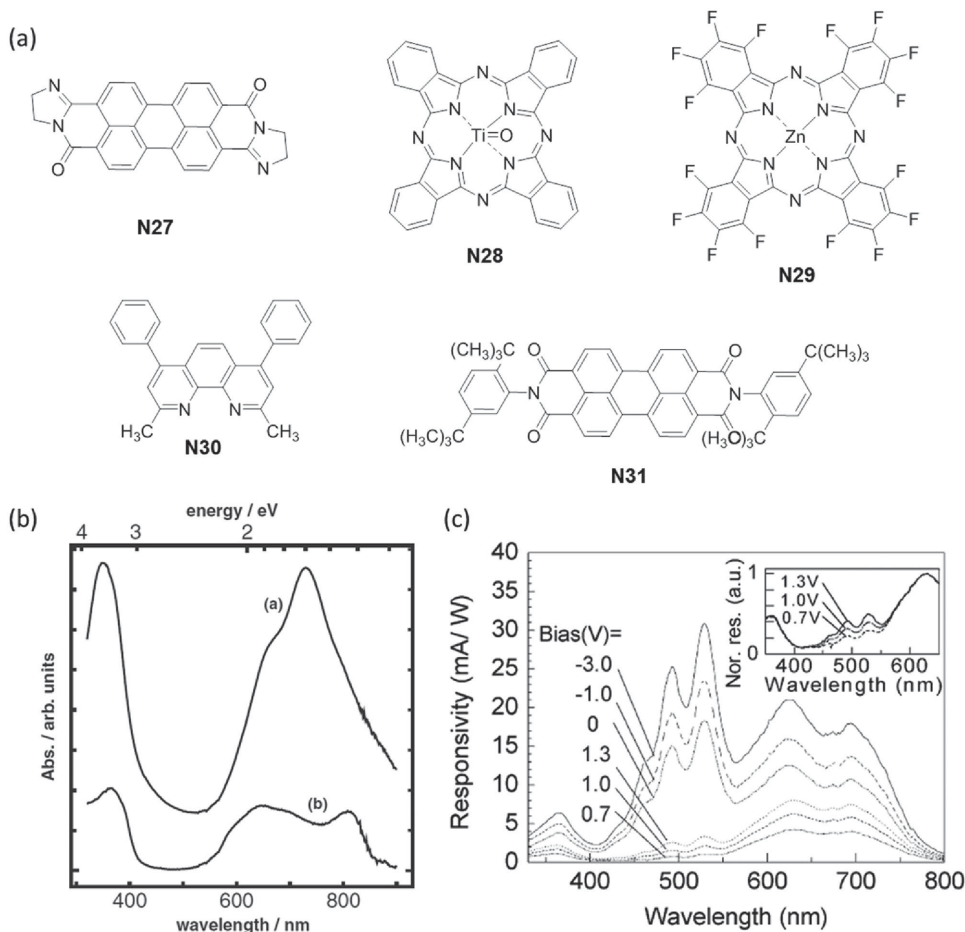


Figure 16. (a) Chemical structures of **N27-N31**; (b) film absorption spectra of **N28** line (a) and **N29** line (b); (c) photocurrent spectra of BHJ devices of **N28** and **N29** under a range of biases. b) Reproduced with permission.^[236] Copyright 2003, Japan Society of Applied Physics; (c) reproduced with permission.^[237] Copyright 2006, IEEE.

of the device was significantly reduced, the ease of fabrication had been enhanced. Building on these results, Morimune et al. (in the same group) then developed a single-layer device consisting of a blend of CuPc (**N24**) with n-type *N,N'*-bis(2,5-di-*tert*-butylphenyl)-3,4,9,10-perylenedicarboximide (BPPC, **N31**), in a device structure of ITO/**N24:N31/Au**.^[237] Figure 16c shows the photocurrent spectra for the device under a range of biases (both forward and reverse). It is evident that under both forward and reverse biases that a broad photoresponse is observed, which is not adequate for realizing a red-sensitive OPD, although the red SCR is somewhat more favorable under a low forward bias.

3.3.1.4. Summary of Materials-based Approaches: In the previous sections, the focus has been on the FWHM response of the OPDs comprising materials designed to absorb specific wavelengths. However, the reports also include a range of other OPD characteristics (e.g., the responsivity, LDR, speed of response and detectivity), although such FOM are not always reported in a consistent fashion. Some of the further metrics of the OPD devices are summarized in Table 3 and for comparison the performance metrics of the separate RGB components of a silicon photodiode (Hamamatsu **S7505-01**)^[246] are included.

The silicon photodiode employs a color filter array to achieve color selectivity in the B, G and R.

In summary, although significant strides towards blue, green, and red-sensitive OPDs have been achieved, the major challenge associated with the materials-only approach is obtaining electron donor and acceptor compounds that collectively (in a BHJ configuration) exhibit a narrow (i.e., a FWHM \leq 100 nm) that is blind outside the spectral window and with a predictable spectral photoresponse (i.e., λ_{max}) in the solid-state. Several factors complicate this approach including the acceptor material absorbing light outside of the profile of the donor material (which occurs with the commonly used fullerene acceptors due to their broad absorption), the broadening and red-shifting of the spectral response of the donor material in the solid state (compared to in solution), and the spectral response of the donor changing when it is blended with the acceptor. The three main materials strategies that have been pursued to overcome these challenges include: (i) the isolation of the light-absorbing chromophores so as to reduce inter-chromophore interactions through the use of either doping the chromophore molecule within a polymer or by encapsulating the chromophore within a dendritic architecture; (ii) the control of the spectral response through careful choice of the electron accepting material, so

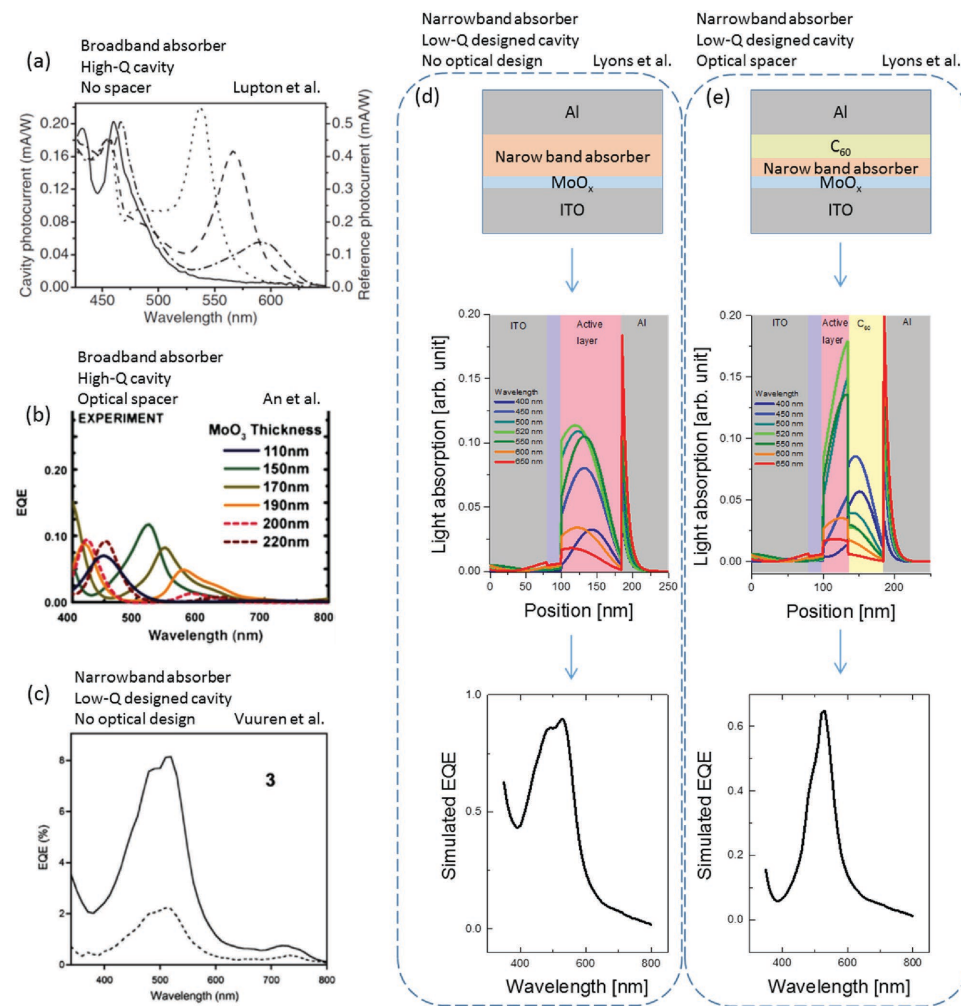


Figure 17. (a) Utilizing semitransparent electrodes enhancing the Q-factor of the photodiode cavity containing broadband absorbers. No optical spacer is used and changing the active layer thickness results in tuning the spectral window. The contribution of fullerene at wavelengths <550 nm is significant; (b) utilising semitransparent electrodes in photodiodes made of broadband absorbers along with optical spacers of different thicknesses can tune the spectral window with less undesired contribution from fullerene absorption; (c) use of a narrowband green absorber in a low Q-factor photodiode (ITO/active layer/metal electrode) with no optical spacer; (d) device structure, optical field distributions, and simulated external efficiency in photodiodes with a narrowband green absorber:PC₇₁BM active layer using a low Q-factor cavity and no optical spacer. The contribution of fullerene in the photoreponse is present but undesired. Utilising a C₆₀ optical spacer in this design; (e) optical modelling showing how by using the optimum active layer and spacer thicknesses, the undesired fullerene contribution can be minimized. The resultant EQE is ultimately narrow with minimum contribution from the fullerene. a) Reproduced with permission.^[119] Copyright 2003, John Wiley & Sons; (b) reproduced with permission.^[121] Copyright 2009, Elsevier; (c) reproduced with permission.^[118b] Copyright 2013, Royal Society of Chemistry; (d) and (e) were reproduced with permission.^[162] Copyright 2014, Elsevier.

as to absorb either the same wavelengths of light as the donor material or to be transparent over the visible spectrum, and (iii) the use of stacked devices that consist of additional layers containing materials able to absorb light complementary to the desired wavelengths; e.g., blue-green light absorbed to realize a red-responsive OPD. There is still significant scope for the development of materials-based approaches for controlling the position and FWHM of the OPD response and the EQE.

3.3.2. Device Optics Engineering

OPDs normally consist of a thin (≈ 100 nm) active layer sandwiched between two partially reflecting electrodes. One of the

electrodes is normally chosen to be completely reflective to increase the absorption within the active layer and the other one is chosen to be transparent in order for the light coupling into the device to be efficient. As such, organic photodiodes are 'low finesse' cavities where the light absorption in the active layer is governed by the cavity mode(s), which provides an opportunity for tuning the spectral response.^[247] Lupton et al. used semitransparent electrodes to enhance the Q-factor of a cavity consisting of broadband absorbers and were able to tune the maximum sensitivity wavelength (λ_{\max}) by changing the active layer thickness (changing the cavity length), although the FWHM was poor due to the fullerene response^[119] (Figure 17a). An et al. reported using a semi-transparent electrode approach to fabricate narrowband OPDs by using a broadband absorbing

bilayer with MoO_x as both hole-transport layer and optical spacer.^[121] A narrow spectral response (FWHM ≈ 100 nm) was achieved for a device with the structure Al/MoO_x/CuPc(N24)/C₆₀(N19)/BCP(N30)/Ag. A key result of the work of An et al. was that by increasing the optical spacer thickness it was possible to tune in more than one mode within the cavity and as a result a bimodal response could be obtained, although this of course affects the monochromaticity (Figure 17b). However, a general challenge faced by Q-factor enhanced cavities is that the proportion of the light coupled into the device decreases the EQE and they have a strong angular dependent spectral response.

Lyons et al. reported another approach to further narrow the spectral bandwidth for a green absorbing OPD that combined the ‘materials’ and ‘microcavity’ approaches.^[162] As discussed in Section 3.3.1, narrowband donors need to be blended with acceptors, and in the case of Lyons et al. narrow green absorbing ketocyanine-based donors (Figure 17c) were blended with a fullerene acceptor that gave an undesired blue response. The blue response was suppressed by employing C₆₀ as an optical spacer layer, which also acted as a hole blocking layer. Figure 17d and Figure 17e demonstrate the structure, photo-carrier distribution profile and predicted EQE of an OPD consisting of a narrowband active layer with and without the C₆₀ optical spacer.

Two final examples are given with potential applications in colorimetry and artificial vision development. Antognazza et al. also reported narrowband OPDs by varying the thickness of the P3HT(B1):PC₆₁BM(B7) photoactive layer and exploiting the filter effect of the optical absorption.^[51] Gautam et al.

demonstrate single-pixel, single-polymer based OPDs as tri-color sensors: the spectral response of the OPD depends on the “characteristic polarity and temporal profile of the photocurrent signal” of the active polymer layer in response to the various incident colors.^[248]

3.3.2.1. Pixelated Multilayer (Stacked) OPD Color Imaging: As previously discussed, Higashi et al. and Lamprecht et al. introduced extra layers into the OPD devices to absorb wavelengths outside the desired spectral window to give a narrower response. An extension of the concept is to make multilayer (stacked) OPD sensors for imaging, which is a similar approach to that used in the Foveon X3^[42] (Figure 18a), with the work largely built on the seminal work by Tang.^[249]

NHK (Nippon Hoso Kyokai – the Japan Broadcasting Corporation^[250]) have worked extensively on developing this concept. Their preliminary work (2003) involved the development of a stacked sensor that employed three organic semiconductor films - each sensitive to only one of red, green, and blue light, in order to separate the incident light into colors according to the depth of the image sensor.^[251,252] The sensor was therefore designed with the blue-sensitive layer on the top, the green-sensitive layer in the middle and the red-sensitive layer on the bottom of the stack, with transparent readout circuits separating the three layers (Figure 18b). The chemical structures of the materials employed [blue: coumarin 6, ‘C6’ (N32)-doped poly(*n*-hexyloxyphenyl)phenylsilane (N33) (C6:PHPSS); green: rhodamine 6G, ‘R6G’ (N3)-doped poly(methylphenylsilane) (N34) (R6G:PMPS); red: zinc phthalocyanine (N35)/aluminium

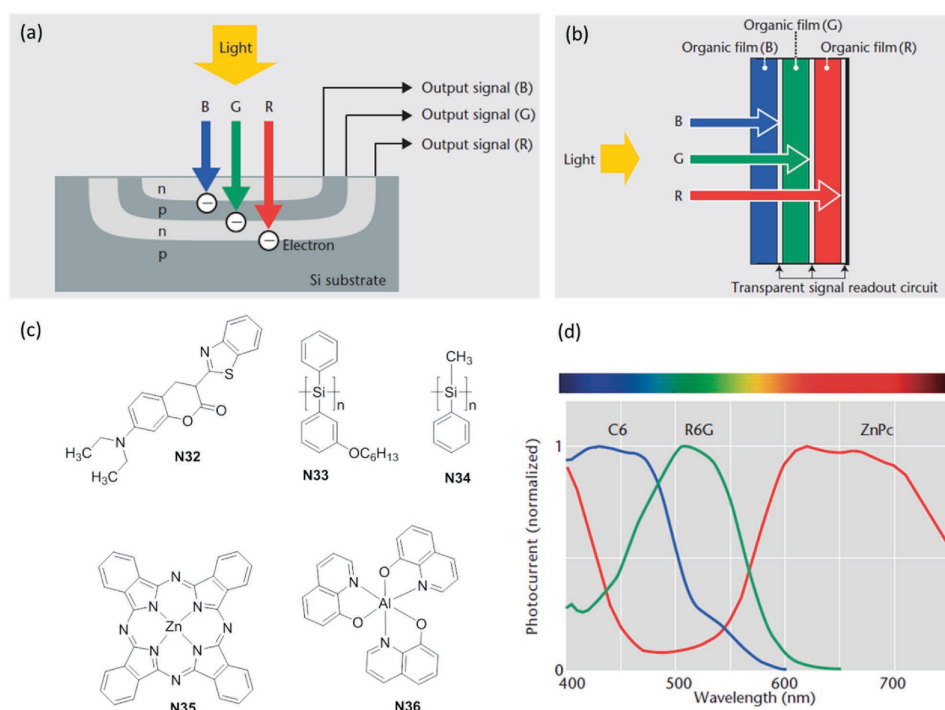


Figure 18. (a) Cartoon showing the basic principle of color recognition within a Foveon X3® sensor; (b) schematic showing the basic architecture of an OPD-based stacked device; (c) chemical structures of materials N32 – N36; (d) spectral photoresponses of each of the B-, G- and R-sensitive OPD layers a), (b) and (d) reproduced with permission.^[253] Copyright 2012, NHK STRL.

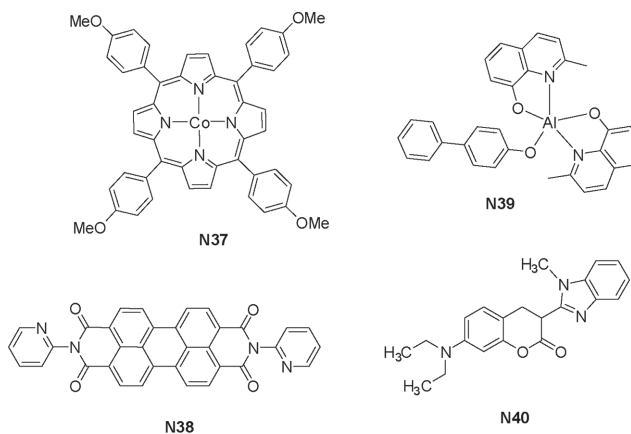


Figure 19. Chemical structures of materials N37 – N40 (used in fabricating multilayer devices).

tris(8-hydroxyquinolinato) (N36) bilayer (ZnPc/Alq₃) are shown in Figure 18c. In a preliminary study, separate OPDs containing the red, green, and blue-sensitive films were fabricated and analysed. The photo-response spectra of the separate OPDs (Figure 18d) showed that there would be some resolution of the colors, although the FWHM of all the colors was greater than the 100 nm required for illuminant-independent color discrimination. For example, the red OPD had a FWHM >200 nm and additional undesired photocurrent was generated in the violet/blue region (400–450 nm) (Figure 18d). Furthermore, the IQEs of the OPDs were low: for the blue- (N32:N33), green- (N3:N34) and red-sensitive (N35/N36) OPDs, the IQEs were found to be 0.7%, 0.8% and 20%, respectively.^[252] The higher

IQE for the red OPD was attributed to its broadened spectral photo-response.

A more selective photo-response in the red was obtained when the Alq₃ (N36) was replaced with BCP (N30, Figure 15),^[254] with Satoshi et al. demonstrating a peak quantum efficiency of 14.7% under 620 nm irradiation with a bilayer ZnPc/BCP film and FWHM of 200 nm. However, higher selectivities and sensitivities (EQEs) were, in general, required for the blue- and green-OPDs.

Subsequently, Aihara et al. fabricated a blue-absorbing film comprising a *meso*-tetra(4-methoxyphenyl)porphyrinato cobalt(II) complex (N37)/Alq₃(N36)/BCP(N30) trilayer; this was reported to have an improved EQE of 20% at a field of 2.0×10^6 V/cm.^[255,256] The chemical structure of N37 is shown in Figure 19.

Hokuto et al. (NHK) fabricated a prototype color sensor consisting of three OPDs [Blue: Co-TPP (N37)/Alq₃ (N36); Green: N,N'-dimethylquinacridone (DMQA, N15)/Alq₃ (N36); Red: ZnPc (N35)/Alq₃ (N36)] in a stacked structure.^[145] An interesting feature was observed: while the quantum efficiencies of the individual OPD devices (5–8%) were still insufficient to meet imaging requirements, the light selectivity was shown to be markedly improved in the stacked structure. That is, the FWHMs of the absorptions were narrow due to parasitic absorption of each of the layers as the photons penetrated through the image sensor (Figure 20a).

The same group then developed a stacked device in which a transparent zinc oxide (ZnO) thin-film transistor (TFT) was incorporated between each layer to read out the signals generated within each OPD (Figure 20b).^[48,257] In a preliminary study, only green [DMQA (N15)/Py-PTC (N38)] and red

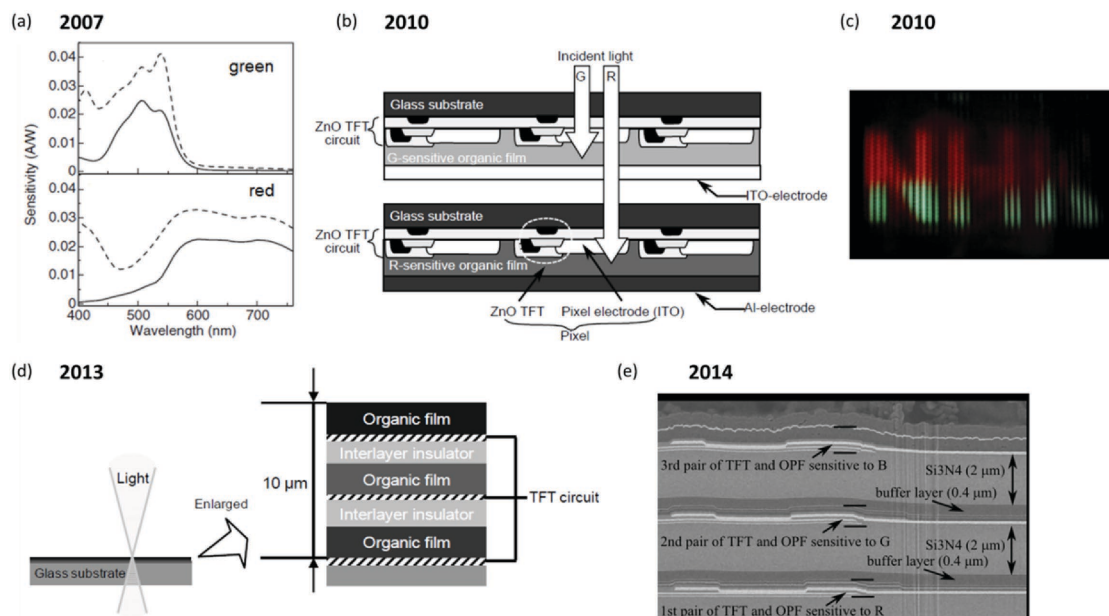


Figure 20. (a) A comparison of output signal currents from single devices (dashed lines) and stacked structures (solid lines) for green and red devices; (b) a cross sectional view of an image sensor fabricated in which a ZnO TFT is inserted between each layer to read out the signals generated within each OPD; (c) a full-color reproduced image taken with the stacked sensor shown in (b); (d) cross-sectional view of a stacked organic image sensor; (e) three pairs of OPDs and TFTs separated by 2 μm-thick-Si₃N₄ and 0.4 μm-thick-buffer layers. a) Reproduced with permission.^[145] Copyright 2007, Japan Society of Applied Physics; (b) and (c) reproduced with permission.^[48] Copyright 2010, Society of Photo Optical Instrumentation Engineers; (d) reproduced with permission^[258] Copyright 2013, Society of Photo Optical Instrument Engineers; (e) reproduced with permission.^[259] Copyright 2014, IEEE.

[ZnPc (N35)/titanyl phthalocyanine (TiOPc, N28)] stacked devices were fabricated, and these had EQEs of 5% and 20% at -1 and -5 V, respectively.^[257] The authors followed up by fabricating a full image sensor consisting of a stack of green-sensitive [DMQA (N15)/Py-PTC (N38)] and red-sensitive [ZnPc (N35)/TiOPc (N28)/ aluminium(III) bis(2-methyl-8-quinolinolato) (*p*-phenylphenolato) 'Balq' (N39)] OPDs, each integrated with ZnO TFT read-out circuits,^[48] which gave satisfactory color separation and resulted in the recognition of a full-color image [Figure 20(c)]. The EQEs of the green- and red-sensitive OPDs were 5% and 20% (at -5 V), respectively.

In the next stage of development, NHK realised an image sensor consisting of 12,288 (128×96) pixels (for each of R, G and B), with each pixel measuring 100 × 100 μm².^[260] The stacked image sensor consisted of the following OPDs: blue-sensitive [coumarin 30 (N40):C₆₀ (N19)], green-sensitive [DMQA (N15)/Py-PTC (N38)] and red-sensitive [ZnPc (N35)/TiOPc (N28)] pixels. Despite variable EQEs for each of the OPDs (7.6% at -10 V, 7.0% at -3 V and 18% at -15 V, respectively), and relatively large pixels, the image sensor was able to produce a color image at 10 frames per second (fps), with a resolution corresponding to the pixel number. Replacing the ZnO with optically transparent indium-gallium-zinc-oxide (InGaZnO) as the TFT semiconductor in the imaging array and using ITO electrodes enabled an increase in frame rate to 30 fps that could produce clear video images at this speed,^[261] and is comparable to an equivalent silicon photodiode.^[262] However, the optics of such multilayer stacks are complex and in a final evolution the authors developed thin 10 μm inter-layer insulation films (epoxy-based) and TFT circuits between the organic films^[258] (Figure 20d). The authors noted that the solvent used in the wet-coating process to form the epoxy film damaged the organic films and so the epoxy-based insulators were replaced with silicon nitride (Si₃N₄) to give a three-layer stacked image sensor, i.e., consisting of B [Coumarin 30 (N40):C₆₀(N19)], G (quinacridone:N15) and R (ZnPc:N35) sensitive layers^[259] (Figure 20e).

In an effort to mimic the performance of conventional color film (based on negatives), workers at Fujifilm initially investigated the possibility of an image sensor which makes use of three stacked organic films (RGB) fabricated on a single pixel to replace the use of the green color filter.^[263] A prototype was constructed containing one organic layer, which comprised the green-absorbing dye DMQA (N15) whilst the red and blue light signals were obtained via filters in combination with silicon PDs. This hybrid configuration (i.e., a green OPD and red/blue Si PDs) was proposed to solve the pixel-signal circuit connection problems posed by the Foveon X3 image sensor since it is far simpler and thus able to reduce the production costs significantly.^[64] The rationale is that the blue and red light are transmitted through this layer and absorbed by silicon photodiodes beneath (each fitted with the appropriate color filter), whilst the green-sensitive OPD captures green light without the need for a color filter, enabling the capture of monochromatic images.^[47,263] Minimal variation of the spectral responses compared with simulated responses warranted further material and device optimization.^[264] Fujifilm has since partnered with Panasonic in developing this

idea further. The collaboration employs a hybrid approach in which an organic semiconductor-based photoactive layer is combined with CMOS circuitry.^[265] The result is a hybrid organic/CMOS image sensor that outperforms conventional image sensors in geometric 'fill factor' (enhanced light harvesting), dynamic range (88 dB) and a wider range of light incident angles (up to 60°) – producing better color reproducibility (without color mixing). The image sensor also provides greater lens design flexibility, which means that the overall camera size can be reduced. The two companies plan to promote this new technology – once it is fully developed – in a wide range of applications, e.g., security and vehicle cameras.^[265]

A key advantage of the layered OPD approach is that it has the potential to achieve a geometric fill factor of close to 100%, but electrical connection to the individual OPDs is complex and the overall reduction of light transmission through the layers limits the efficiency of the devices. Connecting the stacked layers so as to reduce crosstalk between the layers has always been a major challenge for multilayer image sensing devices.^[9] Lim et al. (Samsung) have been able to overcome this challenge with their initial research (introduced in an earlier section) culminating in the fabrication of a prototypical image sensor in which a green-sensitive OPD consisting of a blend of *N,N'*-dimethyl-2,9-dimethylquinacridone (DM-2,9-DMQA, N41 – see Figure 21a) with sub-phthalocyanine N14 was built onto a CMOS circuit with Si photodiodes fitted with color filters to absorb the blue and red light.^[242] The tetramethylated quinacridone N41 was selected over N15 as it demonstrated superior optoelectronic properties (i.e., it acts as a better p-type semiconductor) when in the solid state. Preliminary characterisation and optimization of BHJs fabricated with N41 and N14 (ITO/MoO_x/N41:N14/Al) demonstrated that the optimal structure consisted of a 70 nm-thick BHJ with the materials in a ratio of 1:1 (Table 3). To realise an organic-on-Si hybrid CMOS color image sensor, the G OPD was then constructed with transparent ITO electrodes on both sides of the sensor; i.e., as a transparent inverted OPD with the structure ITO/MoO_x:Al/N41:N14(1:1)/MoO_x/ITO. Although the EQE of this device was lower (41% at -3 V) than for the optimised devices (57% at -3 V), the EQEs of the RGB PDs were well balanced (i.e., of similar values) (Figure 21b). Of significance, the total number of charges generated per pixel was 1.6 times higher than in conventional inorganic systems. Figure 21c shows a tiled scanning electron microscopy (SEM) image of the bottom ITO arrays: the B and R color filters and the CMOS circuit with Si PDs are beneath the bottom ITO array. The G-sensitive OPD pixels demonstrate a linear response to illumination under a reverse bias of 3 V (Figure 21d) even when the temperature was gradually increased up to 140 °C, indicating their thermal stability (Figure 21e). The multi-stacked organic-on-Si hybrid CMOS color image sensor was then integrated within a camera and able to produce a full-color, 5-megapixel image (Figure 21f) – showing distinct B, G, and R colors and a stable white color (indicative of the balanced B, G, and R OPD EQEs). This is clearly a significant step in realizing color selective organic semiconductor-containing image sensors and the benefits that they are able to contribute towards high sensitivity imaging.

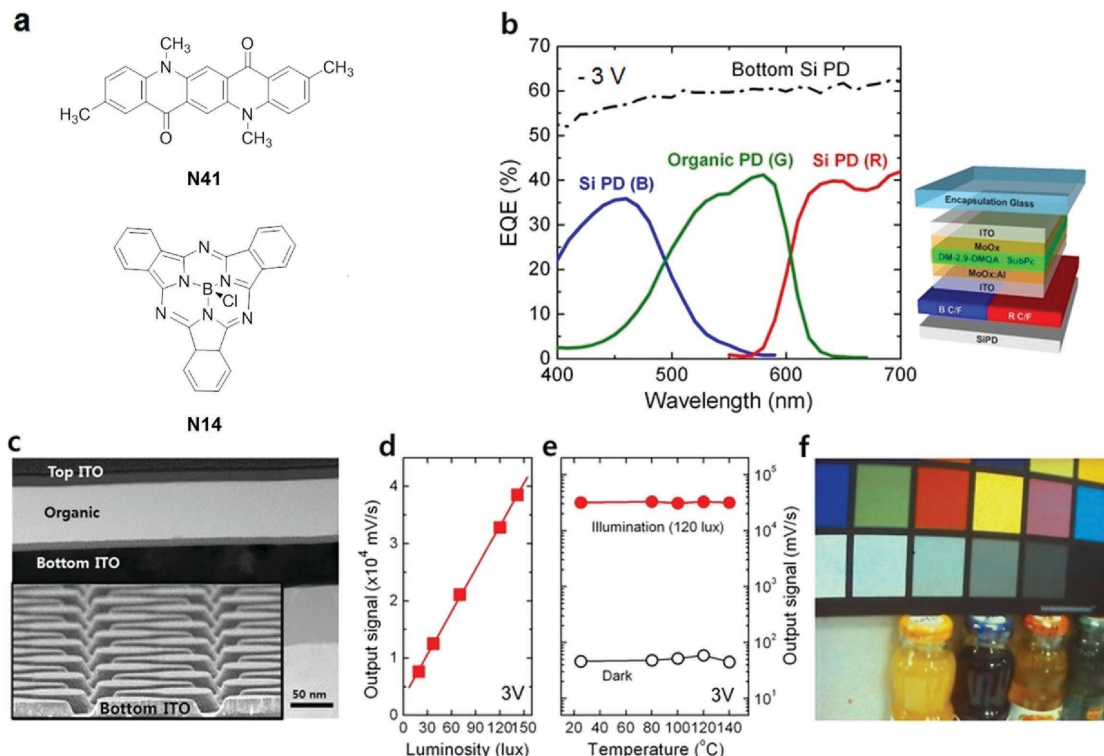


Figure 21. Development of organic-on-Si CMOS color image sensor by Lim et al. (Samsung): (a) Chemical structures of the green absorbers (donor N41 and acceptor N14) used to construct the green-sensitive OPD; (b) EQE curves of the Si B- and R-PDs and the G-OPD (measured at -3 V); (c) cross-sectional TEM and SEM (inset) images of the hybrid CMOS color image sensor array of G OPD pixels. The B and R color filters and the CMOS circuit with Si PDs are located under the bottom ITO array; (d) output signal as a function of light intensity of the G OPD pixels under a bias of -3 V; (e) thermal stability of the output signal under illumination at 120 lux and in the dark in G OPD pixels at a bias of -3 V; (f) a full-color image acquired using a camera integrated with a 5-megapixel organic-on-Si hybrid CMOS color image sensor. b-f) Reproduced with permission.^[242] Copyright 2015, Nature Publishing Group.

3.3.2.2. Manipulating the IQE to Achieve Narrowband Width: In the previous sections, the approach to narrowing the spectral response utilised thin active layers and in this section we discuss the use of thick films. Before doing so, it should be noted that the $EQE(\lambda)$ of any light harvesting device can be written as:

$$EQE(\lambda) = \eta_{\text{abs}}(\lambda) \eta_{\text{gen}} \eta_{\text{coll}} = \eta_{\text{abs}}(\lambda) \cdot \text{IQE}, \quad (11)$$

where η_{abs} corresponds to light absorption within the active layer, η_{gen} to the charge carrier generation quantum yield via exciton and charge transfer state dissociation,^[266] and η_{coll} to charge carrier collection efficiency by the electrodes. The flatness of the IQE in OPDs has been shown to originate from the energy independence of the generation efficiency^[267] and efficient charge transport in thin devices at reverse bias. It has been recently reported that the IQE can be spectrally narrowed to deliver OPDs with a defined spectral response.^[142] Armin et al. used thick PCDTBT(B3):PC₇₁BM(B4) and poly[2,5-(2-octyldodecyl)-3,6-diketopyrrolopyrrole-*alt*-5,5-(2,5-di(thien-2-yl)thieno[3,2-*b*]thiophene)] (DPP-DTT, B19):PC₇₁BM(B4) junctions ($\approx 2 \mu\text{m}$) in which the response was narrowed to the absorption onset of the BHJ layer (see Figure 22), leading to visible-blind and tuneable red and NIR narrow band responses [FWHM of $\approx 65 \text{ nm}$ ($\lambda_{\text{max}} = 680 \text{ nm}$; $EQE \approx 18\%$, -1 V) and $\approx 80 \text{ nm}$ ($\lambda_{\text{max}} = 705 \text{ nm}$, $EQE \approx 8\%$, -1 V), respectively].^[142] The use of thick

junctions had been previously proposed for broadband IR detection by Yang et al.,^[268] and further developed by Arca et al., but in these cases the OPDs utilised weak charge transfer absorptions.^[269] The ‘charge-collection narrowed’ (CCN) approach of Armin et al.^[142] utilises the fact that the short wavelengths are absorbed close to the transparent electrode with the generated charges not collected due to recombination processes while the longer wavelengths are absorbed throughout the bulk with the generated charges leading to a response. An extra advantage of the use of thick junctions is that the dark current (and hence noise) is dramatically reduced. This approach is material-agnostic and has recently been employed in realizing narrowband responses using solution processed^[270] and single crystal^[271] lead halide perovskite photodiodes.

4. Future Applications of OPDs

The major advances in image sensing technology since the first CCD image sensor was invented in 1970 and the first digital camera in 1975 are shown in Figure 23, along with some of the important landmarks in OPD-based imaging. It can be seen from Figure 23 that although the first OPD for color sensing was realized in 1981, it is only over the last two decades that the technological potential of OPDs has begun to be realized.

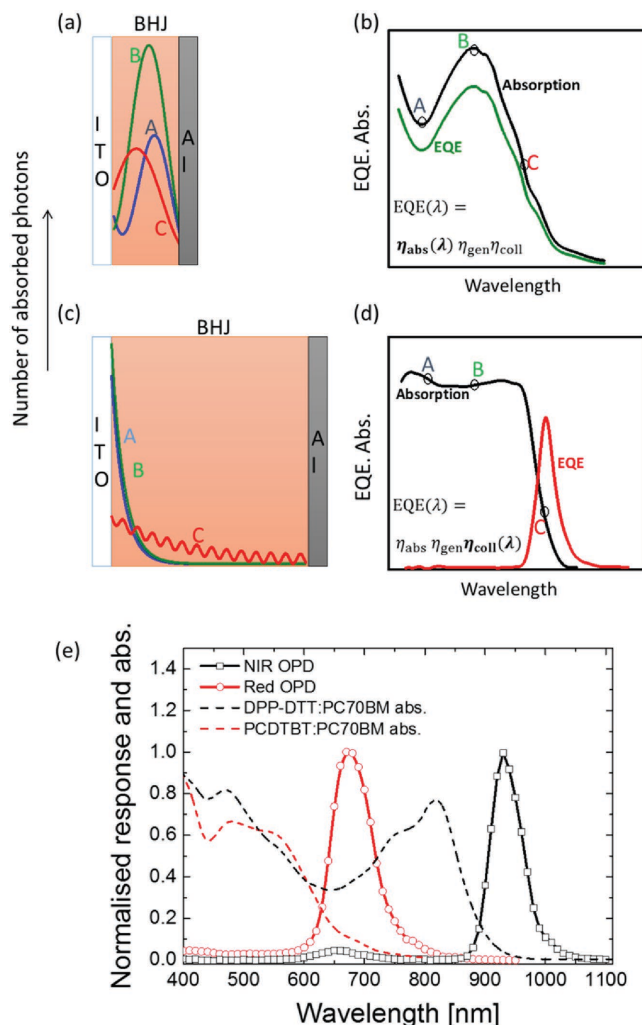


Figure 22. The photodiode structures are shown with the absorbed photon distribution for selected wavelengths marked on the absorption spectra within the active layer (A, B and C); conventional narrowband OPD (a) and (b): in this case, photo-excitations are distributed within the active layer volume for all three wavelengths A, B and C. The spectral behavior of the EQE then follows the absorption spectrum within the active layer modified by any cavity interference effects; charge collection-narrowed (CCN) OPD (c, d): using a thick bulk heterojunction photo-active layer, shorter wavelength photons (A and B) are absorbed near the indium tin oxide (ITO) side, therefore the extraction of photo-generated electrons is hindered. In this case, the charge collection efficiency, Z_{coll} , is spectrally narrowed to only the wavelengths that are near the onset of the absorption (C) where the junction extinction coefficient is low. The EQE therefore peaks sharply at the onset of the absorption; (e) the normalized EQE of the narrowband CCN OPDs comprising thick junctions of PCDTBT (B3) (red) and DPP-DTT (B19) (NIR) blended with PC₇₁BM (B4). The normalized absorption of PCDTBT(B3):PC₇₁BM(B4) and DPP-DTT(B19):PC₇₁BM(B4) blends are also shown (dashed lines). The photoresponse peaks at the absorption edge as predicted under the CCN regime. Reproduced with permission.^[142] Copyright 2015, Nature Publishing Group.

As CMOS technology continues to evolve (e.g., the development of curved CMOS imagers), OPD imagers can bring distinct advantages to image sensing. Factors such as reduced film thickness and increased geometric fill factor (the measure of

surface area available for light sensing) of the photo-sensing pixel in OPDs could simplify the optical design required to capture light over a larger angle of incidence. Organic semiconductors are considered intrinsically flexible, making them more suitable to curved, moldable or conformable photodetectors. The most advanced non-planar inorganic image sensor to date has been reported by Ko et al., in which a silicon-based hemispherical image sensor with elastomeric interconnects was able to achieve a wide field of view (akin to the human eye).^[272] This follows the seminal work of Mahowald and Mead in initially developing a silicon-based retina.^[273] Xu et al. have since employed OPDs in developing human-eye mimicking vision systems.^[274,275] The development of mechanically flexible image sensors is particularly important for aberration-free conformal imaging with the wide field of view required for medical and security applications. Mechanical flexibility is therefore an important attribute in choosing the light sensing material for designing the next generation of image sensors.^[276,277] Material attributes such as solubility have enabled low temperature processing and conformal coating of organic semiconductors as well as direct printing of OPDs on large area flexible substrates, including paper.^[102] The first flexible image sensor based on organic semiconductors was demonstrated in 2005 by Someya et al.^[278] and this has been followed by more recent examples of evaporated^[279] and solution-processed^[156] image sensors.

Three key areas of development have been identified including machine vision systems and surveillance, flexible large-area OPDs for position and X-ray detection, and bioelectronics (e.g., artificial vision and biosensing). The following sub-sections explain how the properties offered by OPDs are predicted to be able to fulfil the needs within each of these applications.

4.1. Machine Vision Systems and Surveillance

Automated solutions for lower cost and increased efficiency in high volume production are important for the modern manufacturing and packaging industry. Robot-guided vision systems are now a norm in performing routine tasks such as the placement of labels on packaged goods, screws in an electrical component, and lids or caps on food containers.^[280] Image sensing under uniform lighting forms an integral part of a machine vision system - where images of objects are taken and processed to guide robots whilst performing tasks with great precision. In conventional cameras, the spectral properties of the illumination source can affect the color of an object in an image, which is caused, at least in part, by the broad spectral coverage and limited dynamic range of conventional sensors. The reflections and glare from the object surface limits the quality of color information in an image.^[75,281] Producing images with high color constancy is therefore a key technological challenge once the dynamic range of the scene (in which the object is located) becomes larger than that of the sensor, a condition often encountered in uncontrolled lighting situations. For this reason, current image sensors are unable to distinguish variability in object color under non-uniform lighting conditions. All machine vision systems therefore rely on the use of a controlled light illumination and infrared image sensors to mitigate

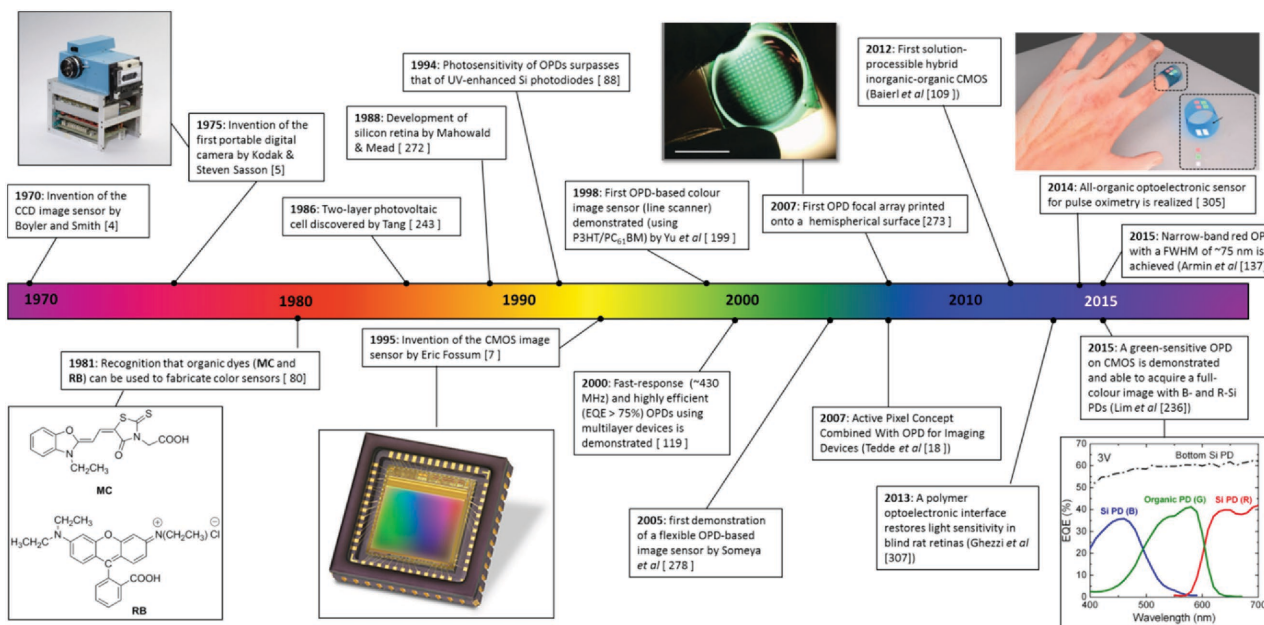


Figure 23. Progress made with OPDs since their conception in the 1980s, shown along with other landmark image-sensing achievements (since 1970). Reproduced with permission: spectrum,^[242] copyright 2015, Nature Publishing Group; hemispherical focal array,^[274] copyright 2008, Elsevier; optoelectronic sensor^[306] copyright 2014, Nature Publishing Group; Kodak prototype digital camera, copyright George Eastman House (Eastman Kodak Company, accession number L15.0005.0007); CMOS image sensor, copyright e2v technologies (<http://www.e2v-us.com/products/imaging/cmos-image-sensors/>).

the color accuracy problem. Furthermore, a high level of color purity is usually required for applications such as real-time video surveillance that demand greater accuracy in imaging objects in natural scenes such as the recognition of humans and their activities.^[282] If robot-guided vision systems are to tackle tasks in real-life situations, the vision system has to mimic the human eye. A theoretical approach to overcome the vision impairment of current image sensors was presented by Finlayson in which the use of a combination of narrow spectral responses and a logarithmic pixel was proposed to create an image that is invariant to the change in lighting conditions.^[49] This theoretical work underpins the developments in materials and device design for spectrally selective OPDs discussed in the previous sections.

4.2. Flexible Large-area OPDs for Position and X-ray Detection

In contrast to conventional color imaging systems, X-ray imaging techniques require the use of so called indirect-conversion detectors where a scintillator layer, under exposure to X-ray photons, emits UV or optical photons. Upon exposure to X-rays, scintillators such as terbium-doped gadolinium oxysulfide, (Gd₂O₂S:Tb) emit green photons that are detected with photodetector arrays composed of amorphous silicon.^[283] Development of a photoconductor material that enables conformable and large-area OPDs for use in X-ray imaging is an emerging topic. The important criteria for materials selection for X-ray imaging is being able to coat the sensing material over a large area (typically 30×30 cm or larger) and to have photodetectors with very low dark currents (10–1000 pA/cm²).^[284] Processing organic semiconductors over large areas on flexible substrates with the spatial resolution required for X-ray imaging (typically 150 μm) is relatively simple.

Furthermore, as discussed earlier, integration of OPDs with different transistor technologies for image readout can be achieved, and hence there is increased technological interest in replacing inorganic photoconductors with wide optical gap (>2 eV) organic semiconductors for X-ray imaging.^[156]

The first demonstration of large area active matrix arrays of OPDs for application in X-ray imaging was reported by Street et al. in 2002.^[123] More recently, Keivanidis et al. reported reasonable X-ray hardness of organic blends composed of fullerene and non-fullerene acceptors used in conjunction with a Gd₂O₂S:Pr scintillator.^[285] The X-ray “hardness” is a material property that is defined by the resistance of material against damage caused by doses of high energy ionizing radiation. The photocurrents reported from P3HT:PC₆₁BM, TFB:PDI, and F8BT:PDI blends exhibited a linear dependence on the X-ray dose; however a drop in EQE of 17% under X-ray exposure was reported for a P3HT:PC₆₁BM blend.^[285] Blackesley et al.^[286] and Gelinck et al.^[287] further explored the potential of OPDs in replacing inorganic photodetectors and concluded that a reduction in OPD dark current was required for good X-ray imaging. To this end, Agostinelli et al. demonstrated that an extremely low dark current density of ≈50 pA/cm² was achievable by thickness optimization of the OPD photoactive layer.^[288] Kingsley et al. improved the X-ray hardness of P3HT:PC₆₁BM blends by taking advantage of the ability to form a relatively thin organic layer of ≈150 nm and reported a loss in EQE of just 2% after prolonged X-ray exposure.^[289] Most recently, Arca et al. have shown that solution-processable P3HT:PC₆₁BM-based OPD imagers can meet the industrial specifications for X-ray imaging.^[290] Takada et al. have also reported the compatibility of OPDs fabricated directly onto the plastic scintillating layer plates, which gave rise to an increased X-ray sensitivity.^[291]

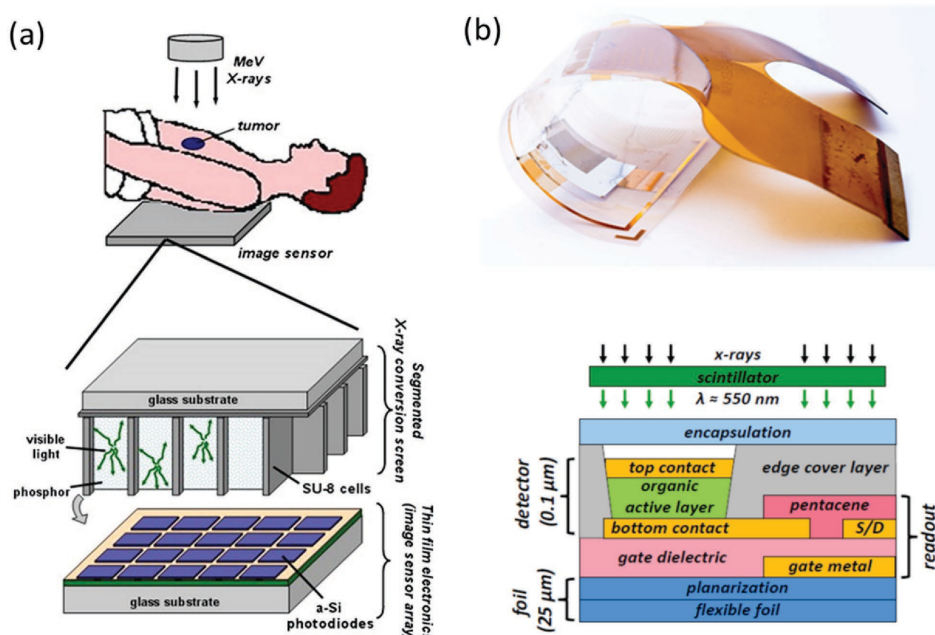


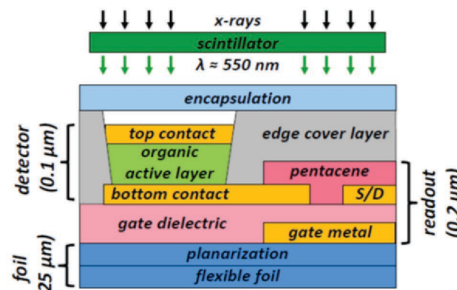
Figure 24. (a) X-ray imaging using high energy X-rays to treat a tumour and to image its location. The conventional X-ray imager shown here uses a segmented scintillating phosphor screen and an array of a-Si photodetectors that detect visible photons emitted by the scintillator layer; (b) a fully flexible OPD-based X-ray imager developed by researchers at IMEC for sensing visible light emitted by the scintillating layer. The pixel cross-section image shows monolithic integration of an organic active layer with a pentacene-based transistor read out on plastic foil. a) Adapted with permission.^[283] Copyright 2007, Elsevier; pixel cross-section image reproduced with permission.^[292] Copyright 2013, International Image Sensor Society; (b) reproduced with permission. Copyright 2015, IMEC.^[298]

With the advantage of flexibility, Malinowski et al. demonstrated a 32×32 OPD flexible pixel array based on a SubPc (N30)/C₆₀ (N13) active bilayer, which used an organic transistor based readout circuit on plastic foil.^[292] Figure 24 shows the typical layout used for medical X-ray imaging and the role of photodetector arrays in locating the position of a tumour.

The more general suitability of lateral position-sensitive photodetection using organic semiconductors in large area devices has been described.^[132,293] Someya et al. have used the pressure sensitivity of flexible electronic circuits composed of organic field effect transistors for pressure-sensitive artificial skins.^[294] In an interesting development, Koeppen et al. have combined the position and pressure sensing ability of organic semiconductors and reported a large area OPD based position sensitive image sensor for applications such as artificial skin for robots.^[295] Likewise, Benisty et al. have reported large area OPDs with resolution of the order of 50 μm for novel flat capture photonic architectures.^[296] Finally, Lamet et al. (ISORG Technologies) have described the development of organic sensor-based surfaces for contactless user interfaces using OPDs, although this is yet to reach full commercialization.^[265,297] Thus, there is considerable scope for using OPDs in large area detection technologies.

4.3. Organic Photodiodes in Bioelectronics, Artificial Vision and Biosensing

Bionics, bioelectronics and bio-nanoelectronics are terms variously used to describe the general concept of creating artificial functional interfaces with biological systems.^[299–301] This



concept can arguably be traced back to the 18th century when Luigi Galvani used externally applied voltages to stimulate movement in the detached legs of frogs. Modern manifestations of such endeavours include implantable cardio-defibrillators (ICDs) to treat sudden heart failure, and the cochlear implant to restore hearing. “Organic bioelectronics” was a term coined by Berggren and Richter-Dahlfors to describe the use of organic optoelectronic materials as the bioelectronic transducing interface in their seminal review on the subject in 2007.^[301] In principle, organic semiconductors offer considerable advantages over their inorganic counterparts in this regard: mechanical flexibility, biological compatibility and even affinity, low cost and wide ranging functionality. Malliaras noted recently that “one observation we made a few years ago was that there is a shift from the use of organic electronic coatings to the use of organic electronic devices.”^[302] This undoubtedly indicates that the field is becoming more technologically sophisticated and furthermore that real, functional organic bioelectronic prototypes are emerging.

The overwhelming majority of bioelectronic applications to date have involved the direct transduction of electrical signals. The ICD and cochlear devices are classic examples, as is the revolutionary neural interfacing work of Fromherz and colleagues.^[303] An alternative to delivering the external stimuli by direct electrical means (i.e., the application of a voltage or driving of a current) is the concept of opto-electrical transduction in which the input signal using electromagnetic radiation (UV, visible or NIR light for example) and soliciting an electrical or photochemical response directly in the biological entity or some secondary transducing element. In principle, the opposite

transducing pathway is also possible – read-out of an electrical signal via an output electro-optical transducer. This presents a clear opportunity for organic photodiodes operating under bias or at short circuit, and reports are now emerging along these lines in two main areas – biosensing, and the stimulation of neurones and artificial vision. Recent progress and opportunities in these two emerging areas will now be discussed.

4.3.1. OPD-based Biosensors

The key focus in this area is the *in vivo* or *in vitro* detection of biochemical moieties. Two main methodologies have been reported. The first involves integration of an OPD with a functionalised substrate, which subsequently emits chemiluminescence upon binding of a specific target. This is an attractive methodology for a simple biosensor since no source of photoexcitation is required and the OPD can be operated in “photovoltaic mode” at short circuit (no power consumption). An archetypal example of this modality is the miniaturised biosensor of Wojciechowski et al.^[304] This device is composed of a disposable chip containing a classic acceptor-donor bulk heterojunction OPD [P3HT (**B1**):PC₆₁BM (**B7**)] and a sensing surface coated with a chemiluminescent immobilised capture antibody. The biosensor was designed to detect Staphylococcal enterotoxin B and could do so reliably down to concentrations as low as a 0.5 ng/mL. There are many other similar examples such as those from the de Mello group for detecting H₂O₂^[198] utilising relatively standard broadband OPDs with modest performance metrics compared with current state-of-the-art. The second methodology is arguably more complex and requires the integration of a light source (such as a light emitting diode – LED) with the OPD in combination with a target sensing surface. This architecture requires external power, but is potentially more sensitive and versatile than the chemiluminescent methodology. Again, there are many reports of such biosensors in the literature, but a typical example using a LED and OPD is that reported by Sagmeister et al.^[305] for an optochemical oxygen sensor. This device was configured with the OPD operating in forward bias to suppress the response time in order to measure phosphorescent lifetimes of two sensor dyes. The OPD was fabricated in a ring geometry and was a modified Tang-type linear p-n heterojunction composed of copper phthalocyanine (**N38**) and PTCBI (**N27**). This device was ultimately capable of making lifetime measurements down to 5 μs over a large range of oxygen concentrations (0–20%). Another more sophisticated and in fact state-of-the-art example of an integrated light source-OPD-based biosensor is that reported by Lochner et al.^[306] This sensor was created to be an *in vitro* pulse oximeter (i.e., could measure human pulse and blood oxygen content) and used green and red organic LEDs (OLEDs) and two spatially separated broadband OPDs. The sensing configuration is shown in Figure 25a and the OPDs were composed of a bulk heterojunction blend of poly({4,8-bis[2-ethylhexyloxy]benzo[1,2-b:4,5-b']dithiophene-2,6-diyl} {3-fluoro-2-[2-ethylhexyl]carbonyl}thienol[3,4-b]thiophenediyl}) (**PTB7**, Figure 25b) and PC₇₁BM (**B4**) yielding external quantum efficiencies as high as 80% with a leakage current of ≈1 nA/cm² at -2 V and with a -3 dB cut-off frequency >10 kHz. These metrics are

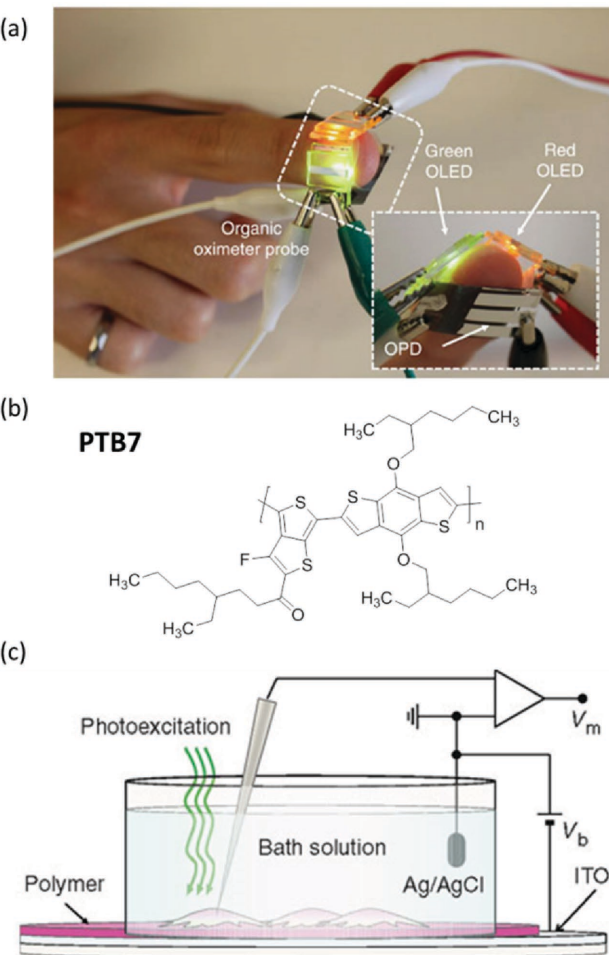


Figure 25. (a) Photograph showing the OLED-OPD configuration for pulse oximeter of Lochner et al. The red and green light is transmitted through the finger and detected by the backside OPD (**PTB7:PC₇₁BM**); (b) chemical structure of **PTB7**; (c) schematic of the photosensing interface from Ghezzi et al. The neurones were grown directly on the P3HT:PC₆₁BM OPD and enclosed within an electrolytic solution. Neurone action potentials were measured in the electrolytic solution using a standard patch clamp set-up and the OPD illuminated from above with a pulsed photoexcitation. a) Reproduced with permission.^[306] Copyright 2014, Nature Publishing Group; (c) reproduced with permission.^[307] Copyright 2011, Nature Publishing Group.

more than adequate for pulse and oximetry measurements. The device was ultimately capable of measuring pulse rate and oxygenation with errors of 1% and 2%, respectively and is notable because it was created on a flexible substrate, with the active layers of the sensor deposited by spin-coating and printing.

4.3.2. Neuronal Photoactivation, Mimicking Natural Photodetectors and Artificial Vision

Several recent reports have emerged of using standard bulk heterojunction photodiodes to stimulate or sense response in neuronal models. For example, Ghezzi et al. demonstrated that a network of primary neurones could be grown directly on top of

a P3HT:PC₆₁BM BHJ (minus the top metallic cathode).^[307] The neurons remained viable on the BHJ surface for many days and their biological functionality was not affected. Furthermore, the optoelectronic properties of the OPD were likewise retained. The configuration for the experiment is shown in Figure 25a with the “read” circuit essentially consisting of an electrical bath and electrode. Using this simple approach the authors were able to trigger and measure action potentials in the neurones in a “temporally reliable and spatially selective manner with short pulses of visible light”. The OPD in this case was operated in photovoltaic mode at short circuit. The transduction mechanism was not entirely clear however, and a number of options were postulated: i) a purely resistive mechanism where photogenerated charge migrates from the BHJ into the electrolyte giving rise to Faradaic currents, membrane depolarization in the neurons and subsequent firing; or ii) a capacitive mechanism involving the establishment of two oppositely charged Helmholtz layers at the BHJ/electrolyte and electrolyte/neuronal membrane interfaces – the redistribution of charge in the latter leading to membrane depolarization; or iii) a combination of both effects. The authors favored a purely capacitive mechanism because of the very low photocurrents generated by the OPD in PV mode. The same group recently took this light-enabled stimulation of neurones one step further, and using a neat P3HT OPD this time restored light sensitivity in blind rat retinas.^[308]

The authors used an almost identical experimental protocol, but in this case elicited a photo-stimulated response in explants of rat retinas with light induced photoreceptor degeneration. The results suggest exciting opportunities for such devices to play a role in subretinal prosthetic implants, i.e., realising the ultimate goal of artificial vision. Similar results are now emerging from other groups. A notable example is the work of Gautam et al. who recently demonstrated a BHJ [poly(alkylthiophene):N2200] deposited on a multi-electrode array (MEA).^[309] This device was capable of stimulating a blind rat retina and simultaneously recording its electrophysiological activity. These early reports of OPD-enabled bioelectronics clearly demonstrate the utility of organic optoelectronic interfaces, and if progress in the rest of the field is as rapid then the first *in vivo* demonstration of an artificial vision system is likely to be in the not too distant future. OPDs fabricated on hemispherical image planes have already contributed significantly to progress in development of the “synthetic eye”.^[274,310,311]

In summary, in this short section we have briefly outlined the current status of OPDs in the rapidly emerging field of organic bioelectronics. Main applications to date include bio-sensing and neuronal stimulation with opto-electrical transduction. The OPDs used so far are invariably broadband and relatively modest in their performance metrics. With the recent advent of broadband silicon diode-like OPD performance^[126] and strategies for sub-100 nm FWHM spectral responses,^[142] new applications requiring spatially, temporally and spectrally selective stimuli or responses are now within reach.

5. Conclusions and Future Outlook

Organic semiconductors have been used to realize photodiodes that are able to overcome some of the limitations of their

inorganic counter parts, e.g., color constancy, whilst offering easier processing on large area, lightweight and flexible substrates, and biocompatibility. Thus organic OPDs have much promise for future image-sensing applications, which will be difficult to fulfil with conventional inorganic semiconductor-based photodiodes. However, the structural disorder and excitonic nature of organic semiconductors provides challenges for OPDs in terms of their performance metrics, e.g., the junction thickness, speed of response and the LDR, which need to be addressed for them to become fully commercial. There is thus a major focus on improving the mobilities of organic semiconductors (this includes polymers and small molecules). Such a drive has already led to organic solar cells with enhanced efficiencies,^[126,317,318] and it is likely that these learnings will translate into the OPD field.

With respect to realizing filter-less, narrowband photodetection with OPDs, a variety of approaches have been highlighted in this review: the advent of novel narrowband absorbers (donor and acceptor), the use of either transparent donor or acceptor materials, the insertion of additional layers to absorb light with undesired wavelengths, and the development of stacked OPDs. However, there is still significant scope for research in this area.

More recently, the emergence of hybrid organic-inorganic materials such as the lead organohalide perovskites for use in solution-processed solar cells has transitioned into the area of photodiodes. The electro-optical properties of these perovskites can be also tailored^[314] and they exhibit non-excitonic charge generation and large charge carrier mobility.^[315] Recently, Lin et al.,^[316] Dou et al.,^[317] Fang et al.^[318] and Sutherland et al.^[319] have reported low noise broadband organohalide perovskite photodiodes for visible NIR-blind detection. These photodiodes exhibited a large LDR,^[316] fast temporal response^[318] and high EQEs,^[320] even in relatively thick junctions (>300 nm) due to the non-excitonic nature of lead organohalide perovskites. Most recently, Fang et al.^[271] and Lin et al.^[270] have reported narrowband photodiodes with FWHM of <100 nm based on the charge collection narrowing (CCN) concept introduced by Armin et al.,^[142] and this area of research is likely to expand in the future.^[321]

Acknowledgements

We thank The University of Queensland (R.J.v.V.) and the Australian Renewable Energy Agency (A.A. and A.K.P.) for financial support. P.L.B. is a University of Queensland Vice-Chancellor's Research Focused Fellow and P.M. is an Australian Research Council Discovery Outstanding Research Award Fellow.

Received: November 2, 2015

Revised: December 16, 2015

Published online:

- [1] A. E. Becquerel, *Comptes Rendus Hebdomadaires des Séances de L'Academie des Sciences* **1848**, 26, 181.
- [2] L. Godowsky, L. D. Mannes (Eastman Kodak Co.), US1997493, 1935.
- [3] W. A. Adcock, (Texas Instruments Incorporated), US4057830 A, 1977.

- [4] W. Boyle, G. Smith, US3792322 A, **1974**.
- [5] G. A. Lloyd, S. J. Sasson (Eastman Kodak Co.), US4131919 (A), **1978**.
- [6] S. K. Mendis, *IEEE J. Solid-State Circuits* **1997**, *32*, 187.
- [7] E. R. Fossum, *Tech. Dig. of IEEE International Electron Devices Meeting* **1995**, pp. 17–25.
- [8] R. Lineback, *O-S-D Report: A Market Analysis and Forecast for the Optoelectronics, Sensors/Actuators, and Discretes*, IC Insights, Arizona, USA, **2014**, pp. 4–28.
- [9] J. Ohta, in *Smart CMOS Image Sensors and Applications*, CRC Press, Boca Raton, FL, USA, **2007**, Ch. 3.
- [10] A. N. Belbachir, P. M. Göbel, *Smart Cameras: A Historical Evolution in Smart Cameras* (Ed: A.N. Belbachir), Springer, New York, **2010**, pp. 3–17.
- [11] R. Lineback (IC Insights), personal communication, August 2015.
- [12] M. Freebody, *Photon. Spectra August* **2011**, 50.
- [13] J. Nakamura, in *Image Sensors and Signal Processing for Digital Still Cameras* (Ed: J. Nakamura), **2005**, CRC Press, Boca Raton, FL, USA, Ch. 3.
- [14] R. Lukac, *J. Real-Time Image Process.* **2006**, *1*, 45.
- [15] S. Ratnasingam, S. Collins, *J. Opt. Soc. Am. A* **2010**, *27*, 286.
- [16] K. Aizawa, K. Sakae, Y. Suenaga, *Image Processing Techniques: Algorithms, Sensors, and Applications*, CRC Press, Boca Raton, FL, USA, **2004**, Ch. 2 & 7.
- [17] B. Tang, K. F. Lee, in *IEEE International Conference on Acoustics, Speech, and Signal Processing, (ICASSP '04)*, IEEE, NJ, USA **2004**, *3*, 105.
- [18] F. Zhang, J. Zhang, C. Yang, X. Zhang, *IEEE Trans. Electron Dev.* **2010**, *57*, 788.
- [19] M. Vieira, P. Louro, A. Fantoni, M. Fernandes, M. A. Vieira, M. Barata, in *6th International Multi-Conference on Systems, Signals and Devices (SSD)*, IEEE, NJ, USA, **2009**, 1–6.
- [20] P. Louro, A. Fantoni, M. Fernandes, M. Vieira, in *6th International Multi-Conference on Systems, Signals and Devices (SSD)*, IEEE, NJ, USA, **2009**, 1–4.
- [21] T. N. Ng, R. A. Lujan, S. Sambandan, R. A. Street, S. Limb, W. S. Wong, *Appl. Phys. Lett.* **2007**, *91*, 063505.
- [22] Q. Zhu, S. Coors, B. Schneider, P. Rieve, M. Bohm, *IEEE Trans. Electron. Dev.* **1998**, *45*, 1393.
- [23] S. Tedde, E. S. Kaus, J. Furts, D. Henseler, P. Lugli, *IEEE Electron. Dev. Lett.* **2007**, *28*, 893.
- [24] J. Ohta, in *Smart CMOS Image Sensors and Applications*, **2007**, CRC Press, Boca Raton, FL, USA, Ch. 4.
- [25] G. Langfelder, A. Longoni, F. Zaraga, *Nucl. Instrum. Meth. A* **2009**, *610*, 50.
- [26] P. B. Catrysse, B. A. Wandell, *J. Opt. Soc. Am. A* **2003**, *20*, 2293.
- [27] A. Tetsuya, A. S. Kenji, A. Yutaka, *Jpn. J. Appl. Phys.* **2014**, *53*, 04EC02.
- [28] G. De Cesare, F. Irrera, F. Lemmi, F. Palma, *IEEE Trans. Electron Dev.* **1995**, *42*, 835.
- [29] Y. Ohmori, H. Kajii, *Proc. IEEE* **2009**, *97*, 1627.
- [30] K.-J. Baeg, M. Binda, D. Natali, M. Caironi, Y.-Y. Noh, *Adv. Mater.* **2013**, *25*, 4267.
- [31] H. Dong, H. Zhu, Q. Meng, X. Gong, W. Hu, *Chem. Soc. Rev.* **2012**, *41*, 1754.
- [32] G. Konstantatos, E. H. Sargent, *Proc. IEEE* **2009**, *97*, 1666.
- [33] a) C. Lan, *J. Mater. Chem. C* **2015**, *3*, 8074; b) X. Wang, *Chem. Soc. Rev.* **2014**, *43*, 1400.
- [34] P. Parreira, E. Torres, C. Nunes, C. N. de Carvalho, G. Lavareda, A. Amaral, M. J. Brites, *Sensor. Actuat. B-Chem.* **2012**, *161*, 901.
- [35] K. Spaulding, K. Parulski, in *Digital Color Imaging Handbook* (Ed: G. Sharma), CRC Press, Boca Raton, FL, USA, **2002**, Ch. 12.
- [36] A. Theuwissen, in *33rd European Solid State Circuits Conference (ESSCIRC)* IEEE, NJ, USA **2007**, 21.
- [37] H. Lee, S. Nam, H. Kwon, S. Lee, J. Kim, W. Lee, C. Lee, J. Jeong, H. Kim, T. J. Shin, Y. Kim, *J. Mater. Chem. C* **2015**, *3*, 1513.
- [38] G. Konstantatos, E. H. Sargent, *Nat. Nanotechnol.* **2010**, *5*, 391.
- [39] S. Nau, C. Wolf, S. Sax, E. J. W. List-Kratochvil, *Adv. Mater.* **2015**, *27*, 1048.
- [40] G. Konstantatos, J. Clifford, L. Levina, E. H. Sargent, *Nat. Photon.* **2007**, *1*, 531.
- [41] A. Goetzberger, C. Hebling, *Sol. Energ. Mater. Sol. Cells* **2000**, *62*, 1.
- [42] D. Knipp, P. G. Herzog, H. Stiebig, *IEEE Trans. Electron. Dev.* **2002**, *49*, 170.
- [43] T. Lule, S. Benthien, H. Keller, F. Mutze, P. Rieve, K. Seibel, M. Sommer, M. Bohm, *IEEE Trans. Electron Dev.* **2000**, *47*, 2110.
- [44] W. Bludau, A. Onton, W. Heinke, *J. Appl. Phys.* **1974**, *45*, 1846.
- [45] R. Lukac, K. N. Plataniotis, D. Hatzinakos, *IEEE Trans. Circ. Syst. Vid.* **2005**, *15*, 1475.
- [46] P. Degenaar, K. Nikolic, L. Chen, in *Next Generation Artificial Vision Systems: Reverse Engineering the Human Visual System* (Eds: A. Bharath, M. Petrou), Artech House, Norwood, MA, USA, **2008**, Ch. 10.
- [47] M. Ihama, M. Hayashi, Y. Maehara, M. Tetsurou, S. Takada, *Proc. SPIE* **2007**, *6656*, 66560A.
- [48] H. Seo, S. Aihara, M. Namba, T. Watabe, H. Ohtake, M. Kubota, N. Egami, T. Hiramatsu, T. Matsuda, M. Furuta, H. Nitta, T. Hirao, *Proc. SPIE Sensors, Cameras and Systems or Industrial/Scientific Applications XI* **2010**, *7536*, 753602.
- [49] G. D. Finlayson, S. D. Hordley, *J. Opt. Soc. Am. A* **2001**, *18*, 253.
- [50] M. R. Antognazza, U. Scherf, P. Monti, G. Lanzani, *Appl. Phys. Lett.* **2007**, *90*, 163509.
- [51] M. R. Antognazza, D. Musitelli, S. Perissinotto, *Org. Electron.* **2010**, *11*, 357.
- [52] M. Yamaguchi, *J. Soc. Photographic Sci. Techn. Jpn.* **2002**, *65*, 21.
- [53] P. B. Catrysse (Palo Alto), B.A. Wandell (Menlo Park), US7248297 (B2), **2007**.
- [54] S. Nishiaki, T. Nakamura, M. Hiramoto, T. Fujii, M. Suzuki, *Nat. Photon.* **2013**, *7*, 240.
- [55] Y. Kanamori, M. Shimono, K. Hane, *IEEE Photonic Tech. Lett.* **2006**, *18*, 2126.
- [56] S. Yokogawa, S. P. Burgos, H. A. Atwater, *Nano Lett.* **2012**, *12*, 4349.
- [57] T. Xu, Y.-K. Wu, X. Luo, L. J. Guo, *Nat. Commun.* **2010**, *1*, 59.
- [58] Y. Gu, L. Zhang, J. K. W. Yang, S. P. Yeo, C.-W. Qiu, *Nanoscale* **2015**, *7*, 6409.
- [59] S. Feruglio, G.-N. Lu, P. Garda, G. Vasilescu, *Sensors* **2008**, *8*, 6566.
- [60] R. F. Lyon, P. M. Hubel, in *Proc. IS & T/TSID 10th Color Imaging Conference* **2002**, 349.
- [61] D. L. Gilblom, S. K. Yoo, P. Ventura, *Proc. SPIE Infrared Technology and Applications XXIX* **2003**, *5074*, 318.
- [62] R. B. Merrill, (Foveon Inc.), US 5965875(A), **1999**.
- [63] K. M. Findlater, D. Renshaw, J. E. D. Hurwitz, R. K. Henderson, T. E. R. Bailey, S. G. Smith, M. D. Purcell, J. M. Raynor, in *IEEE Workshop on CCDs*, IEEE, NJ, USA **2001**, 4.
- [64] M. Inuuya, (Fuji Photo Film Co., Ltd.), US2006/0208162 A1, **2006**.
- [65] A. Longoni, F. Zaraga, G. Langfelder, L. Bombelli, *IEEE Electr. Device Lett.* **2008**, *29*, 1306.
- [66] M. A. Martínez, E. M. Valero, J. Hernández-Andrés, J. Romero, G. Langfelder, *Appl. Optics* **2014**, *53*, C14.
- [67] H. Park, Y. Dan, K. Seo, Y. J. Yu, P. K. Duane, M. Woher, K. B. Crozier, *Nano Lett.* **2014**, *14*, 1804.
- [68] H. Park, K. B. Crozier, *ACS Photon.* **2015**, *2*, 544.
- [69] G. de Cesare, F. Irrera, F. Lemmi, F. Palma, *Appl. Phys. Lett.* **1995**, *66*, 1178.
- [70] G. De Cesare, F. Irrera, F. Lemmi, F. Palma, M. Tucci, *MRS Symp. Proc.* **1994**, *36*, 885.
- [71] a) T. Zhai, X. Fang, M. Liao, X. Xu, L. Li, B. Liu, Y. Koide, Y. Ma, J. Yao, Y. Bando, D. Golberg, *ACS Nano* **2010**, *4*, 1596; b) J. Yoo, S. Jeong, S. Kim, J. H. Je, *Adv. Mater.* **2015**, *27*, 1712.

- [72] R. B. Jacobs-Gedrim, N. Shanmugam, N. Jain, C. A. Durcan, M. T. Murphy, T. M. Murray, R. J. Matyi, R. L. Moore, B. Yu, *ACS Nano* **2014**, *8*, 514.
- [73] D. Kufer, I. Nikitskiy, T. Lasanta, G. Navickaite, F. H. L. Koppens, G. Konstantatos, *Adv. Mater.* **2015**, *27*, 176.
- [74] J. A. Marchant, N. D. Tillett, C. M. Onyango, *Cybernet. Syst.* **2004**, *35*, 19.
- [75] D. H. Foster, *Trends Cogn. Sci.* **2003**, *7*, 439.
- [76] A. Chakrabarti, W. T. Freeman, T. Zickler, in *IEEE International Conference on Computational Photography (ICCP)* **2014**, *1*.
- [77] M. Ebner, *Algorithms for Color Constancy under Nonuniform Illumination in Color Constancy*, John Wiley & Sons, Hoboken, NJ, USA, **2007**, Ch. 7.
- [78] J. Liu, Z. Shao, Q. Cheng, *Opt. Lett.* **2011**, *36*, 4821.
- [79] H. Burkhardt, B. Neumann, B. Funt, K. Barnard, L. Martin, *Lecture Notes in Computer Science*, Springer, Berlin/Heidelberg, Germany **1998**, 445.
- [80] S. Ratnasingam, S. Collins, in *Image Analysis and Processing (ICIAP)*, Springer, Berlin/Heidelberg, Germany **2009**, 748–756.
- [81] J. Vazquez-Corral, M. Bertalmio, *Sensors* **2014**, *14*, 3965.
- [82] D. H. Foster, *Vision Res.* **2011**, *51*, 674.
- [83] X. Xu, L. Zhuo, J. Zhang, L. Shen, *J. Electron. (China)* **2009**, *26*, 681.
- [84] A. Chakrabarti, A. K. Hirakawa, T. Zickler, in *IEEE Conference on Computer Vision and Pattern Recognition (CVPR)*, IEEE, NJ, USA **2008**, pp. 1–6.
- [85] K. Kudo, T. Moriizumi, *Appl. Phys. Lett.* **1981**, *39*, 609.
- [86] G. J. Hedley, A. J. Ward, A. Alekseev, C. T. Howells, E. R. Martins, L. A. Serrano, G. Cooke, A. Ruseckas, I. D. W. Samuel, *Nat. Commun.* **2013**, *4*, 1.
- [87] M. Knupfer, *Appl. Phys. A* **2003**, *77*, 623.
- [88] D. C. Coffey, B. W. Larson, A. W. Hains, J. B. Whitaker, N. Kopidakis, O. V. Boltalina, S. H. Strass, G. Rumbles, *J. Phys. Chem. C* **2012**, *116*, 8916.
- [89] A. A. Bakulin, S. D. Dimitrov, A. Rao, P. C. Y. Chow, C. B. Nielsen, B. C. Schroeder, I. McCulloch, H. J. Bakker, J. R. Durrant, R. H. Friend, *J. Phys. Chem. Lett.* **2013**, *4*, 209.
- [90] S. H. Park, A. Roy, S. Beaupré, S. Cho, N. Coates, J. S. Moon, M. Daniel, M. Leclerc, K. Lee, A. J. Heeger, *Nat. Photon.* **2009**, *3*, 297.
- [91] G. Yu, J. Gao, J. C. Hummelen, F. Wudl, A. J. Heeger, *Science* **1995**, *270*, 1789.
- [92] R. Shinar, J. Shinar, *Organic Electronics in Sensors and Biotechnology*, McGraw-Hill Professional Publishing, New York, **2009**, Ch. 6.
- [93] G. Yu, K. Pakbaz, A. J. Heeger, *Appl. Phys. Lett.* **1994**, *64*, 3422.
- [94] X. Gong, M. Tong, Y. Xia, W. Cai, J. S. Moon, Y. Cao, G. Yu, C.-L. Shieh, B. Nilsson, A. J. Heeger, *Science* **2009**, *325*, 1665.
- [95] F. Guo, Z. Xiao, J. Huang, *Adv. Opt. Mater.* **2013**, *1*, 289.
- [96] Z. Su, F. Hou, X. Wang, Y. Gao, F. Jin, G. Zhang, Y. Li, L. Zhang, B. Chu, W. Li, *ACS Appl. Mater. Interfaces* **2015**, *7*, 2529.
- [97] D. Yang, D. Ma, *J. Mater. Chem. C* **2013**, *1*, 2054.
- [98] D.-S. Leem, K.-H. Lee, Y.-N. Kwon, D.-J. Yun, K.-B. Park, S.-J. Lim, K.-S. Kim, Y. W. Jin, S. Lee, *Org. Electron.* **2015**, *24*, 176.
- [99] A. Armin, I. Kassal, P. E. Shaw, M. Hambach, M. Stolterfoht, D. M. Lyons, J. Li, Z. Shi, P. L. Burn, P. Meredith, *J. Amer. Chem. Soc.* **2014**, *136*, 11465.
- [100] T. Someya, Y. Kato, I. Shingo, Y. Noguchi, T. Sekitani, H. Kawaguchi, T. Sakurai, *IEEE Trans. Electron Dev.* **2005**, *52*, 2502.
- [101] E. Kraker, A. Haase, G. Jakopic, J. R. Krenn, S. Köstler, C. Konrad, S. Heusing, P. W. Oliveira, M. Veith, *Thin Solid Films* **2009**, *518*, 1214.
- [102] a) B. Lamprecht, R. Thünauer, M. Ostermann, G. Jakopic, G. Leising, *Phys. Status Solidi A* **2005**, *202*, R50; b) R. S. Aga, J. P. Lombardi, C. M. Bartsch, E. M. Heckman, *IEEE Phot. Techn. Lett.* **2014**, *26*, 305.
- [103] F. Arca, S. F. Tedde, M. Sramek, J. Rauh, P. Lugli, O. Hayden, *Sci. Report.* **2013**, *3*, 13224.
- [104] Z. Liu, K. Parvez, R. Li, R. Dong, X. Feng, K. Müllen, *Adv. Mater.* **2015**, *27*, 669.
- [105] K.-H. Lee, D.-S. Leem, J. S. Castrucci, K.-B. Park, X. Bulliard, K.-S. Kim, Y. W. Jin, S. Lee, T. P. Bender, S. Y. Park, *ACS Appl. Mater. Interfaces* **2013**, *5*, 13089.
- [106] I. K. Kim, B. N. Pal, M. Ullah, P. L. Burn, S.-C. Lo, P. Meredith, E. B. Namdas, *Adv. Opt. Mater.* **2015**, *3*, 49.
- [107] R. Eckstein, T. Rödlmeier, T. Glaser, S. Valouch, R. Mauer, U. Lemmer, G. Hernandez-Sosa, *Adv. Electron. Mater.* **2015**, *1*, 1500101.
- [108] E. Saracco, B. Bouthinon, J.-M. Verilhac, C. Celle, N. Chevalier, D. Mariolle, O. Dhez, J.-P. Simonato, *Adv. Mater.* **2013**, *25*, 6534.
- [109] G. Azzellino, A. Grimoldi, M. Binda, M. Caironi, D. Natali, M. Sampietro, *Adv. Mater.* **2013**, *25*, 6829.
- [110] G. Pace, A. Grimoldi, D. Natali, M. Sampietro, J. E. Coughlin, G. C. Bazan, M. Caironi, *Adv. Mater.* **2014**, *26*, 6773.
- [111] A. Pierre, I. Deckman, P. B. Lechêne, A. C. Arias, *Adv. Mater.* **2015**, doi: 10.1002/adma.201502238.
- [112] S. F. Tedde, J. Kern, T. Sterzl, J. Fürst, P. Lugli, O. Hayden, *Nano Lett.* **2009**, *9*, 980.
- [113] A. Falco, L. Cinà, G. Scarpa, P. Lugli, A. Abdellah, *ACS Appl. Mater. Interfaces* **2014**, *6*, 10593.
- [114] D. Baierl, L. Pancheri, M. Schmidt, D. Stopka, G.-F. Dalla Betta, G. Scarpa, P. Lugli, *Nat. Commun.* **2015**, *3*, 1175.
- [115] A. Falco, A. M. Zaidi, P. Lugli, A. Abdellah, *Org. Electron.* **2015**, *23*, 186.
- [116] P. Peumans, Y. Aharon, S. R. Forrest, *J. Appl. Phys.* **2003**, *93*, 3693.
- [117] F. Guo, B. Yang, Y. Yuan, Z. Xiao, Q. Dong, Y. Bi, J. Huang, *Nat. Nanotechnol.* **2012**, *7*, 798.
- [118] a) R. D. Jansen-van Vuuren, P. C. Deakin, S. Olsen, P. L. Burn, *Dyes Pigments*, **2014**, *101*, 1; b) R. D. Jansen-van Vuuren, A. Pivrikas, A. K. Pandey, P. L. Burn, *J. Mater. Chem. C* **2013**, *1*, 3532.
- [119] J. M. Lupton, R. Koeppe, J. G. Müller, J. Feldmann, U. Scherf, U. Lemmer, *Adv. Mater.* **2003**, *15*, 1471.
- [120] J. Qi, J. Han, X. Zhou, D. Yang, J. Zhang, W. Qiao, D. Ma, Z. Y. Wang, *Macromolecules* **2015**, *48*, 3941.
- [121] K. H. An, B. O'Connor, K. P. Pipe, M. Shtein, *Org. Electron.* **2009**, *10*, 1152.
- [122] R. A. Street, M. Mulato, R. Lau, J. Ho, J. Graham, Z. Popovic, J. Hor, *Appl. Phys. Lett.* **2001**, *78*, 4193.
- [123] R. A. Street, J. Graham, Z. D. Popovic, A. Hor, S. Ready, J. Ho, *J. Non-Cryst. Solids* **2002**, *299–302*, 1240.
- [124] P. Peumans, V. Bulovic, S. R. Forrest, *Appl. Phys. Lett.* **2000**, *76*, 3855.
- [125] H.-J. Yun, M. C. Hwang, S. M. Park, R. Kim, D. S. Chung, Y.-H. Kim, S.-K. Kwon, *ACS Appl. Mater. Interfaces* **2013**, *5*, 6045.
- [126] A. Armin, M. Hambach, I. K. Kim, P. L. Burn, P. Meredith, E. B. Namdas, *Laser Photonics Rev.* **2014**, *8*, 924.
- [127] J. P. Clifford, G. Konstantatos, K. W. Johnston, S. Hoogland, L. Levina, E. H. Sargent, *Nat. Nanotechnol.* **2009**, *4*, 40.
- [128] D. S. Chung, Y. Rho, M. Ree, S.-K. Kwon, Y.-H. Kim, *ACS Appl. Mater. Interfaces* **2012**, *4*, 4758.
- [129] P. E. Keivanidis, P. K. H. Ho, R. H. Friend, N. C. Greenham, *Adv. Funct. Mater.* **2010**, *20*, 3895.
- [130] P. E. Keivanidis, S.-H. Khong, P. K. H. Ho, N. C. Greenham, R. H. Friend, *Appl. Phys. Lett.* **2009**, *94*, 173303.
- [131] G. A. H. Wetzel, M. Kuik, M. Lenes, P. W. M. Blom, *Appl. Phys. Lett.* **2011**, *99*, 153506.
- [132] U. Shafique, C. Santato, K. S. Karim, *IEEE Trans. Electron Devices* **2014**, *61*, 3465.
- [133] Y. Fang, F. Guo, Z. Xiao, J. Huang, *Adv. Opt. Mater.* **2014**, *2*, 348.
- [134] T. N. Ng, W. S. Wong, R. A. Lujan, R. A. Street, *Adv. Mater.* **2009**, *21*, 1855.

- [135] S. Cook, H. Ohkita, Y. Kim, J. J. Benson-Smith, D. D. C. Bradley, J. R. Durrant, *Chem. Phys. Lett.* **2007**, *445*, 276.
- [136] H. Seo, S. Aihara, K. Misao, N. Egami, *Jpn. J. Appl. Phys.* **2010**, *49*, 111601.
- [137] S. Sahu, A. J. Pal, *J. Nanosci. Nanotech.* **2009**, *9*, 450.
- [138] A. Armin, G. Juska, M. Ullah, M. Velusamy, P. L. Burn, P. Meredith, A. Pivrikas, *Adv. Energy Mater.* **2014**, *4*, 1300954.
- [139] J. Huang, G. Li, Y. Yang, *Appl. Phys. Lett.* **2005**, *87*, 112105.
- [140] A. M. Goodman, A. Rose, *J. Appl. Phys.* **1971**, *42*, 2823.
- [141] M. Ramuz, L. Bürgi, C. Winnewisser, P. Seitz, *Org. Electron.* **2008**, *9*, 369.
- [142] A. Armin, R. D. Jansen-van Vuuren, N. Kopidakis, P. L. Burn, P. Meredith, *Nat. Commun.* **2015**, *6*, 6343.
- [143] H. Jin, A. Armin, M. Hambach, Q. Lin, P. L. Burn, P. Meredith, *Phys. Status Solidi A* **2015**, *212*, 2246.
- [144] A. J. Moulé, J. B. Bonekamp, K. Meerholz, *J. Appl. Phys.* **2006**, *100*, 094503.
- [145] S. Hokuto, S. Aihara, T. Watabe, H. Ohtake, M. Kubota, N. Egami, *Jpn. J. Appl. Phys.* **2007**, *46*, L1240.
- [146] M. Iizuka, K. Kudo, S. Kuniyoshi, K. Tanaka, *Synthetic Met.* **2000**, *115*, 181.
- [147] T. Fukuda, M. Komoriya, R. Kobayashi, R. Ishimaru, N. Kamata, *Jpn. J. Appl. Phys.* **2009**, *48*, 04C161.
- [148] F. Martínez-Verdú, J. Pujol, P. Capilla, *J. Imaging Sci. Techn.* **2002**, *46*, 15.
- [149] J. Wang, G. Yu, G. Srdanov, A. J. Heeger, *Org. Electron.* **2000**, *1*, 33.
- [150] D. Gadia, G. Lasco, A. Rizzi, D. Marini, M. Antognazza, in *5th European Conference on Color in Graphics, Imaging and Vision (CGIV)*, IS&T, Virginia, USA **2010**, 132.
- [151] R. D. Jansen-van Vuuren, K. D. Johnstone, S. Ratnasingam, H. Barcena, P. C. Deakin, A. K. Pandey, P. L. Burn, S. Collins, I. D. W. Samuel, *Appl. Phys. Lett.* **2010**, *96*, 253303.
- [152] M. El-Desouki, D. M. Jamal, Q. Fang, L. Liu, F. Tse, D. Armstrong, *Sensors* **2009**, *9*, 430.
- [153] I. Nausieda, K. Ryu, I. Kyrmisis, A. I. Akinwande, V. Bulovic, C. G. Sodini, *IEEE Trans. Electron Devices* **2008**, *55*, 527.
- [154] R. A. Street, J. Graham, Z. Popovic, A. Hor, M. Mulato, R. Lau, J. Ho, *Mat. Res. Soc. Symp. Proc.* **2001**, *665*, 281.
- [155] W. S. Wong, R. Lujan, J. H. Daniel, S. Limb, *J. Non-Cryst. Solid* **2006**, *352*, 1981.
- [156] T. N. Ng, W. S. Wong, M. L. Chabiny, S. Sambandan, R. A. Street, *Appl. Phys. Lett.* **2008**, *92*, 3.
- [157] Y. Gang, Y. Cao, (Uniax Corp.), *WO9909603 (A1)*, **1999**.
- [158] Y. Zhang, Y. B. de Boer, P. W. M. Blom, *Adv. Funct. Mater.* **2009**, *19*, 1901.
- [159] A. Armin, G. Juska, B. W. Philippa, P. L. Burn, P. Meredith, R. D. White, A. Pivrikas, *Adv. Energy Mater.* **2013**, *3*, 321.
- [160] A. J. Morfa, A. M. Nardes, S. E. Shaheen, N. Kopidakis, J. van de Lagemaat, *Adv. Funct. Mater.* **2011**, *21*, 2580.
- [161] X. Gong, M.-H. Tong, S. H. Park, M. Liu, A. Jen, A. J. Heeger, *Sensors* **2010**, *10*, 6488.
- [162] D. M. Lyons, A. Armin, M. Stolterfoht, R. C. R. Nagiri, R. D. Jansen-van Vuuren, B. N. Pal, P. L. Burn, S.-C. Lo, P. Meredith, *Org. Electron.* **2014**, *15*, 2903.
- [163] T. Martin, R. Landauer, *Phys. Rev. B* **1992**, *45*, 1742.
- [164] E. L. Dereniak, G. D. Boreman, *Infrared Detectors & Systems* (Ed: John Wiley & Sons., USA), **1996**, 152.
- [165] V. Mitin, L. Reggiani, L. Varani, in *Noise and Fluctuations Control in Electronic Devices*, (Ed: A. A. Balandin), American Scientific Publishers: U.S.A, **2002**, Ch. 2.
- [166] K. Kaku, A. T. Williams, B. G. Mendis, C. Groves, *J. Mater. Chem. C* **2015**, *3*, 6077.
- [167] A. Carbone, P. Mazzetti, *J. Appl. Phys.* **1996**, *80*, 1559.
- [168] G. Konstantatos, I. Howard, A. Fischer, S. Hoogland, J. Clifford, E. Klem, L. Levina, E. H. Sargent, *Nature* **2006**, *442*, 180.
- [169] J. Lee, P. Jadhav, M. A. Baldo, *Appl. Phys. Lett.* **2009**, *95*, 033301.
- [170] R. Dong, C. Bi, Q. Dong, F. Guo, Y. Yuan, Y. Fang, Z. Xiao, J. Huang, *Adv. Opt. Mater.* **2014**, *2*, 549.
- [171] S.-T. Chuang, S.-C. Chien, F.-C. Chen, *Appl. Phys. Lett.* **2012**, *100*, 013309.
- [172] F.-C. Chen, S.-C. Chien, G.-L. Cious, *Appl. Phys. Lett.* **2010**, *97*, 103301.
- [173] H.-Y. Chen, M. K. F. Lo, G. Yang, H. G. Monbouquette, Y. Yang, *Nat. Nanotechnol.* **2008**, *3*, 543.
- [174] L. Li, F. Zhang, J. Wang, Q. An, Q. Sun, W. Wang, J. Zhang, F. Teng, *Sci. Rep.* **2015**, *5*, 9181.
- [175] W. Wang, F. Zhang, L. Li, M. Zhang, Q. An, J. Wang, Q. Sun, *J. Mater. Chem. C* **2015**, *3*, 7386.
- [176] M. Stolterfoht, A. Armin, B. Philippa, R. D. White, P. L. Burn, P. Meredith, G. Juška, A. Pivrikas, *Sci. Rep.* **2015**, *5*, 9949.
- [177] S. Sahu, S. K. Batabyal, A. J. Pal, *Appl. Phys. Lett.* **2007**, *90*, 142112.
- [178] I. H. Campbell, B. K. Crone, *Appl. Phys. Lett.* **2012**, *101*, 023301.
- [179] Y. Che, H. Huang, M. Xu, C. Zhang, B. R. Bunes, X. Yang, L. Zang, *J. Am. Chem. Soc.* **2011**, *133*, 1087.
- [180] K. Kato, S. Hata, J. Yoshida, A. Kozen, in *Fourth International Conference on Indium Phosphide and Related Materials*, Newport, USA, **1992**, 254.
- [181] K. Kato, *IEEE Trans. Microw. Theory* **1999**, *47*, 1265.
- [182] M. Taichiro, K. Hirotake, O. Yutaka, *Jpn. J. Appl. Phys.* **2006**, *45*, 546.
- [183] T. Hamasaki, T. Morimune, H. Kajii, S. Minakata, R. Tsuruoka, T. Nagamichi, Y. Ohmori, *Thin Solid Films* **2009**, *518*, 548.
- [184] D. Baierl, B. Fabel, P. Lugli, G. Scarpa, *Org. Electron.* **2011**, *12*, 1669.
- [185] W.-W. Tsai, Y.-C. Chao, E.-C. Chen, H.-W. Zan, H.-F. Meng, C.-S. Hsu, *Appl. Phys. Lett.* **2009**, *95*, 213308.
- [186] D. Yang, X. Zhou, D. Ma, *Org. Electron.* **2013**, *14*, 3019.
- [187] B. Li, *Mod. Phys. Lett. B* **2012**, *26*, 1250100.
- [188] G. Zhang, W. Li, B. Chu, F. Yan, J. Zhu, Y. Chen, *Appl. Phys. Lett.* **2010**, *96*, 073301.
- [189] A. Armin, M. Velusamy, P. Wolfer, Y. Zhang, P. L. Burn, P. Meredith, A. Pivrikas, *ACS Photonics* **2014**, *1*, 173.
- [190] M. S. Arnold, J. D. Zimmerman, C. K. Renshaw, X. Xu, R. R. Lunt, C. M. Austin, S. R. Forrest, *Nano Lett.* **2009**, *9*, 3354.
- [191] J. Qi, L. Ni, D. Yang, X. Zhou, W. Qiao, M. Li, D. Ma, Z. Y. Wang, *J. Mater. Chem. C* **2014**, *2*, 2431.
- [192] L. Li, Y. Huang, J. Peng, Y. Cao, X. Peng, *J. Mater. Chem. C* **2014**, *2*, 1372.
- [193] S. M. Menke, R. Pandey, R. J. Holmes, *Appl. Phys. Lett.* **2012**, *101*, 223301.
- [194] Q. Zafar, Z. Ahmad, K. Sulaiman, A. S. Hamzah, Z. A. Rahman, *Sensor. Actuat. A -Phys.* **2014**, *206*, 138.
- [195] C.-M. Yang, P.-Y. Tsai, S.-F. Horng, K.-C. Lee, S.-R. Tzeng, H.-F. Meng, J.-T. Shy, C.-F. Shu, *Appl. Phys. Lett.* **2008**, *92*, 083504.
- [196] S. Valouch, C. Hönes, S. W. Kettlitz, N. Christ, H. Do, M. F. G. Klein, H. Kalt, A. Colsmann, U. Lemmer, *Org. Electron.* **2012**, *13*, 2727.
- [197] D. Baierl, B. Fabel, P. Gabos, L. Panzeri, P. Lugli, G. Scarpa, *Org. Electron.* **2010**, *11*, 1199.
- [198] X. Wang, M. Amatongchai, D. Nacapricha, O. Hofmann, J. C. de Mello, D. D. C. Bradley, A. J. de Mello, *Sensor. Actuat. B-Chem.* **2009**, *140*, 643.
- [199] I. K. Kim, X. Li, M. Ullah, P. E. Shaw, R. Wawrzinek, E. B. Namdas, S.-C. Lo, *Adv. Mater.* **2015**, *27*, 1521.
- [200] X. Sheng, C. Yu, V. Malyarchuk, Y.-H. Lee, S. Kim, T. Kim, L. Shen, C. Horng, J. Lutz, N. C. Giebink, J. Park, J. A. Rogers, *Adv. Opt. Mater.* **2014**, *2*, 314.
- [201] Y.-Y. Lin, C.-W. Chen, W.-C. Yen, W.-F. Su, C.-H. Ku, J.-J. Wu, *Appl. Phys. Lett.* **2008**, *92*, 233301.

- [202] L. Zhu, Q. Dai, Z.-F. Hu, X.-Q. Zhang, Y.-S. Wang, *Opt. Lett.* **2011**, *36*, 1821.
- [203] W. Li, K. H. Hendriks, W. S. C. Roelofs, Y. Kim, M. M. Wienk, R. A. J. Janssen, *Adv. Mater.* **2013**, *25*, 3182.
- [204] G. Yu, J. Wang, J. McElvain, A. J. Heeger, *Adv. Mater.* **1998**, *10*, 1431.
- [205] G. Yu, G. Srdanov, J. Wang, H. Wang, Y. Cao, A. J. Heeger, *Synthetic Met.* **2000**, *111–112*, 133.
- [206] H. Arora, P. E. Malinowski, A. Chasin, D. Cheyns, S. Steudel, S. Schols, P. Heremans, *Appl. Phys. Lett.* **2015**, *106*, 143301.
- [207] B. Arredondo, B. Romero, J. M. S. Pena, A. Fernández-Pacheco, E. Alonso, R. Vergaz, C. de Sios, *Sensors* **2013**, *13*, 12266.
- [208] F. F. So, S. R. Forrest, *IEEE Trans. Electron Dev.* **1989**, *36*, 66.
- [209] Hamamatsu, S2551 (Designed for Visible to Infrared Precision Photometry), <http://www.hamamatsu.com/eu/en/product/category/3100/4001/4103/S2551/index.html>, (accessed: December 2015).
- [210] Optoelectronics, O. UV Enhanced Series (Inversion Layer and Planar Diffused Silicon Photodiodes), <http://www.osiopoelectronics.com/Libraries/Datasheets/UV-Enhanced-Planar-Diffused-IR-Supressed-Photodiodes.sflb.ashx>, (accessed: December 2015).
- [211] M. Ihama, H. Koguchi, H. Inomata, H. Asano, Y. Imada, Y. Mishima, Y. Kato, Y. Hirose, M. Segawa, T. Ueda, S. Kishimura, in *International Image Sensor Workshop (IISW)* (Co-chairs: E. R. Fossum, B. Fowler), International Image Sensor Society, Snowbird, UT, USA **2013**.
- [212] M. Ihama, T. Mitsui, K. Nomura, Y. Maehara, H. Inomata, T. Gotou, Y. Takeuchi, *FUJIFILM Research Development* **2010**, *55*, 14.
- [213] M. Mori, Y. Hirose, M. Segawa, I. Miyanaga, R. Miyagawa, T. Ueda, H. Nara, H. Masuda, S. Kishimura, T. Sasaki, Y. Kato, Y. Imada, H. Asano, H. Inomata, H. Koguchi, M. Ihama, Y. Mishima, in *Symposium on VLSI (Very-Large-Scale Integration) Technology Digest of Technical Papers*, Kyoto, Japan, **2013**, T22.
- [214] J. Griffiths, in *Color and Constitution of Organic Molecules*, Academic Press, New York, **1976**, 72.
- [215] N. Nijegorodov, P. V. C. Luhanga, J. S. Nkoma, D. P. Winkoun, *Spectrochim. Acta A* **2006**, *64*, 1.
- [216] T. Fukuda, M. Komoriya, R. Mori, Z. Honda, K. Takahashi, N. Kamata, *Mol. Cryst. Liq. Cryst.* **2009**, *504*, 212.
- [217] T. Fukuda, R. Kobayashi, N. Kamata, S. Aihara, H. Seo, K. Hatano, D. Terunuma, *Jpn. J. Appl. Phys.* **2010**, *49*, 01AC05.
- [218] S. Kimura, T. Fukuda, Z. Honda, N. Kamata, K. Mori, K. Hatano, *Mol. Cryst. Liq. Cryst.* **2012**, *566*, 54.
- [219] T. Fukuda, S. Kimura, Z. Honda, N. Kamata, *Mol. Cryst. Liq. Cryst.* **2011**, *539*, 202/[542].
- [220] R. Kobayashi, T. Fukuda, Y. Suzuki, K. Hatano, N. Kamata, S. Aihara, H. Seo, D. Terunuma, *Mol. Cryst. Liq. Cryst.* **2010**, *519*, 206.
- [221] T. Fukuda, S. Kimura, Z. Honda, N. Kamata, K. Mori, K. Hatano, *Phys. Status Solidi A* **2012**, *209*, 2324.
- [222] T. Fukuda, S. Kimura, R. Kobayashi, A. Furube, *Phys. Status Solidi A* **2013**, *210*, 2674.
- [223] T. Sanji, H. Ishiwata, T. Kaizuka, M. Tanaka, H. Sakurai, R. Nagahata, K. Takeuchi, *Chem. Lett.* **2005**, *34*, 1130.
- [224] Y. Ohmori, T. Hamasaki, H. Kajii, T. Morimune, *Proc. SPIE – Optical Sensors*, Prague, Czech Republic, **2009**, 7536, 73560W.
- [225] A. K. Pandey, K. D. Johnstone, P. L. Burn, I. D. W. Samuel, *Sensor. Actuat. B-Chem.* **2014**, *196*, 245.
- [226] Y. A. M. Ismail, T. Soga, T. Jimbo, *Jpn. J. Appl. Phys.* **2010**, *49*, 52301.
- [227] T. Fukuda, S. Kimura, Z. Honda, N. Kamata, *Mol. Cryst. Liq. Cryst.* **2012**, *566*, 67.
- [228] T. Fukuda, S. Kimura, N. Kamata, K. Mori, K. Hatano, *Mol. Cryst. Liq. Cryst.* **2013**, *578*, 119.
- [229] D.-S. Leem, K.-H. Lee, K.-B. Park, S.-J. Lim, K.-S. Kim, Y. Wan Jin, S. Lee, *Appl. Phys. Lett.* **2013**, *103*, 043305.
- [230] J. Meiss, M. Hummert, A. Petrich, S. Pfuetzner, K. Leo, M. Riede, *Sol. Energ. Mat. Sol. C* **2011**, *95*, 630.
- [231] B. T. Lim, I. Kang, C. M. Kim, S. Y. Kim, S.-K. Kwon, Y.-H. Kim, D. S. Chung, *Org. Electron.* **2014**, *15*, 1856.
- [232] X. Cheng, M. Caironi, Y.-Y. Noh, J. Wang, C. Newman, H. Ye, A. Facchetti, H. Sirringhaus, *Chem. Mater.* **2010**, *22*, 1559.
- [233] B. Lamprecht, R. Thünauer, S. Köstler, G. Jakopic, G. Leising, J. R. Krenn, *Phys. Status Solidi R* **2008**, *2*, 178.
- [234] Y. Ishimaru, M. Wada, T. Fukuda, N. Kamata, *IEICE Trans. Electron.* **2011**, *E94.C*, 187.
- [235] Y. Higashi, K.-S. Kim, H. G. Jeon, M. Ichikawa, *J. Appl. Phys.* **2010**, *108*, 034502.
- [236] M. Kaneko, T. Taneda, T. Tsukagawa, H. Kajii, Y. Ohmori, *Jpn. J. Appl. Phys.* **2003**, *42*, 2523.
- [237] T. Morimune, H. Kajii, Y. Ohmori, *IEEE Phot. Tech. Lett.* **2006**, *18*, 2662.
- [238] L. Dong, X. Liu, G. Dong, L. Duan, D. Zhang, H. Zhao, L. Wang, Y. Qiu, *Laser Photonics Rev.* **2014**, *8*, 316.
- [239] K. Segi, S. Nakai, H. Okada, *J. Photopolym. Sci. Tec.* **2014**, *27*, 343.
- [240] A. Satoshi, K. Miyakawa, Y. Ohkawa, T. Matsubara, T. Takahata, S. Suzuki, M. Kubota, K. Tanioka, N. Kamata, D. Terunuma, *Jpn. J. Appl. Phys.* **2005**, *44*, 3743.
- [241] Hamamatsu, Silicon Photodiode: Blue Color Sensor (S6428-01), <http://www.hamamatsu.com/jp/en/product/alpha/M/4154/S6428-01/index.html> (accessed: December 2015).
- [242] S.-J. Lim, D.-S. Leem, K.-B. Park, K.-S. Kim, S. Sul, K. Na, G. H. Lee, C.-J. Heo, K.-H. Lee, X. Bulliard, R.-I. Satoh, T. Yagi, T. Ro, D. Im, J. Jung, M. Lee, T.-Y. Lee, M. G. Han, Y. W. Jin, S. Lee, *Sci. Rep.* **2015**, *5*, 7708.
- [243] Hamamatsu, Silicon Photodiode: Green Color Sensor (S6429-01), <http://www.hamamatsu.com/us/en/product/alpha/M/4154/S6429-01/index.html>, (accessed: December 2015).
- [244] D. Yang, L. Zhang, H. Wang, Y. Wang, Z. Li, T. Song, C. Fu, S. Yang, B. Zou, *IEEE Photon. Tech. Lett.* **2015**, *27*, 233.
- [245] Hamamatsu, Silicon Photodiode: Red Color Sensor (S6430-01), <http://www.hamamatsu.com/jp/en/product/alpha/M/4154/S6430-01/index.html> (accessed: December 2015).
- [246] Hamamatsu, S7505-01 RGB Color Sensor, <http://www.hamamatsu.com/jp/en/product/alpha/R/4153/S7505-01/index.html> (accessed: December 2015).
- [247] L. A. A. Pettersson, L. S. Roman, O. Inganäs, *J. Appl. Phys.* **1999**, *86*, 487.
- [248] V. Gautam, M. Bag, K. S. Narayan, *J. Am. Chem. Soc.* **2011**, *133*, 17942.
- [249] C. W. Tang, *Appl. Phys. Lett.* **1986**, *48*, 183.
- [250] NHK Corporate Information, <http://www.nhk.or.jp/corporateinfo/> (accessed: December 2015).
- [251] S. Aihara, Y. Hirano, T. Tajima, K. Miyakawa, Y. Ohkawa, T. Matsubara, T. Takahata, S. Suzuki, N. Egami, K. Tanioka, M. Abe, N. Saito, *Proc. IEEE - Workshop on Charge-Coupled Devices and Advanced Image Sensors*, IEEE, NJ, USA **2003**, *7*.
- [252] S. Aihara, Y. Hirano, T. Tajima, K. Tanioka, M. Abe, N. Saito, N. Kamata, D. Terunuma, *Appl. Phys. Lett.* **2003**, *82*, 511.
- [253] S. Aihara, M. Kubota, *Broadcast Tech.* **2012**, *49*, 14.
- [254] S. Aihara, K. Miyakawa, Y. Ohkawa, T. Matsubara, T. Takahata, S. Suzuki, N. Egami, N. Saito, K. Tanioka, N. Kamata, D. Terunuma, *Jpn. J. Appl. Phys.* **2003**, *42*, L801.
- [255] S. Aihara, K. Miyakawa, Y. Ohkawa, T. Matsubara, T. Takahata, S. Suzuki, M. Kubota, K. Tanioka, N. Kamata, D. Terunuma, *Jpn. J. Appl. Phys.* **2005**, *44*, 3743.
- [256] N. Suzuki, (FUJIFILM Corp.), US7858433 B2, **2010**.
- [257] S. Aihara, H. Seo, M. Namba, T. Watabe, H. Otake, M. Kubota, N. Egami, T. Hiramatsu, T. Matsuda, M. Furuta, H. Nitta, T. Hirao, *IEEE Trans. Electron. Dev.* **2009**, *56*, 2570.
- [258] T. Sakai, H. Seo, S. Aihara, M. Kubota, M. Furuta, *Proc. SPIE - Sensors, Cameras, and Systems for Industrial and Scientific Applications XIV*, SPIE, Bellingham, WA, USA, **2013**, 8659, 86590G.

- [259] H. Seo, T. Sakai, H. Otake, M. Furuta, *IEEE – Sensors*, Valencia, Spain, **2014**, 1672.
- [260] H. Seo, S. Aihara, T. Watabe, H. Otake, T. Sakai, M. Kubota, N. Egami, T. Hiramatsu, T. Matsuda, M. Furuta, T. Hirao, *Jpn. J. Appl. Phys.* **2011**, 50, 024103.
- [261] S. Toshikatsu, H. Seo, S. Aihara, M. Kubota, N. Egami, D. Wang, M. Furuta, *Jpn. J. Appl. Phys.* **2012**, 51, 010202.
- [262] Omnivision, *Omnivision Image Sensor OV16820/OV16825 16-Megapixel*, http://www.ovt.com/download_document.php?type=sensor&sensorid=116, accessed online: December 2015.
- [263] S. Takada, M. Ihama, M. Inuiya, *Proc SPIE - Sensors, Cameras, and Systems for Scientific/Industrial Applications VII*, SPIE, Bellingham, WA, USA, **2006**, 6068, 60680A.
- [264] T. Shunji, M. Ihama, M. Inuiya, T. Komatsu, T. Saito, *Proc. SPIE IS & T Electronic Imaging - Digital Photography III*, SPIE, Bellingham, WA, USA, **2007**, 6502, 650207.
- [265] R. Bogue, *Sensor Rev.* **2014**, 34, 143.
- [266] S. R. Forrest, *MRS Bull.* **2005**, 30, 28.
- [267] F. C. Jamieson, T. Agostinelli, H. Azimi, J. Nelson, J. R. Durrant, *J. Phys. Chem. Lett.* **2010**, 1, 3306.
- [268] C.-M. Yang, P.-Y. Tsai, S.-F. Horng, K.-C. Lee, S.-R. Tzeng, H.-F. Meng, J.-T. Shy, C.-F. Shu, *Appl. Phys. Lett.* **2008**, 92, 083504.
- [269] F. Arca, M. Sramek, S. F. Tedde, P. Lugli, O. Hayden, *IEEE J. Quantum Electron.* **2013**, 49, 1016.
- [270] Q. Lin, A. Armin, P. L. Burn, P. Meredith, *Nat. Photon.* **2015**, 9, 687.
- [271] Y. Fang, Q. Dong, Y. Shao, Y. Yuan, J. Huang, *Nat. Photon.* **2015**, 9, 679.
- [272] H. C. Ko, M. P. Stoykovich, J. Song, V. Malyarchuk, W. M. Choi, C.-J. Yu, J. B. Geddes III, J. Xiao, S. Wang, Y. Huang, J. A. Rogers, *Nature* **2008**, 454, 748.
- [273] C. A. Mead, M. A. Mahowald, *Neural Networks* **1988**, 1, 91.
- [274] X. Xu, M. Davanco, X. Qi, S. R. Forrest, *Org. Electron.* **2008**, 9, 1122.
- [275] X. Xu, M. Mihnev, A. Taylor, S. R. Forrest, *Appl. Phys. Lett.* **2009**, 94, 043313.
- [276] S. R. Forrest, *Nature* **2004**, 428, 911.
- [277] A. F. Abouraddy, O. Shapira, M. Bayindir, J. Arnold, F. Sorin, D. S. Hinczewski, J. D. Joannopoulos, Y. Fink, *Nat. Mater.* **2006**, 5, 532.
- [278] T. Someya, S. Iba, Y. Kato, T. Sekitani, Y. Noguchi, Y. Murase, H. Kawaguchi, T. Sakurai, in *Electron Devices Meeting, IEDM Technical Digest (IEEE International)*, IEEE, NJ, USA **2004**, 365.
- [279] T. Someya, Y. Kato, I. Shingo, Y. Noguchi, T. Sekitani, H. Kawaguchi, T. Sakurai, *IEEE Trans. Electron. Dev.* **2005**, 52, 2502.
- [280] A. Soini, in *Proc. of the 2nd Int. Symp. On Image and Signal Processing and Analysis (ISPA)*, IEEE, NJ, USA, **2001**, 332.
- [281] S. Ratnasingam, S. Collins, J. Hernández-Andrés, *J. Opt. Soc. Am. A* **2010**, 27, 2198.
- [282] R. Chellappa, A. K. Roy-Chowdhury, S. K. Zhou, in *Synthesis Lectures on Image, Video, and Multimedia Processing*, Morgan & Claypool, San Rafael, CA, USA, **2005**, 1, pp. 1–173.
- [283] J. H. Daniel, A. Sawant, M. Teepe, C. Shih, R. A. Street, L. E. Antonuk, *Sensor. Actuat. A-Phys.* **2007**, 140, 185.
- [284] M. Kabir, S. Kasap, J. Rowlands, in *Springer Handbook of Electronic and Photonic Materials* (Eds: S. Kasap, P. Capper), Springer, New York, **2006**, pp. 1121–1137.
- [285] P. E. Keivanidis, N. C. Greenham, H. Sirringhaus, R. H. Friend, J. C. Blakesley, R. Speller, M. Campoy-Quiles, T. Agostinelli, D. D. C. Bradley, J. Nelson, *Appl. Phys. Lett.* **2008**, 92, 023304.
- [286] J. C. Blakesley, P. E. Keivanidis, M. Campoy-Quiles, C. R. Newman, Y. Jin, R. Speller, H. Sirringhaus, N. C. Greenham, J. Nelson, P. Stavrinou, *Nucl. Instrum. Methods Phys. Res.* **2007**, 580, 774.
- [287] G. H. Gelinck, A. Kumar, D. Moet, J.-L. van der Steen, U. Shafique, P. E. Malinowski, K. Myny, B. P. Rand, M. Simon, W. Rütten, A. Douglas, J. Jorritsma, P. Heremans, R. Andriessen, *Org. Electron.* **2013**, 14, 2602.
- [288] T. Agostinelli, M. Campoy-Quiles, J. C. Blakesley, R. Speller, D. D. C. Bradley, J. Nelson, *Appl. Phys. Lett.* **2008**, 93, 203305.
- [289] J. W. Kingsley, A. J. Pearson, L. Harris, S. J. Weston, D. G. Lidzey, *Org. Electron.* **2009**, 10, 1170.
- [290] F. Arca, E. Kohlstädt, S. F. Tedde, P. Lugli, O. Hayden, *IEEE Trans. Electron Dev.* **2013**, 60, 1663.
- [291] E. Takada, K. Fujii, H. Imai, H. Okada, Y. Namito, T. Nakamura, *J. Nucl. Sci. Technol.* **2014**, 52, 104.
- [292] P. E. Malinowski, A. Kumar, D. J. D. Moet, D. Cheyns, B. P. Rand, J.-L. P. J. van der Steen, K. Myny, S. Steudel, M. Simon, G. Gelinck, P. Heremans, in *International Image Sensors Workshop (IISW)*, International Image Sensor Society, Snowbird, UT, USA, **2013**.
- [293] D. Kabra, T. B. Singh, K. S. Narayan, *Appl. Phys. Lett.* **2004**, 85, 5073.
- [294] T. Someya, T. Sekitani, S. Iba, Y. Kato, H. Kawaguchi, T. Sakurai, *Proc. Natl. Acad. Sci. USA* **2004**, 101, 9966.
- [295] R. Koeppe, P. Bartu, S. Bauer, N. S. Sariciftci, *Adv. Mater.* **2009**, 21, 3510.
- [296] H. Benisty, V. Raulot, M. Flury, A. Moriceau, D. Richard, *IEEE J. Sel. Top. Quant. Electron.* **2016**, 22, 4500108.
- [297] J. Y. Gomez, L. Jamet, E. Guerineau, C. Premont, (ISORG), WO2013045780 (A1) **2013**.
- [298] IMEC, *Imec and Holst Center Unveil Fully Organic Imager*, http://www2.imec.be/be_en/press/imec-news/imecholstorganicimager.html, (accessed: December 2015).
- [299] P. Meredith, C. J. Bettinger, M. Irimia-Vladu, A. B. Mostert, P. E. Schwenn, *Rep. Prog. Phys.* **2013**, 76, 034501.
- [300] A. Noy, *Adv. Mater.* **2011**, 23, 807.
- [301] M. Berggren, A. Richter-Dahlfors, *Adv. Mater.* **2007**, 19, 3201.
- [302] G. G. Malliaras, *Biochim. Biophys. Acta Gen. Subjects* **2013**, 1830, 4286.
- [303] P. Fromherz, *ChemPhysChem* **2002**, 3, 276.
- [304] J. R. Wojciechowski, L. C. Shriver-Lake, M. Y. Yamaguchi, E. Füreder, R. Pieler, M. Schamesberger, C. Winder, H. J. Prall, M. Sonnleitner, F. S. Ligler, *Anal. Chem.* **2009**, 81, 3455.
- [305] M. Sagmeister, A. Tschepp, E. Kraker, T. Abel, B. Lamprecht, T. Mayr, S. Köstler, *Anal. Bioanal. Chem.* **2013**, 405, 5975.
- [306] C. M. Lochner, Y. Khan, A. Pierre, A. C. Arias, *Nat. Commun.* **2014**, 5, 5745.
- [307] D. Ghezzi, M. R. Antognazza, M. Dal Maschio, E. Lanzarini, F. Benfenati, G. Lanzani, *Nat. Commun.* **2011**, 2, 166.
- [308] D. Ghezzi, M. R. Antognazza, R. Maccarone, S. Bellani, E. Lanzarini, N. Martino, M. Mete, G. Pertile, S. Bisti, G. Lanzani, F. Benfenati, *Nat. Photon.* **2013**, 7, 400.
- [309] V. Gautam, K. S. Narayan, *Organogenesis* **2014**, 10, 9.
- [310] X. Xin, Q. Xiangfei, M. Davanco, S. R. Forrest, in *20th Annual Meeting of the IEEE Lasers and Electro-Optics Society (LEOS)*, Lake Buena Vista, FL, USA **2007**, 578.
- [311] X. Xin, M. Davanco, S. R. Forrest, in *21st Annual Meeting of the IEEE Lasers and Electro-Optics Society (LEOS)*, Acapulco, Mexico, **2008**, 356.
- [312] S. Liu, P. You, J. Li, J. Li, C.-S. Lee, B. S. Ong, C. Surya, F. Yan, *Energ. Environ. Sci.* **2015**, 8, 1463.
- [313] Q. Zhang, B. Kan, F. Liu, G. Long, X. Wan, X. Chen, Y. Zuo, W. Ni, H. Zhang, M. Li, Z. Hu, F. Huang, Y. Cao, Z. Liang, M. Zhang, T. P. Russell, Y. Chen, *Nat. Photon.* **2015**, 9, 35.
- [314] Q. Lin, A. Armin, R. C. R. Nagiri, P. L. Burn, P. Meredith, *Nat. Photon.* **2015**, 9, 106.
- [315] C. Wehrenfennig, G. E. Eperon, M. B. Johnston, H. J. Snaith, L. M. Herz, *Adv. Mater.* **2014**, 26, 1584.
- [316] Q. Lin, A. Armin, D. M. Lyons, P. L. Burn, P. Meredith, *Adv. Mater.* **2015**, 27, 2060.
- [317] L. Dou, Y. (M) Yang, J. You, Z. Hong, W.-H. Chang, G. Li, Y. Yang, *Nat. Commun.* **2014**, 5, 5404.
- [318] Y. Fang, J. Huang, *Adv. Mater.* **2015**, 27, 2804.
- [319] B. R. Sutherland, A. K. Johnston, A. H. Ip, J. Xu, V. Adinolfi, P. Kanjanaboos, E. H. Sargent, *ACS Photonics* **2015**, 2, 1117.
- [320] B. Conings, L. Baeten, C. De Dobbelaere, J. D'Haen, J. Manca, H.-G. Boyen, *Adv. Mater.* **2014**, 26, 2041.
- [321] M. B. Johnston, *Nat. Photon.* **2015**, 9, 634.